

The syn-rift tectono-stratigraphic record of rifted margins (Part II): A new model to break through the proximal/distal interpretation frontier

Pauline Chenin, Gianreto Manatschal, Jean-François Ghienne, Peng Chao

▶ **To cite this version:**

Pauline Chenin, Gianreto Manatschal, Jean-François Ghienne, Peng Chao. The syn-rift tectono-stratigraphic record of rifted margins (Part II): A new model to break through the proximal/distal interpretation frontier. Basin Research, In press, 10.1111/bre.12628 . insu-03473206

HAL Id: insu-03473206
https://insu.hal.science/insu-03473206

Submitted on 9 Dec 2021

HAL is a multi-disciplinary open access archive for the deposit and dissemination of scientific research documents, whether they are published or not. The documents may come from teaching and research institutions in France or abroad, or from public or private research centers.

L'archive ouverte pluridisciplinaire **HAL**, est destinée au dépôt et à la diffusion de documents scientifiques de niveau recherche, publiés ou non, émanant des établissements d'enseignement et de recherche français ou étrangers, des laboratoires publics ou privés.

The syn-rift tectono-stratigraphic record of rifted margins (Part II): A new model to break through the proximal/distal interpretation frontier

Pauline Chenin[1*], Gianreto Manatschal[1], Jean-François Ghienne[1], Peng Chao[1]

[1] Université de Strasbourg, CNRS, ITES UMR 7063, 5 rue Descartes, 67084 Strasbourg, France

* corresponding author: chenin@unistra.fr

Keywords: hyperextended margin, rifting, tectono-stratigraphic record

Highlights

- A new tectono-stratigraphic model to help break through the proximal/distal interpretation frontier
- Each rift domain is associated with specific structures and sedimentary architectures
- Each rift domain displays a specific ratio of vertical vs horizontal accommodation space creation
- Rift deformation localizes sequentially, inducing a younging of the base of passive infill oceanward
- The early syn-rift stratigraphic record is largely discontinuous/broken up in the distal margin

Abstract

One fundamental lesson from the last decades research into rifted margins is that stratigraphic horizons cannot be simply correlated from the proximal into distal domain, which makes the interpretation of poorly calibrated and largely inaccessible distal margins difficult. In this contribution, we propose a new tectono-stratigraphic model to help break through the proximal/distal interpretation frontier. After reviewing the scientific advances on rifted margins achieved during the last century, we describe the primary spatio-temporal evolution of active deformation during rifting. We show that different rift domains are associated with specific (1) periods of active deformation; (2) tectonic structures and related stratigraphic architecture; (3) amounts of accommodation creation owing to specific ranges of horizontal widening and vertical deepening; and (4) depositional environments. We demonstrate that the sequential localization of extension during rifting results in a younging of the base of passive infill (i.e., sediment deposited in a non-tectonic setting) oceanward. We propose a panel of few to few tens of My time intervals related to specific tectonic events – our *Tectonic Sequences* – that may be correlated more or less easily and continuously across rifted margins. This study underlines the value of an iterative approach between fieldwork on fossil rifted margins and offshore geophysical studies, where field studies offer easy-to-access and high-resolution calibration of dismembered rifted margin remnants, while geophysical studies provide comparatively low-resolution imaging of entire, intact but largely inaccessible, rifted margins. It also highlights the necessity of jettisoning outdated dogma on rifted margins and changing our routines when interpreting seismic sections and outcrops.

1. Introduction

Rifting is a process involving extension of the crust and upper mantle, during which accommodation is created by both horizontal widening and vertical deepening. The involved sedimentary systems record the timing, location and type of tectonic

deformation, the distribution of depocenters, the reorganization of sedimentary sources, and the evolution of water depths. Yet, distal parts of present-day rifted margins have remained largely inaccessible to date, including to drilling, which makes the interpretation of their syn-rift stratigraphic architecture, the determination of their sedimentary facies, and their correlation with more proximal parts of the margin difficult.

Over the last decades, the scientific community has made significant progress in understanding the processes at play during rifting. The iterative workflow between onshore and offshore studies, together with the improvement of imaging, dating and modelling techniques, enabled us to identify the characteristics common to rift systems, and to recognize a systematic deformation sequence during their formation. The ensuing question is: does a comparable formation history among rift systems imply a similar tectono-stratigraphic record, despite the differences in their local sedimentary sources and depositional environments?

In this contribution, we propose a new conceptual tectono-stratigraphic model synthetizing the evolution of deformation over space and time during rifting. We review *when*, *where* and *how* accommodation is created, and show that specific domains of rifted margins are associated with specific (1) periods of tectonic activity; (2) style of deformation and tectono-stratigraphic architectures; (3) ratios of horizontal vs vertical accommodation creation; and (4) depositional environments. After briefly summarizing the historical evolution of models for rifted margins, we describe our tectono-stratigraphic model and compare it with observations from both present-day and fossil rifted margins. Then, we discuss how this template can help interpreting seismic sections in poorly calibrated rift systems and to correlate remnants of dismembered margins embedded in orogens (e.g., Alps, Pyrenees, Oman, Timor, Zagros). Finally, we examine the limitations of our model, in particular the correlation of timelines/time intervals both along dip and strike of rifted margins, the effect of sedimentation rates with respect to the rates of

subsidence, the impact of magma, and the challenge of including a three-dimensional perspective at segmented and multiphase rift systems.

2. Historical overview

Rifting has always been regarded as a process creating accommodation space that is filled with sediments and/or volcanic products and/or water, both during and after the termination of deformation (McKenzie, 1978). However, our understanding of *when*, *where* and *how* accommodation is created and filled has been significantly evolving over the last decades (e.g., Bond and Kominz, 1988; De Graciansky *et al.*, 2011; Gawthorpe *et al.*, 1994; Gawthorpe and Leeder, 2000; Olsen and Morgan, 2006; Schlische, 1995; Withjack *et al.*, 2002).

2.1. The Geosyncline Theory (from the late 1850's to the 1960's)

The premise of tectonics emerged from the work of Hall (1859), who first recognized the existence of vertical movements (subsidence and uplift) of the Earth surface and the folding of sedimentary series (Figure 1a). Hall suggested that folding occurred at the *axis* of *synclinal* structures that resulted from Earth surface deformation. Dana (1873) suggested that the subsidence of *Geosynclines* (which corresponded to Hall's synclinal axis) was balanced by the rising of adjacent *Geanticlines*, both resulting from Earth contraction-driven lateral compression. A few decades later, Haug (1900) introduced the distinction between shallow- and deep-water facies, and emphasized their lateral change between the margins and the axial part of a Geosyncline. He also suggested that Geosynclines were mobile zones located at the boundary between two stable continental masses. These basic concepts were further developed during subsequent decades with the work of Argand (1916), Kay (1951), Kober (1923) and

Stille (1913, 1924, 1936), among others. For further details on the birth and evolution of the Geosyncline Theory see the review by Aubouin (1965).

2.2. The early stages of Plate Tectonic Theory: Pure-Shear vs Simple-Shear models and the birth of seismic stratigraphy (from the 1970's to the early 1990's)

Based on the first reflection seismic sections at rifted margins (e.g., Montadert *et al.* 1979), rift systems and rifted margins were envisioned as essentially comprising oceanward-dipping, high-angle (ca. 60 °) normal faults separating a series of tilted fault blocks and associated half-graben/graben whose size decreased oceanward (Figure 1b). The oceanic crust was supposed to start directly where thinned continental crust terminated, which implied a localized and instantaneous breakup related to the onset of steady-state magma emplacement. McKenzie (1978) and Jarvis and McKenzie (1980) envisioned rifting as Pure-Shear (depth-uniform) thinning of the lithosphere, resulting in both rapid ("instantaneous") subsidence associated with crustal thinning, and subsequent protracted, progressively decreasing subsidence related to thermal relaxation of the thinned lithospheric mantle.

A few years later, Lemoine *et al.* (1987) suggested that Wernicke's (1985) alternative Simple-Shear Model would better explain the ancient Alpine Tethys rift system (Figure 1c). Indeed, observations from the Alpine Tethys margins exposed in the Alps diverged from the Pure-Shear Model predictions in that: (1) the topographic and thermal evolution of the former conjugate margins appeared to be largely asymmetric (Lemoine, 1985), contrasting with the predictions of the symmetrical Pure-Shear Model; (2) at least one of the two margins was uplifted during rifting (e.g., the Briançonnais Block; Lemoine *et al.*, 1986), while the Pure-Shear model only predicted subsidence; and (3) no evidence for a Penrose-type oceanic crust could be found; instead, Alpine geologists had evidenced exhumation of subcontinental mantle to the seafloor (Decandia and Elter, 1972, 1969).

Contemporaneously, Falvey (1974) laid the ground for modern rifted margin stratigraphy. He stated that the onset of rifting was marked by an unconformity generated by a phase of thermal doming, which he named the *Rift Onset Unconformity* (*ROU*). He also mentioned the existence of a so-called *Breakup Unconformity* (*BU*), associated with the onset of rapid subsidence of the entire margin. This phase of rapid subsidence, modelled a few years later as an isostatic adjustment following the mechanical breakup of the lithosphere by Braun and Beaumont (1989), was thought to be expressed by the progradation of sedimentary deposits over the shelf and continental slope.

Hubbard (1988) introduced the term “megasequence”, which he defined as a “major sedimentary package” bounded by “the most prominent regional unconformities”. He suggested that these prominent regional unconformities “record the principal periods of change in basin geometry and polarity”. Hubbard (1988), and then Prosser (1993), recognized three types of megasequences, namely pre-, syn- and post-rift megasequences, deposited respectively prior to the onset of rifting, during rifting and after the termination of rifting.

In the 1980’s–early 1990’s, the architecture of the pre-, syn and post-rift megasequences were conceptualized with the help of analytical (Barr, 1991, 1987), analogue (Buchanan and McClay, 1991), and numerical modelling (Hardy, 1993). The pre-rift megasequence was supposed to be coupled to the underlying basement, except in the presence of low frictional, efficiently decoupling materials like salt or clays. In the absence of pre-rift tectonic events, pre-rift deposits are essentially comprised of parallel strata (i.e., without growth structures; violet sediments in Figures 1b and 1c).

The syn-rift megasequence was regarded as comprised of wedge-shape sedimentary deposits that thicken toward the adjacent normal fault (blue sediments in Figures 1b and 1c). However, the nature of the isostatic compensation (none, local or regional),

155 the geometry of the normal fault involved (planar or listric), sedimentation rates and
156 climate may result in various stratal geometries of these syn-rift deposits (e.g., Barr,
157 1991; Buchanan and McClay, 1991; Prosser, 1993).

158 The post-rift megasequence was interpreted to be made of un-extended sedimentary
159 packages that drape or onlap against preexisting topography, or downlap onto
160 oceanic crust (green sediments in Figures 1b and 1c). In isolated basins, when the
161 sedimentation rate is very low compared to the rate of subsidence, these deposits are
162 parallel and horizontal. Otherwise, they display clinoform shapes (e.g., significant
163 thickening of strata toward the basin center; Fig. 5 of Waltham *et al.*, 1993).

164 In the “rigid domino fault blocks” models for rifted margins (Figures 1b and 1c), all
165 faults and intervening tilted blocks are required to move and stop moving
166 simultaneously, and thus the syn-rift megasequence is synchronous across the entire
167 margin (blue sediments in Figures 1b and 1c; Waltham *et al.*, 1993). Both the base
168 and top of the syn-rift megasequence are therefore ideally marked by an isochronous
169 change in stratal dip across the entire margin, either between parallel pre-rift deposits
170 and wedge-shape syn-rift deposits in the former case, or between wedge-shape syn-
171 rift deposits and parallel post-rift deposits in the latter.

172

173

174 2.3. Toward a Polyphase Rifting Model (from the 1990’s to the early 2010’s)

175 Stratigraphic studies from both the Alps (Froitzheim and Eberli, 1990) and the Iberia–
176 Newfoundland margins (Murillas *et al.*, 1990; Tucholke *et al.*, 2007; Wilson *et al.*,
177 2001) highlighted that Alpine Tethys and southern North-Atlantic rifting were achieved
178 via two main, distinct and successive extensional phases. During the first phase,
179 numerous and broadly distributed half-graben depocenters, bounded by high-angle
180 normal faults, formed over a wide region (dark blue sediments in Figure 1d). At this

stage, crustal and lithospheric thinning were minor ($1/\beta << 1.5$, where $1/\beta$ corresponds to the ratio *crust thickness prior to extension / crust thickness at the end of extension*; McKenzie, 1978). During the second phase, tectonic activity was localized only in the future distal margins. There, significant crustal thinning ($1.5 < 1/\beta < \infty$) was achieved via both normal and extensional detachment faulting, as well as via the attenuation of ductile middle- and/or lower crustal layers (Manatschal *et al.* 2001; light blue sediments in Figure 1d). Crustal thinning was accompanied by significant lithospheric thinning.

Using numerical models, Lavier and Manatschal (2006) suggested that rifting was achieved via successive and distinct deformation modes, which we call here *Polyphase Rifting*. In their model, deformation evolved from initially distributed extension with limited crustal and lithospheric thinning (the so-called *stretching phase*) to increasingly localized deformation with significant crustal and lithospheric thinning (the so-called *thinning* and (*mantle*) *exhumation* phases). At the shift between the *stretching* and *thinning* phases, deformation stopped in the future proximal domain while rifting was still active in the future distal domain. This numerical model was consistent with the observation of passive infill sedimentation in the proximal domain at a time when rifting was not achieved yet, as in the Alpine Tethys (Froitzheim and Eberli, 1990; Masini *et al.*, 2013) and in Iberia–Newfoundland (Manatschal and Bernoulli, 1999; Murillas *et al.*, 1990; Péron-Pinvidic *et al.*, 2007; Tucholke *et al.*, 2007).

The observation of passive infill deposits emplaced during rifting required the refinement of the term *syn-rift*. Following Masini *et al.* (2013), we here restrict the use of *syn-rift* to its temporal dimension with respect to the overall rifting event, and use the terms *pre-tectonic*, *syn-tectonic* and *post-tectonic* to characterize the architecture of sedimentary deposits with respect to local tectonic activity (Figures 2a–2d). In this perspective, pre-rift sediments are necessarily pre-tectonic and post-rift sediments

are necessarily post-tectonic. However, syn-rift sediments may be either pre-, syn- or post-tectonic (Figure 2e).

In the absence of pre-rift tectonic events and inherited topography, pre-tectonic sediments display horizontal and parallel strata of constant thickness (Figure 2a). Syn-tectonic sediments are usually wedge-shaped, but their architecture varies depending on the type of fault they are associated with (Figure 2f). Indeed, while normal faults generate only minor horizontal extension (< 5 km), extensional detachment faults may exhume basement over more than 15 km (e.g., Epin and Manatschal, 2018). We qualify deposits as *half-graben wedge-shaped* when associated with a high-angle normal fault (Figure 2b) and *supra-detachment wedge-shaped* when related to an extensional detachment fault (Figure 2c). Note that the development of such growth structures is conditional on a sufficient syn-tectonic sedimentation rate. Extensional detachment faults are generally associated with cataclastic breccias and black gouges (Chester and Logan, 1986; Froitzheim and Eberli, 1990; Manatschal *et al.*, 2000), and, when exhumed to the seafloor, their surface is typically overlain by tectono-sedimentary breccias (e.g., Collettini, 2011, and references therein; Masini *et al.*, 2011). Post-tectonic deposits (Figure 2d) are either made of strata onlapping against, downlapping onto, or draping residual rift-related topography. Away from rift-related faults and/or in the absence of rift-related topography or intervening syn-tectonic deposits, pre- and post-tectonic deposits may practically be indistinguishable and only a paraconformity might capture the intervening syn-tectonic stage.

3. Building a stratigraphic model for idealized rifted margins

Over the last decade, the intense iterative workflow between field studies at remnants of rifted margins exposed on land (e.g., Andersen *et al.*, 2012; Masini *et al.*, 2013;

Mohn *et al.*, 2010; Epin *et al.*, 2017; Gawthorpe *et al.*, 2018; Ribes *et al.*, 2019b; Serck *et al.*, 2021; Stockli and Bosworth, 2018), interpretation of rifted margin seismic sections with ever higher resolutions (e.g., Causer *et al.*, 2020; Clerc *et al.*, 2018; Gillard *et al.*, 2016; Haupert *et al.*, 2016; Lymer *et al.*, 2019; Osmundsen *et al.*, 2016; Whiting *et al.*, 2020; Yang and Welford, 2021; Zhang *et al.*, 2019) and numerical modelling (e.g., Huismans and Beaumont, 2011; Brune *et al.*, 2014; Chenin *et al.*, 2020; Duretz *et al.*, 2020; Jourdon *et al.*, 2020; Naliboff *et al.*, 2017; Pérez-Gussinyé *et al.*, 2020; Petri *et al.*, 2019) have allowed to considerably improve our understanding of the architecture and evolution of rifted margins.

3.1. Benefits and pitfalls of using a template to guide interpretation

In this contribution, we propose a tectono-stratigraphic model to guide seismic and field interpretations in correlating observations from proximal margins into their distal continuation. Although model-driven approaches have historically caused significant misinterpretations and remain problematic when blindly applied (e.g., review by Manatschal *et al.*, 2021), having a first-order template may help when attempting to unravel the tectono-stratigraphic-record of uncalibrated distal domains. Indeed, sedimentary facies of given age may vary between the shallow-water proximal domain and deep-water hyperextended domain, and thus one cannot rely on the seismic signature/sedimentary field observations to correlate sedimentary units. Furthermore, as new real estate (i.e., new depositional surface) is created via the exhumation of basement along extensional detachment faults, the stratigraphic record may be largely discontinuous (e.g., sediments older than the age of exhumation are missing over the corresponding new real estate). This implies that seismic/field interpretations should not attempt to find continuous pre-rift or early syn-rift deposits in distal margins, where extensional detachment faults are likely.

The tectono-stratigraphic model we propose aims to describe an interpretation philosophy rather than providing a template to be copy-pasted, and we stress that careful seismic observations, rigorous application of the first principles of stratigraphy, and mindful consideration of the local geological history remain crucial to reliable interpretations.

3.2. Preliminary concepts and definitions

3.2.1. A spatial framework for rifted margins: definition of rift domains

Based on the geometry of top basement and Moho, which are two of the most consensual interfaces observed on seismic sections (red lines on Figure 3a), Sutra *et al.* (2013) identified four systematic rift domains. From the continent to the oceans, these domains are: (1) the *proximal domain*, where top basement and Moho are sub-horizontal and parallel, and where the 30 ± 5 km-thick crust displays only minor thinning. When the lithosphere was equilibrated prior to rifting (i.e. sub-horizontal top basement, Moho and base of the lithosphere), crustal thickness in the proximal domain may be used as a proxy for pre-rift crustal thickness; (2) the necking *domain*, where the crust is thinned from 30 ± 5 km to ca. 10 km; (3) the *hyperextended domain*, where the crust is thinned from ca. 10 km to 0 km. Compared with the necking domain, the angle of aperture between top basement and Moho is lower and more consistent in the hyperextended domain (Nirrengarten *et al.*, 2016; Sutra and Manatschal, 2012; Figure 3a); and (4) the *exhumed mantle domain*, where subcontinental lithospheric mantle is exhumed to the seafloor (Figure 3a).

Based on a worldwide compilation of seismic sections across magma-poor rifted margins and rift systems (i.e., < 6 km thickness of magmatic addition prior to lithospheric breakup; Tugend *et al.*, 2020), Chenin *et al.* (2017) proposed that

each domain displays a typical range of width, specifically: necking domains range between 10 and 100 km, with an average of 55 km; hyperextended domains between 20 and 70 km, with an average of 50 km; and exhumed mantle domains between 20 and 110 km with an average of 60 km (Figure 3b). They highlighted the absence of correlation between the width of the different domains for a given margin (Figure 3c).

3.2.2. Linking domains to rheological architecture and deformation processes

The variability in the angle of aperture between top basement and Moho among the different domains of rifted margins (red lines in Figure 3a) is interpreted to reflect along-dip changes in the rheology of the continental crust and underlying mantle, which may arise from composition, strain-rate, structural and/or temperature evolution during rifting (Chenin *et al.*, 2017; Nirrengarten *et al.*, 2016; Sutra and Manatschal, 2012; Brune *et al.*, 2014; Ros *et al.*, 2017; Figures 3d and 3e). In the proximal domain, crustal thinning is minor, broadly distributed, and largely accommodated by ductile deformation within the middle- to lower crust, which accounts for the horizontal and parallel position of both top basement and Moho (Sutra *et al.*, 2013). In the necking domain, the convergence between top basement and Moho is interpreted to reflect the progressive removal of ductile layers (Pérez-Gussinyé *et al.*, 2003; Sutra *et al.*, 2013). In the hyperextended domain, the lower dip angle of top basement is thought to express the frictional thinning of a fully brittle continental crust over a weak, serpentinized mantle (Nirrengarten *et al.*, 2016).

Following Péron-Pinvidic *et al.* (2013), we propose that each domain is linked to a specific deformation mode at play during rifting (Figure 3f): (1) the proximal domain displays numerous and broadly distributed half-graben depocenters formed during the *stretching phase* of Lavier and Manatschal (2006). The

tectono-thermal evolution of this domain is essentially ruled by the McKenzie (1978) model; (2) the necking domain is largely shaped by viscoplastic necking of the lithosphere (Chenin *et al.*, 2018). This *necking phase* corresponds to the early thinning phase of Lavier and Manatschal (2006). It is characterized by focusing of deformation into a narrower region compared to the early stretching phase (20–100 km according to the analytical study by Fletcher and Hallet, 1983; the seismic observations by Chenin *et al.*, 2017; and the numerical models by Chenin *et al.*, 2018). There, significant crustal thinning is achieved via detachment faulting (Mohn *et al.*, 2012; Osmundsen and Péron-Pinvidic, 2018; Ribes *et al.*, 2020); (3) the hyperextended domain is essentially shaped by Coulomb Wedge-type frictional thinning of fully brittle continental crust (Nirrengarten *et al.*, 2016). Here, crustal thinning is achieved via in-sequence detachment faulting in highly damaged continental crust (Epin and Manatschal, 2018; Lymer *et al.*, 2019; Manatschal, 1999). The *hyperextension phase* corresponds to the late thinning phase of Lavier and Manatschal (2006); and (4) the exhumed mantle domain records the exhumation of subcontinental mantle (i.e., the *mantle exhumation phase* of Lavier and Manatschal, 2006) via first in-sequence detachment faulting and then out-of-sequence or "flip-flop" detachment faulting (Epin *et al.*, 2019; Gillard *et al.*, 2016a; Reston and McDermott, 2011). Flip-flop mantle exhumation generates relatively symmetrical mantle exhumation (Gillard *et al.*, 2016b).

3.2.3. Constraining the spatio-temporal evolution of rifting using the stratigraphic record

Recently, Ribes *et al.* (2019b) studied the migration of deformation across the Adriatic margin during Alpine Tethys rifting. In each rift domain they identified

341 syn-tectonic sedimentary packages and placed them into a chronostratigraphic
342 time framework by comparing their position with respect to established timelines
343 (i.e., sedimentary markers tied to dated global events; Figure 4). From this
344 analysis, they concluded that: (1) Alpine Tethys rifting was associated with strain
345 localization, namely the region of active deformation (pink color in Figure 4)
346 became narrower as rifting advanced, and finally focused into the region of
347 future breakup; (2) the focusing of deformation was achieved through discrete
348 steps (i.e., *sequential*) rather than progressively (see the staircase architecture
349 of the roof of the syn-tectonic sequence, which climbs up between the proximal,
350 necking, hyperextended and exhumed mantle domain in Figure 4); and (3)
351 significant amounts of *new real estate* were locally created due to basement
352 (crust or mantle) exhumation via extensional detachment faults (Figure 4). This
353 newly exhumed material could only collect sediments that are younger than its
354 exhumation age, which implies a discontinuous stratigraphic record along dip of
355 the margin.

356 Comparable conclusions were drawn from the study of high-resolution reflection
357 seismic sections in the South China Sea by Chao *et al.* (2021) and Luo *et al.*
358 (2021), in the Porcupine Basin by Whiting *et al.* (2020), in the North Atlantic by
359 Sharp *et al.* (2017), and from numerical models by Pérez-Gussinyé *et al.* (2020):
360 all recognized a sequential localization of deformation into the distal domain as
361 rifting progresses, and/or increasing fragmentation of the pre-rift top basement
362 with ever wider domains of new real estate created between older fragments
363 oceanward.

364 Considering that each rift domain (*proximal, necking, hyperextended* and
365 *exhumed mantle domain*) is dominantly controlled by one specific deformation
366 mode (*stretching, necking, hyperextension* and *mantle exhumation*, respectively;
367 Figure 3f), and assuming that these deformation modes are active during distinct

periods of time, Ribes *et al.* (2019b) defined four *system tracts*, namely the *stretching, necking, hyperextension* and *mantle exhumation system tracts*. In the following, we will refer to these periods as *Tectonic Sequences* (*TS;* see next section for a discussion of terminology-related issues). A *Tectonic Sequence* encompasses all the sediments deposited during the period of activity of the corresponding deformation mode.

3.2.4. A short discussion on the complexity of finding accurate and illustrative terminology in an already jargon-rich field

In seismic interpretation calibrated by well data, it is common to map seismic *sequences* along rifted margins and to assign them a non-interpretive name linked to their relative age (e.g., J10, J20, J30, K19, K20, etc.; for instance Alves *et al.*, 2003). In contrast, in field studies or in interpretation of seismic images where chronostratigraphic constraints are lacking, it is common to map *system tracts*/depositional sequences or seismic *packages* according to the characteristic structures they display (e.g., Posamentier and Vail, 1988; Prosser, 1993; Ribes *et al.*, 2019b). Both these "non-interpretative" and “sequence stratigraphy" approaches are equivalent in 2D, however differences arise when it comes to analyze the stratigraphy of a propagating or segmented rift system in 3D: In the system tract approach, one correlates deformation phases without regard on their timing (i.e., the age of their upper and lower boundary may change ages across the rift system). In contrast, in the non-interpretative approach, one correlates timelines/isochronous seismic packages without regard to the tectonic processes they record (i.e., one package of given age may display the characteristic deformation patterns of the stretching phase in one segment, and of the hyperextension phase in the adjacent segment).

While the term *sequence* often has a time connotation, the term *system tract* rather relies on sedimentary architectures (e.g., stratal terminations). The term *package* is probably the most neutral term that can be used to present observations. Here we chose to use the term *Tectonic Sequence (TS)* to refer to the sediment body deposited during a given deformation phase to underline that (1) they are related to and coeval with a specific deformation mode; and (2) the upper- and lower limit of these packages are isochrons along dip of a given rifted margin transect (2D). We discuss in section 6.4.3 the difficulties raised by studying rifted margins in 3D.

3.3. Characteristic Tectonic Sequences (TSs) of an idealized 2D along-dip transect across a rifted margin

In the present section, we describe the characteristics of the TSs of our idealized model (Figure 5a–5g) without going through the details of construction. The observations on which this model was built derive essentially from the Alps and are presented in Part I (companion paper by Manatschal *et al.,* this volume). The present contribution aims to present our idealized model and show its application. Of course, because it is idealized, our model is simplified (see discussion in section 6.1). It aims to capture the first-order structures and patterns that can generally be identified at rifted margins; however, when applying this model, one must always keep in mind that each rift system is unique and builds on its own inheritance.

Based on the field and seismic observations, conceptual models and numerical modelling results presented in section 3.2, we present the Wheeler diagram of idealized two-dimensional rifted margins. By *idealized* we mean that the seven following hypotheses are fulfilled: (1) rifting is achieved via **four distinct and successive extension phases** that are the stretching, necking, hyperextension and mantle exhumation phases; (2) these extension phases **do not overlap in time**,

421 therefore **each** one is **associated with one single Tectonic Sequence**, namely
422 stretching, necking, hyperextension and mantle exhumation TS; (3) each extension
423 phase is **controlled by a single deformation mode**, namely stretching, necking,
424 hyperextension and mantle exhumation; (4) the **structures** formed during a
425 deformation phase are **characteristic and specific to the corresponding**
426 **deformation mode**; (5) each **deformation mode is spatially restricted to the rift**
427 **domain(s) it affects** (a deformation mode may affect several rift domains); (6) when
428 a **rift domain** is affected by a deformation mode, its **entire width is affected**; and
429 (7) rifting is a localizing process during which the **successive deformation modes**
430 **affect an ever narrower region**.

431

432 3.3.1. The stretching TS

433 The stretching TS records the stretching phase, which is characterized by a low-
434 β (β << 1.5, where β corresponds to the ratio *length prior to extension / length at*
435 *the end of extension*; McKenzie, 1978) pure shear extension of the lithosphere
436 accommodated by broadly distributed, high-angle normal faulting of brittle layers
437 (usually the upper crust and upper mantle) and plastic deformation of ductile
438 ones (usually the middle- and lower crust). The corresponding half-graben
439 depocenters are distributed over the entire rift domain (Figures 5b and 5g1). The
440 **stretching TS** will thus display **comparable depositional characteristics in**
441 **the future proximal, necking and hyperextended domains** (fifth line of Figure
442 6a), although it will be increasingly overprinted and dismembered by subsequent
443 extensional events in the distal domains (fifth line of Figure 6b). In contrast, the
444 stretching TS will be absent in the exhumed mantle domain since no mantle is
445 exhumed to the seafloor during the stretching phase.

446 The stretching TS is characterized by **wedge-shaped sedimentary deposits**
447 that thicken toward the main controlling normal faults (Figure 5g1 and fifth line of

448 Figure 6a). Related deposits often include breccias derived from the adjacent
449 footwall crest and fault plane. Indeed, the activity of a normal fault is usually
450 associated with footwall uplift and erosion due to the rotation of the fault block
451 (Yielding, 1990) and/or to the flexural response of the lithosphere (Kusznir and
452 Ziegler, 1992). Most of the infill is however linked to axial sedimentation
453 (Gawthorpe and Leeder, 2000; Leeder and Gawthorpe, 1987).

454 Accommodation creation during the stretching phase is predominantly created
455 by fault-controlled subsidence within rift basins. No significant lithospheric
456 thinning occurs during this stage, so that only limited accommodation is created
457 outside the basins, and only minor subsequent thermal subsidence is recorded
458 across the future proximal domain. Moreover, the usually high ratio between the
459 sedimentation- and accommodation creation rates hampers the formation of
460 significant bathymetry during the stretching phase (fifth line of Figure 6c).

461

462 3.3.2. The necking TS

463 The necking TS records the major phase of crustal thinning, from ca. 30 to
464 10 km ($1.5 < 1/\beta < 3$). During the early stages of the necking phase, a few large-
465 offset (up to few tens of km; e.g., Osmundsen and Péron-Pinvidic, 2018; Ribes
466 *et al.*, 2020; Sutra *et al.*, 2013) detachment faults form on either side of a largely
467 undeformed crustal ***keystone*** (*H-block* in Lavier and Manatschal, 2006; Figure
468 5c). These major **crustal-scale detachment faults**, which may **exhume mid-**
469 **crustal levels to the seafloor** (Ribes *et al.*, 2020), are specific and
470 characteristic structures of the future necking domains. The isostatic uplift
471 resulting from detachment-related tectonic denudation (Spencer, 1984) may
472 result in **erosion** of the exhumed basement and nearby deposition of
473 **siliciclastic sediments/sandstones** (e.g., the *Grès Singuliers* in the Mont

Blanc region; Ribes *et al.*, 2020, and references therein), ideally with a *supra-detachment wedge-shaped* architecture.

At the same time, most of the normal faults formed during the stretching phase are inactivated outside the necking domain. As a result, **the necking TS outside the necking domain is characterized by the sealing of the older half-graben depocenters by post-tectonic, passively infilling sediments** (fourth line of Figure 6a; e.g., Masini *et al.*, 2013). As no mantle is exhumed to the seafloor during the necking phase, the necking TS is absent in the exhumed mantle domain.

The onset of crustal necking is linked to the yield of the strongest lithospheric layer, which is usually the upper mantle in a thermally equilibrated lithosphere (Figure 3d). When the upper crust is mechanically decoupled from the mantle, the mechanical breakdown of the upper mantle is followed by a flexural rebound that tends to bring the necked system back to isostatic equilibrium (Braun and Beaumont, 1989). This flexural rebound accounts for the shallow-water depth, or even the **uplift and local erosion of the keystone** (i.e., the future necking and hyperextended domains) during the necking phase (see erosional unconformity in Figures 5c, 5d and 5g5; Chenin *et al.*, 2019, 2020). Uplift of the keystone may be further increased by the thermal erosion related to the asthenosphere upwelling beneath the rift system.

The late necking phase (Figure 5d) is linked to significant crustal and lithospheric thinning, which will eventually counterbalance the flexural rebound of the lithosphere and cause rapid and significant subsidence (e.g., Ribes *et al.*, 2020). The timing of uplift vs subsidence depends strongly on the rheology of the lithosphere (Chenin *et al.*, 2020). Subsidence might be further enhanced by large sediment supply and by subsequent thermal relaxation of the rift system.

In summary, **in the necking domain of the final margin, the necking TS** is expressed by (fourth line of Figures 6a–6c): (1) **creation of new real estate** due to the exhumation of upper- to middle crustal rocks to the seafloor via extensional detachment faulting; (2) ***supra-detachment wedge-shaped* sedimentary deposits of necking phase age** emplaced **directly onto exhumed basement;** (3) uplift and **erosion of exhumed basement and pre-necking sediments** potentially visible **in both the necking and hyperextended domains; and (4) contemporaneous deposition of basement-derived material in adjacent regions**. These sediments may be "cannibalized" (i.e., remobilized and re-deposited) during the necking phase owing to the progressive exhumation–uplift–rollover of the detachment fault on which the sandstones were deposited.

3.3.3. The hyperextension TS

The hyperextension TS records the localized dismembering of fully brittle continental crust from 10 to 0 km thick ($3 < 1/\beta < \infty$). Hyperextension is the first deformation stage to display a marked asymmetry (Nirrengarten *et al.*, 2016; Ranero and Pérez-Gussinyé, 2010): on the one hand, the future lower-plate margin is extended via in-sequence detachment faulting; and on the other hand, the future conjugate upper-plate margin is delaminated by the slip on the underlying detachment fault (Figures 5e, 5g2 and 5g4; Haupert *et al.*, 2016). Each of these deformation processes results in a particular morphology of the margin (see below).

During hyperextension, the proximal and necking domains are tectonically inactive, which results in continued passive infill in the proximal domain and the sealing of syn-tectonic structures/deposits in the necking domain (third line of

526 Figure 6a). Thus, **in the proximal and necking domains of the future margin,**
527 **the hyperextension TS is characterized by post-tectonic deposits.** Due to
528 the lack of mantle exhumation at this stage, the hyperextension TS is absent in
529 the exhumed mantle domain.

530 The hyperextension phase is associated with **rapid subsidence in both the**
531 **necking and hyperextended domains** (third line of Figure 6c). Subsidence is
532 related to extreme crustal thinning above a mechanically weak mantle (the
533 mechanical breakup of the upper mantle was achieved during the previous
534 necking phase). In the necking domain, subsidence is at this stage essentially
535 driven by thermal relaxation (i.e., lithosphere cooling).

536 In the lower-plate hyperextended domain, each successive in-sequence
537 detachment fault crosscuts the former one, resulting in the typical in-sequence
538 architecture illustrated in Figure 5g2 and 6a (Ranero and Pérez-Gussinyé,
539 2010). These detachment faults create new real estate via the exhumation of
540 basement to the seafloor (Figure 5g2). The amount of basement exhumed by a
541 detachment fault was reckoned to 10–20 km along-dip in the hyperextended
542 domain of the Adriatic lower-plate margin (Alpine Tethys) by Epin and
543 Manatschal (2018). The exhumed basement is typically pre-rift upper- to middle
544 crust. Each detachment fault is associated with a supra-detachment
545 sedimentary basin floored by tectono-sedimentary breccias. These basins are
546 filled with supra-detachment wedge-shaped syn-tectonic sediments emplaced
547 directly onto the detachment surface, getting younger toward the detachment
548 exhumation point (third line of Figure 6a; Masini *et al.*, 2011). As the successive
549 in-sequence detachment faults are active one after another, syn-tectonic
550 sedimentary deposits become younger oceanward (Péron-Pinvidic *et al.*, 2007).
551 Therefore, sedimentary deposits of a given age that are syn-tectonic in one

552 supra-detachment basin are post-tectonic in supra-detachment basins located
553 more continent-ward.

554 In summary, **in the hyperextended domain of the final lower-plate margin,**
555 **the hyperextension TS is expressed by** (third line of Figures 6a– 6c):
556 (1) creation of **new real estate** due to the exhumation of upper- to middle crustal
557 rocks to the seafloor via **in-sequence detachment faults that dip exclusively**
558 **oceanward;** (2) **tectono-sedimentary breccias and overlying *supra-***
559 ***detachment wedge-shaped* sedimentary deposits of hyperextension phase**
560 **age emplaced directly onto exhumed basement;** and (3) a progressive
561 **younging of supra-detachment basins fill oceanward.**

562 The hyperextended domain of upper-plate margins represents the residual part
563 of the initial keystone block (Haupert *et al.*, 2016; Figure 5g4). Compared with its
564 conjugate, the upper-plate hyperextended domain preserves therefore much
565 more of the stretching and necking-related structures and deposits, namely high-
566 angle normal faults that can dip continent- or oceanward. The base of the outer
567 part of the hyperextended domain is a mantle exhumation fault that may
568 eventually bring lower crustal rocks to the seafloor.

569 Ribes *et al.* (2019a) suggested that the individualization of the upper-plate
570 hyperextended domain is often associated with the formation of a *mega-fault*
571 *scarp* at its boundary with the adjacent necking domain. They defined a *mega-*
572 *fault scarp* as a "topographic ramp [formed by a] system of high-angle faults and
573 facing oceanwards a domain of substantial underfilled accommodation space".
574 They noticed that mega-fault scarps are linked with the emplacement of breccias
575 at their toe, over a wide part of the hyperextended domain (Figure 5g4).

576 In summary, **in the hyperextended domain of the final upper-plate margin,**
577 **the hyperextension TS is expressed by:** (1) creation of **a mega-fault scarp**

578 **and** associated **mega-breccias** at the boundary between the necking and future
579 hyperextended domain; (2) good preservation of earlier sedimentary structures
580 due to the **lack of significant new real estate creation;** and (3) possible
581 **exhumation of lower crustal rocks to the seafloor** at the outer edge of the
582 hyperextended domain**.**

583

584 3.3.4. The mantle exhumation TS

585 The mantle exhumation TS records the phase of subcontinental mantle
586 exhumation to the seafloor (Figure 5f). Mantle exhumation occurs while tectonic
587 activity has ceased in the continental domains of the future margin, **therefore**
588 **the mantle exhumation TS in the proximal, necking and hyperextended**
589 **domains is characterized by post-tectonic sedimentation** (second line of
590 Figure 6a). The entire margin keeps on subsiding during the mantle exhumation
591 phase.

592 The exhumed mantle domain is entirely comprised of new real estate, except
593 from few potential allochthonous blocks of continental crust and/or pre to syn-rift
594 sediments. Subcontinental mantle exhumation is achieved via out-of-sequence
595 flip-flop detachment faults that develop successively on either side of the future
596 spreading center, generating a relatively symmetrical pattern (Epin *et al.*, 2019;
597 Gillard *et al.*, 2016b; Figure 5g and second line of Figure 6a). The activity of a
598 mantle exhumation fault is associated with the formation of a topographic high at
599 the detachment fault breakaway (Spencer, 1984), and thus characterized by
600 over-tilted sedimentary sequences (see to the very right of Figure 5g3; Gillard *et*
601 *al.*, 2015). As tectonic activity continuously steps toward the locus of future
602 breakup, the age of the over-tilted sequences decreases (youngs) oceanward.
603 The first sediments overlying the exhumed mantle are tectono-sedimentary

breccias, and if sedimentary sources are available, the next ones are supra-detachment wedge-shaped syn-tectonic sediments deposited directly onto the detachment surface.

The exhumation phase often displays incipient magmatic activity, which results in discontinuous magmatic intrusions and lava flows (Coltat *et al.*, 2019; Epin *et al.*, 2019; Gillard *et al.*, 2016b, 2015). Magmatic flows are syn-tectonic, and thus they are interbedded with sediments of exhumation phase age.

In summary, **in the exhumed mantle domain of the final margin, the mantle exhumation TS is expressed by** (second line of Figures 6a and 6b): (1) **exclusively new real estate basement** comprised of **subcontinental lithospheric mantle** exhumed to the seafloor via **out-of-sequence detachment faulting;** (2) **tectono-sedimentary breccias** and overlying ***supra-detachment wedge-shaped*** **sedimentary deposits** of mantle exhumation phase age emplaced directly onto exhumed mantle; (3) **over-tilted sedimentary packages** at detachment faults breakaway; and (4) a progressive **younging of supra-detachment basins fill oceanward.**

4. Illustration of our model with calibrated natural examples

The best calibrated rifted margins worldwide (i.e., constrained by either outcrop observations or drilling) are by far those of the fossil Alpine Tethys exposed in the Alps. This example is described in detail in the companion paper by Manatschal *et al.* (this volume) and only briefly summarized here (Figures 7c and 7d). Another well calibrated example is the conjugate transect across the Iberia–Newfoundland margins imaged by the TGS–LG 12 and SCREECH 2 reflection seismic profiles, respectively. In addition to drill hole data from the proximal domain and inner part of the necking domain (e.g., Alves *et al.*, 2002, on the Iberian side; Sinclair, 1994 and references therein; Wielens *et al.*,

2006, on the Newfoundland one), deep-water drilling was performed in the Iberian hyperextended domain and in the inner part of the Newfoundland exhumed mantle domain, as part of the Ocean Drilling Program (ODP) Legs 149, 173 and 210. Besides, the viability of the tectono-stratigraphic interpretation by Sutra *et al.* (2013) was supported by its surface-conservative kinematic restoration.

4.1. Geological setting of Mesozoic rifting events in Western Europe

The opening of the Alpine Tethys and North-Atlantic Ocean was part of the fragmentation of the Pangea supercontinent, which progressed both from east to west and from south to north via *multistage rifting* (Figure 7a): it initiated with the opening of the Meliata-Vardar domain at the western end of the Neothethys. It continued with the opening of the Ligurian, Piemonte and Valais domains between the Eurasian/Iberian plate and the Adriatic/African plate, ahead of the northward-propagating Central Atlantic rifting, while the Meliata–Vardar domain was closing. It continued with the opening of the Bay of Biscay and southern North-Atlantic Ocean, while extension had ceased in the Alpine Tethys realm (Angrand *et al.*, 2020; Le Breton *et al.*, 2020).

A broadly distributed extensional event affected a large part of Western Europe and eastern North America from the Permo-Triassic onward (Leleu *et al.*, 2016, and references therein), and is here regarded as the stretching phase of both the Alpine Tethys and Iberia–Newfoundland rifting. In the Alpine Tethys rift system, the onset of localized deformation (necking phase) started at 185 ± 5 Ma (Sinemurian–Pliensbachian), evolved to hyperextension from 175 ± 5 Ma (Toarcian–Aalenian), and culminated with mantle exhumation from 165 ± 5 Ma onward (Bajocian–Bathonian; Manatschal *et al.*, this volume). Rifting stopped in the Alpine Tethys realm before steady-state seafloor spreading occurred in any branch of the Alpine rift system (Picazo *et al.*, 2016). Then, focused deformation started between Iberia and

Newfoundland with the necking phase from Tithonian to Berriasian time, continued with hyperextension from latest Berriasian to Valanginian time, and with mantle exhumation from the Valanginian (Mohn *et al.*, 2015, and references therein) until the late Aptian–early Albian lithospheric breakup (Bronner *et al.*, 2011). Note that the Iberia–Newfoundland rift system comprises three main segments that underwent diachronous extension from south to north (Alves *et al.*, 2009, and references therein). Here we focus on the central segment (i.e., South Iberia Abyssal Plain–Northern Newfoundland Basin).

4.2. The fossil Alpine Tethys rift system

4.2.1. The proximal domains

The former proximal domains of the European and Adriatic margins were associated with numerous half-graben depocenters (Figure 7b), among which the best-exposed are the Bourg d'Oisans Basin on the European margin (Chevalier, 2002; Dumont *et al.*, 2008), the Il Motto Basin on the northern Adriatic margin (Conti *et al.*, 1994; Eberli, 1988; Ribes *et al.*, 2019b), and the Monte Generoso Basin on the former southern Adriatic margin (Bernoulli, 1964; Bertotti *et al.*, 1993).

The sedimentary record is comparable in the three basins, displaying half-graben wedge-shaped deposits from latest Triassic to Sinemurian–Pliensbachian time (Figures 7c and 7d). In the temporal framework of the Alpine Tethys rifting, this corresponds to the early syn-rift history, namely the *stretching phase*. From Pliensbachian–Toarcian time onward, the three basins record passive infill (i.e., post-tectonic deposits belonging to the syn-rift megasequence).

4.2.2. The necking domains

The best described necking domain in the Alps used to belong to the former European margin and now lies in the Mont Blanc region (Ribes *et al.*, 2020; Figure 7b). Necking domains of the former northern- and southern Adriatic margin were respectively identified in the Campo–Grosina region (no sedimentary record available) by Mohn *et al.* (2010), and in the Cusio–Biellese region by Beltrando *et al.* (2015). Besides, the sedimentary record of the intervening keystone block is preserved in the Briançonnais region (Claudel and Dumont, 1999; Haupert *et al.*, 2016).

Observations from the Mont Blanc (Ribes *et al.*, 2020, and references therein) and Cusio–Biellese region (Beltrando *et al.*, 2015, and references therein) show that (Figures 7c and 7d): (1) the base of the necking TS is a tectonic unconformity owing to detachment-related basement exhumation (new real estate) and/or local erosion; (2) the necking domain is a local region of siliciclastic deposits (sandstones) due to local basement exhumation and erosion/deposition; (3) water-depth remained relatively shallow during the necking phase and deposition of related sandstones. Observations from the Briançonnais domain indicate that the keystone block underwent a phase of transient emergence during the necking phase.

4.2.3. The hyperextended domains

The outer edge of a European upper plate is exceptionally well-preserved in the Tasna Nappe of southeastern Switzerland (Manatschal *et al.*, 2006; Ribes *et al.*, 2019c; Figure 7b). The distal edge of the northern Adria lower plate is exposed in the Err and Upper Platta nappes (Figure 7b) in Southeast Switzerland (Epin and Manatschal, 2018; Manatschal and Nievergelt, 1997; Masini *et al.*, 2012).

710 The hyperextended domain of South Adria is recognized in the Canavese region
711 of the Southern Alps. It was recently interpreted as an upper plate by Decarlis *et*
712 *al.* (2017).

713 The tectono-sedimentary record of the Tasna, Err and Canavese nappes is
714 comparable in that the three of them display (Figures 7c and 7d):
715 (1) discontinuous pre-rift sediments only present as/over allochthonous blocks;
716 (2) basement exhumation via detachment faults overlain by tectono-sedimentary
717 breccias; and (3) deep-marine syn-tectonic sedimentary deposits. They differ in
718 that no lower crust seems to be exhumed at former lower plates (Err Nappe), in
719 contrast to former upper plates (Tasna Nappe and Canavese Zone).

720

721 4.2.4. <u>The exhumed mantle domains</u>

722 The best-preserved outcrops of an exhumed mantle domain and embryonic
723 seafloor spreading system in the Alps are exposed in the Lower Platta Nappe
724 (Figure 7b) in southeastern Switzerland (Desmurs *et al.*, 2002; Epin *et al.*, 2019;
725 Ribes *et al.*, 2019b) and at the Chenaillet Ophiolite in the French-Italian Alps
726 (Manatschal *et al.*, 2011).

727 The tectono-sedimentary record of the Platta Nappe and Chenaillet Ophiolite
728 shows that (Figures 7c and 7d): (1) mantle exhumation was achieved via
729 successive in-sequence detachment faults; (2) topography was created during
730 mantle exhumation, which resulted in gravitational sliding and/or onlapping of
731 syn-exhumation magmatic products and sediments; (3) the exhumed mantle
732 was affected by normal faults, which served as feeder channels for the overlying
733 volcanic sequences; (4) no pre- and early syn-rift deposits existed in the
734 exhumed mantle domain; and (5) the first sedimentary deposits (radiolarites)
735 were characteristic of abyssal deposition environments.

736

737 ## 4.3. The Iberia–Newfoundland conjugate margins

738 ### 4.3.1. The proximal domains

739 The proximal domains of the Iberia and Newfoundland margins (Figure 8a) are
740 characterized by minor stretching factors ($\beta < 2$; Mohn *et al.*, 2015), except in
741 the northern Jeanne d'Arc Basin that was affected by later extension related to
742 the formation of the Orphan Basin further north (Skogseid, 2010). Moho and top
743 basement are sub-horizontal at the scale of both proximal domains (Sutra *et al.*,
744 2013; Figures 8b and 8b1). Extension formed half-graben depocenters such as
745 the (South) Jeanne d'Arc, Whale and Horseshoe basins on the Newfoundland
746 side, and the Porto and Lusitanian basins on the Iberian side (Tucholke *et al.*,
747 2007).

748 The northern Lusitanian- and Jeanne d'Arc basins (Figure 8a) display a
749 comparable evolution and sedimentary fill indicating discontinuous tectonic
750 activity from Late Triassic to Late Jurassic (Alves *et al.*, 2002; Sinclair, 1993).
751 The first rift-related deposits in both basins are Late Triassic to Pliensbachian
752 continental and/or lacustrine sediments and evaporites, representative of
753 terrestrial to epicontinental sea environments. They show *half-graben wedge-*
754 *shape* sedimentary architectures, indicative of their syn-tectonic setting
755 (*stretching TS*). Subsequent marine sandstones and carbonates alternating with
756 shales were passively deposited from the Pliensbachian–Callovian in the
757 northern Lusitanian Basin (Iberian margin) and from the Tithonian in the central
758 Lusitanian Basin and at the Newfoundland margin. They were interpreted to
759 record post-tectonic thermal relaxation at both margins (Alves *et al.*, 2002; Alves
760 *et al.*, 2003; Enachescu, 1987; Hubbard, 1988; McAlpine, 1990; Sinclair, 1988;
761 Ravnås *et al.*, 1997).

On both the Iberian and Newfoundland margins, Callovian–Oxfordian deposits were affected by an erosional unconformity (Ian Sharp personal communication). This unconformity preceded renewed extension, during which marine sandstones were deposited in the northern Lusitanian Basin (Alves *et al.*, 2003, 2002; Ravnås *et al.*, 1997). Renewed extension in the Jeanne d'Arc Basin during the Tithonian was preceded or accompanied by erosion (Sinclair, 1993, and references therein) with alternating carbonates and shales being subsequently deposited.

In the Lusitanian Basin, the onset of post-tectonic sedimentation occurred in the late Tithonian–early Berriasian (Ravnås *et al.*, 1997). Sediments younger than Kimmeridgian are comprised of shallow-marine to continental units that display post-tectonic architectures and testify to limited thermal subsidence (Alves *et al.*, 2003). In the Jeanne d'Arc Basin, the onset of post-tectonic sedimentation was recognized during the Valanginian (CNLOPB, 2010; Enachescu, 1987; Sinclair, 1988). Sediments include sandstones and shales. Subsequent tectono-stratigraphic evolution in the Jeanne d'Arc Basin was affected by extensional events in the adjacent Orphan Basin (Skogseid, 2010) and is therefore not discussed here.

4.3.2. The necking domains

Alves *et al.* (2006) interpreted the necking zone of the Iberian margin to be structured by only high-angle normal faults but noticed the lack of evidence for pre-rift sediments in its outer part. Sutra *et al.* (2013) and Mohn *et al.* (2015) also interpreted the inner Iberian necking domain to contain a large normal fault (Figure 8b) but suggested that top basement in the outer part of the necking

787 domain is made of new real estate basement exhumed by a detachment fault
788 (Figure 8b2).

789 The necking domain of the Newfoundland margin has traditionally been
790 regarded as structured by only high-angle normal faults, like the rest of the
791 margin (Causer *et al.*, 2020; Hopper *et al.*, 2006; Welford *et al.*, 2010). However,
792 Péron-Pinvidic and Manatschal (2009), Sutra *et al.* (2013) and Mohn *et al.*
793 (2015) interpreted the inner necking fault of the Newfoundland margin as a high-
794 angle normal fault that started to evolve as a detachment fault (minor amount of
795 basement exhumed at low angle; Figure 8b). Nobody has recognized new real
796 estate creation in the rest of the Newfoundland necking domain so far.

797 Drill holes in the northern part of Carson Basin (Newfoundland margin; Figure
798 8a) indicate a Tithonian unconformity overlain by sandstone deposits, like that
799 reported in the Jeanne d'Arc Basin (Ian Sharp personal communication). A later
800 Albian unconformity in the northern Carson Basin is interpreted to mark the rift to
801 drift transition in the southern segment (Wielens *et al.*, 2006).

802 In the Iberian necking domain (Peniche Basin; Figure 8a), Alves *et al.* (2006)
803 interpreted Triassic–Late Jurassic syn-tectonic deposits in the depocenter
804 adjoining the main necking fault. These would correspond to the sedimentary fill
805 of a stretching phase half-graben depocenter. Such deposits are lacking in the
806 outer part of the necking domain. Latest Berriasian to Aptian sediments cover
807 the entire necking domain and were interpreted as post-tectonic (Alves *et al.*,
808 2006; Mohn *et al.*, 2015). Alves *et al.* (2006) reported toplaps of Albian age,
809 contemporaneous to the erosional unconformity reported in the Carson Basin.

810

811 4.3.3. <u>The hyperextended domains</u>

812 The hyperextended domain of the Iberian margin is consensually interpreted as
813 structured by detachment faults that exhumed upper- to mid-crustal basement to
814 the seafloor (Krawczyk *et al.*, 1996; Manatschal *et al.*, 2001; Reston and
815 McDermott, 2011; Figure 8b3). In contrast, the hyperextended domain of the
816 Newfoundland margin is regarded as essentially controlled by high-angle normal
817 faulting that crosscut the entire crust (Mohn *et al.*, 2015; Péron-Pinvidic and
818 Manatschal, 2009; Sutra *et al.*, 2013). This distinction prompted Manatschal
819 (2004) and Haupert *et al.* (2016) to interpret the Iberian margin as a lower plate
820 and its Newfoundland conjugate as an upper plate.

821 Drill holes in the hyperextended domain of the Iberian margin indicate upper
822 crustal basement affinities (ODP Sites 639, 901, 1065 and 1069). Exhumed
823 middle- or lower crust has been evidenced only at ODP Sites 900 and 1067
824 (outer edge of the hyperextended domain). No drill hole data from the
825 hyperextended domain of the Newfoundland margin is available.

826 None of the drill holes in the Iberian hyperextended domain penetrated Late
827 Triassic–Early Jurassic sediments. However, since all but one of the deep-water
828 drill holes (ODP Site 639 in the northern segment) stopped before reaching the
829 pre-rift top basement, we cannot exclude that such sequences exist, or existed
830 and were eroded prior to hyperextension.

831 In the Iberian hyperextended domain, pre-rift top basement is overlain by
832 concordant Mid- to Late Jurassic sandstones and conglomerates interpreted as
833 emplaced in an offshore shelf environment (ODP Sites 1065 and 1069; Figure
834 8b2). We consider that these syn-rift deposits, which display pre-tectonic
835 architectures, represent the stretching TS in the hyperextended domain. The
836 subsequent Tithonian–Berriasian deposits are still pre-tectonic in the central
837 segment. They comprise clay, silty clay, coarse sands and conglomerates
838 interpreted to reflect a deepening sequence (up to 500–1000 m; ODP Sites 901,

1065 and 1069). We consider that they represent the necking TS in the hyperextended domain. Whether the sands/conglomerates are derived from basement erosion is not resolved to date.

The sedimentary fill of supra-detachment basins was only drilled in the hyperextended domain of the northern Iberian segment (ODP Sites 638–641). There, it consists of debris flow, turbidites and slumps alternating with background sedimentation. The overall sedimentary sequence displays a wedge-shaped architecture (Boillot and Winterer, 1988). In the hyperextended domain of the central Iberian segment, Péron-Pinvidic *et al.* (2007) suggested that the lack of obvious growth structures may be related to syn-basement exhumation sedimentation in a largely sediment-starved rift system (i.e., the sediment-starved version of our *supra-detachment wedge-shaped* sediment architecture; see Figure 2f). They also noticed an oceanward younging of in the sedimentary fill of supra-detachment basins, where coeval sedimentary sequences display post-tectonic architectures in the inner part of the hyperextended domain, and syn-tectonic architectures in the outer part (Figure 8b3).

At ODP Site 1069, nannofossils (chalk) of late Berriasian to early Valanginan age overlie the tilted (pre-tectonic) Tithonian to older sedimentary sequence. These hemipelagic to pelagic sediments were interpreted as being deposited in open-marine outer-shelf to upper-slope environments (> 1500 m; Urquhart, 2001). They highlight the shutdown of the terrigenous input in the outermost part of the hyperextended domain during late hyperextension, possibly due to sediment capture by inner basins (Wilson *et al.*, 2001). Mohn *et al.* (2015) attributed the essentially post-tectonic infill of the supra-detachment basins to the short (5–10 My) duration of the hyperextension phase.

866 4.3.4. The exhumed mantle domains

867 Wilson *et al.* (2001) suggested that exhumation of already serpentinized mantle
868 started during Valanginian–Hauterivian time. While Manatschal (2004) initially
869 envisioned mantle exhumation via a single detachment fault, Gillard *et al.* (2016)
870 identified four successive in- and out-of-sequence detachment faults on the
871 SCREECH 1 seismic profile further north, across the exhumed mantle domain of
872 the Newfoundland margin.

873 At ODP Site 1068 (mantle exhumation point; Figure 8b2), drilling reported
874 tectono-sedimentary breccias supported by a calcareous chalk matrix of
875 Valanginian–Barremian age deposited onto exhumed mantle (Figure 8b4). The
876 next sediments drilled are much younger Campanian turbidites, which onlap
877 against the tilted tectono-sedimentary breccias. This relationship indicates either
878 that ODP Site 1068 was a topographic high already at the onset of mantle
879 exhumation, or that the tectono-sedimentary breccias were tilted and uplifted
880 after their deposition and prior to Campanian time, and that the adjacent basin
881 was progressively filled by turbidites and pelagic sediments. Comparable
882 relationships were documented by Péron-Pinvidic *et al.* (2007) at the conjugate
883 Newfoundland margin (ODP Site 1277; Figure 8b5): breccias of presumably
884 Aptian age and overlying exhumed mantle are over-tilted compared to the Albian
885 to Cenomanian onlapping, sub-horizontal, passive infill.

886 Magmatic activity contemporaneous with lithospheric breakup is evidenced by
887 diabase sills that were emplaced at the Aptian–Albian boundary (Jagoutz *et al.*,
888 2007; Karner and Shillington, 2005).

889

890 4.3.5. Summary

The primary spatio-temporal evolution of deformation in the Iberia–Newfoundland rift system can be deduced from the architecture of the main sedimentary package interfaces (Figure 8b2): in the inner necking domain, the blue interface marks the top of the syn-tectonic succession, while in the hyperextended domain, it marks the top of the pre-tectonic succession. This implies that deformation was active in the inner necking domain when no deformation had occurred in the hyperextended domain yet.

In the hyperextended domain, a comparable evolution can be observed (Figure 8b3): in the inner part, the red horizon lies within a post-tectonic succession, while it marks the top of syn-tectonic sequence in the outer part. The overlying green horizon lies within a post-tectonic succession along the entire hyperextended domain, while it marks the top of a syn-tectonic succession in the adjacent exhumed mantle domain. This indicates that active deformation was progressively advancing oceanward.

The tectono-stratigraphic history of the Iberia–Newfoundland rift system is summarized in Figure 8c. It is consistent with our idealized model in that: (1) it indicates a sequential localization of deformation oceanward; (2) the proximal domain is only affected by high-angle normal faults whose tectonic activity has largely ceased by the end of the stretching phase; (3) syn-stretching and syn-necking deposits in the outer necking and hyperextended domain of the Iberian margin display shallow-water facies comparable to those of the proximal domain; however, they display pre-tectonic stratigraphic architectures in the distal margin, while they are syn-tectonic in the proximal domain; (4) a syn-necking (Tithonian) unconformity overlain by sandstones exists at least in the proximal and necking domain of the Newfoundland margin; (5) the hyperextended Iberian lower plate is structured by in-sequence detachment faults associated with supra-detachment wedge-shaped deposits that become

younger oceanward; and (6) the exhumation domain displays over-tilted syn-rift pre- to syn-tectonic sequences against which post-rift sediments onlap.

Debated questions concern (1) the existence of extensional detachment faults in the necking domain of both the Iberian and Newfoundland margins; and (2) the existence of (dismembered) half-graben wedge-shape deposits in the stretching TS of the hyperextended domain.

5. Application of our model to incompletely calibrated natural examples

In the following, we rely on our model to interpret the tectono-stratigraphic record of an uncalibrated transect across conjugate NW-South China Sea margins; and of transects across the distal domain of the Mid-Norwegian and Socotra margins with support of observations and data from their adjacent, better-calibrated proximal domains.

5.1. The northwest South China Sea conjugate margins

5.1.1. Geological setting

The NW South China Sea is an aborted, V-shaped oceanic basin that benefits from extensive seismic coverage and some drill holes in the most distal part of the margin, ca. 200 km east of the transect presented below (International Ocean Discovery Program (IODP) Legs 349, 367 and 368; Figure 9a). The South China Sea differs largely from Atlantic-type rifts in that the rheology of the pre-rift lithosphere was significantly weaker due to the high geothermal gradient related to its back-arc position and orogenic and post-orogenic history (Li *et al.*, 2018; Sun *et al.*, 2019).

Rifting of the NW South China Sea is considered to have begun at ca. 65 Ma (Xie *et al.*, 2019), although this age is poorly constrained. Besides, because of the propagating nature of extension, rifting was largely diachronous along strike.

943 The onset of seafloor spreading is dated to 30–28 Ma based on the presence of
944 magnetic anomalies in the oceanic crust (Gee and Kent, 2007).

945 The NW South China Sea has been widely studied, for instance by Cameselle,
946 *et al.* (2017); Gao *et al.*, (2016); Larsen *et al.* (2018); Nirrengarten *et al.* (2020);
947 Ren *et al.* (2018); Zhang *et al.* (2021). Here we focus on the CGN-1
948 multichannel high-resolution 2D seismic section, for which Chao *et al.* (2021)
949 recently proposed a detailed tectono-sedimentary interpretation and balanced
950 kinematic restoration. To study the spatio-temporal evolution of deformation
951 during rifting, they grouped seismic packages of same interpreted age along dip
952 into one *Sequence (S)*. In total, they identified five syn-rift *Sequences* (packages
953 of same interpreted age along dip) with distinct evolutions across the conjugate
954 margins.
955

956 5.1.2. The proximal domain of the northern margin

957 The proximal domain of the northern margin is characterized by sub-horizontal
958 top basement and Moho separated by a ca. 22 km-thick continental crust
959 (Figure 9b). Top basement and pre-rift sediments are affected by only minor
960 normal faulting (fault throw < 0.2 sTWT). The faulted top basement is directly
961 overlain by post-rift deposits, which prevents any accurate dating of crustal
962 faulting. The proximal domain of the southern margin is not imaged and thus is
963 not discussed here.
964

965 5.1.3. The necking domains

966 On the northern margin, the inner limit of the necking domain is a crustal-scale
967 high-angle normal fault with a fault throw of 1.5 sTWT. 10–15 km further
968 outboard, a major detachment fault exhumed upper- to mid-crustal basement to

969 the seafloor over more than 15 km along dip (Figures 9b and 9b1; Chao *et al.*,
970 2021). In the outer part of the necking domain, the basement is affected by a
971 series of smaller high-angle normal faults, which created tilted blocks with minor
972 basement exhumation (< 0.5 sTWT fault throw).

973 The oldest sediments reported in the northern margin necking domain (S1) are
974 interpreted as pre-necking, half-graben wedge-shaped deposits that were
975 dismembered during the necking phase (Figure 9b1). They include faulted
976 wedge-shaped remnants capping pre-rift top basement and an allochthonous
977 package overlying the detachment surface itself (Chao *et al.* 2021; see their
978 Fig. 6). The first sedimentary package whose base is not disrupted by tectonic
979 activity is S5, which is thus interpreted as the first post-tectonic package in the
980 necking domain.

981 In-between S1 and S5, sediments of Ss 2–4 are interpreted as syn-tectonic of
982 the necking phase. They overlie the entire necking domain and display various
983 sedimentary architectures: sediments of S2 display a progradational architecture
984 onto the detachment surface and wedge-shaped architectures between the tilted
985 blocks of the outer necking domain. Sediments of S3 and S4 passively overlie
986 those of S2 in the inner part of the necking zone, whereas they are faulted (syn-
987 tectonic) in the outer part.

988 Chao *et al.* (2021) recognized that the tops of Ss 3, 4 and 5 are truncated,
989 suggesting that the necking domain was subaerial or above the storm-wave
990 base during relatively advanced stages of rifting (Figure 9b1). If this assumption
991 is correct, it implies that the necking domain remained at shallow water depths
992 during a large part of the rifting process.

993 On the southern margin, the inner part of necking domain is not imaged. Its
994 outer part is affected high-angle normal faults whose steepness decreases

995 oceanward, ending with a sub-horizontal detachment fault that exhumed upper-
996 to mid-crustal basement to the seafloor over ca. 15 km along dip (Figures 9b
997 and 9b2). The detailed tectono-sedimentary record at this margin is poorly
998 constrained compared to its conjugate because it is not possible to distinguish
999 between deposits related to Ss 1–4 (Chao *et al.* 2021). However, the boundary
1000 between S1–4 and S5 is interpreted as erosional, like along the northern margin.

1001 The careful tectono-stratigraphic restoration by Chao *et al.* (2021) allowed them
1002 to reconstruct the distribution of active faulting through time along the NW-South
1003 China Sea rifted margins: Figure 9c shows that, during the early stages of rifting
1004 (necking phase), faulting was localized into two fault corridors on either side of a
1005 largely undeformed region (active faults shown by red color in Figure 9c). This
1006 event is interpreted as the individualization of a *keystone* block, as predicted by
1007 numerical and analogue models (e.g., McClay 1996; Lavier and Manatschal
1008 2006; Huismans and Beaumont 2011). It ended abruptly with the localization of
1009 deformation and onset of massive sedimentation within the keystone area,
1010 contemporaneous with the abandonment of the former fault corridors on either
1011 side. This rapid switch (< 1 My) was interpreted to mark the transition between
1012 the necking and hyperextension phase (Chao *et al.* 2021).

1013

1014 5.1.4. <u>The hyperextended domains</u>

1015 In contrast to the necking domains, the hyperextended domains of the northern
1016 and southern margins are markedly asymmetrical: on the northern margin, the
1017 hyperextended domain is structured by successive high-angle faults that dip
1018 oceanward and cut through the entire crust (Figures 9b and 9b1). Faults throw
1019 decreases oceanward from 1.5 sTWT to < 0.5 sTWT, together with inter-fault
1020 blocks size. At the southern margin, the hyperextended domain is affected by in-

sequence, oceanward-dipping, low-angle detachment faults that root on one and the same décollement level (Figures 9b and 9b2). Based on these observations, Chao *et al.* (2021) suggested that the southern margin is a lower plate. In contrast, the alternance of ramps and terraces shaping the northern margin tip the scales in favor of an upper plate.

On the northern margin, the hyperextended domain can be subdivided into three sub-domains with distinct characteristics: in the inner sub-domain (He1 in Figure 9b1), the first sediments observed on pre-rift top basement are concordant (pre-tectonic) sedimentary deposits interpreted to belong to S3 (Figure 9b1). The next sediments to be deposited after S3 belong to S4 and display a wedge-shaped architecture. These are overlain by passive deposits interpreted to belong to S5. In the central sub-domain (He2 in Figure 9b1), tilted blocks are overlain by wedge-shaped magmatic products of unknown age. Magmatism is however younger than S5 because corresponding sediments passively overlie this segment. In the outermost sub-domain (He3 in Figure 9b1), only wedge-shaped magmatic products are recognized over the pre-rift basement. They are directly overlain by post-rift deposits, suggesting that magmatism becomes younger oceanward. This hypothesis is consistent with the conclusion drawn by Zhang *et al.* (2021) further east.

The sedimentary record in the hyperextended domain of the southern margin is poorly constrained and does not allow us to distinguish between syn-rift Ss 1–4 (Chao *et al.* 2021). S5 is interpreted as syn-tectonic in the entire hyperextended domain (Figure 9b2).

Looking at the spatio-temporal distribution of active faulting (Figure 9c) highlights a sudden switch from almost no deformation and no sediment deposition onto the keystone block (i.e., the future hyperextended domain), to increasingly localized deformation and significant syn-rift sedimentation limited

to the keystone area until the onset of proto-oceanic seafloor spreading. Keystone individualization (necking phase) is thus associated with extremely shallow water depth and/or emergence of the future hyperextended domain, which causes a lack of sediment deposition (uncovered basement shown by orange color in Figure 9c).

5.1.5. The proto-oceanic domain:

No exhumed mantle has been evidenced in northwest South China Sea, instead, a proto-oceanic domain is described by Larsen *et al.* (2018) and Chao *et al.* (2021). This domain is strongly deformed by high-angle normal faults and overlain by post-rift sediments (Figure 9b).

5.1.6. Summary and predictions:

When looking at the architecture of the main sedimentary package interfaces, we can see that the top of S4 is the base of post-tectonic sedimentation in the necking domains, while it lies within the syn-tectonic sequence in the hyperextended domains. Similarly, the top of S5 is post-tectonic in the necking and inner hyperextended domains, while it belongs to the syn-tectonic sequence further outboard. This indicates a migration of active deformation oceanward as extension progresses. The same trend can be observed in the study of Ren *et al.* (2018; their Fig. 9), where their T80 horizon is post-tectonic in the inner part of the margin and syn-tectonic in more distal domains.

Figure 9c highlights an abrupt switch in the spatio-temporal distribution of active deformation during rifting: deformation is first focused into two fault corridors on either side of an undeformed keystone block that remained at shallow water

depth, or even emerged. Then, deformation shifted “instantaneously” (< 1My) to an opposite situation where deformation was limited to the keystone and the fault corridors became inactive.

The evolution of the NW-South China Sea section described above is summarized in Figure 9d. It is consistent with our idealized model in that: (1) successive discrete deformation phases advanced oceanward as extension progressed; (2) the proximal domain is only structured by high-angle normal faults; (3) the necking domain of both margins display detachment faults that exhumed upper- to mid-crustal basement to the seafloor; (4) pre-tectonic deposits of same age as the necking phase are observed in the hyperextended domain of the northern margin; (5) an erosional unconformity of necking phase age is observed throughout the hyperextended domain of both margins; and (6) extension was achieved via detachment faults in the hyperextended domain of the lower-plate (southern) margin.

Relying on our model, we expect sediments of the necking TS (S2–S4 in Chao et al., 2021) in the hyperextended domain to display shallow water facies and include reworked pre-rift sediments. Deposits on either side of the keystone (necking domains) should display deeper sedimentary facies and be sourced from both the continent (siliciclastics) and from the eroded keystone (reworked pre- to syn-rift sediments).

We expect sediments of the hyperextension TS in both the necking and hyperextended domains to display rapidly deepening sedimentary facies, associated with both tectonic and thermal subsidence related to intense crustal thinning and thermal relaxation beneath the two domains. This hypothesis is supported by drill hole U1501 published by Larsen *et al.* (2018) and the tectono-stratigraphic analysis of the Liwan Basin further east by Zhang *et al.* (2019), both of which indicated a rapid deepening of sedimentary facies from shallow

marine to bathyal depths during the early Oligocene. This time corresponds to the early stages of hyperextension in Chao *et al.* (2021).

5.2. The Mid-Norwegian margin

5.2.1. Geological setting

Rifting between Norway and Greenland was achieved through complex and multistage extension that started during the late Paleozoic and resulted in lithospheric breakup during the Eocene (Péron-Pinvidic and Osmundsen, 2018, and references therein). At the Mid-Norwegian margin, a broadly distributed stretching phase took place discontinuously from Permian to Triassic time, following the Devonian–Carboniferous orogenic collapse of the Caledonian belt (Péron-Pinvidic and Osmundsen, 2018, and references therein). A first phase of localized deformation (the necking phase) started during the Late Jurassic (Tithonian) and ended in the Early Cretaceous (e.g., Brekke, 2000; Doré *et al.*, 1999; Planke *et al.*, 2000). Then, localized deformation stepped further outboard, creating detachment faults that possibly reached mantle exhumation in the Møre and Vøring basins during late Early- to Late Cretaceous (Osmundsen *et al.*, 2016). From the Late Cretaceous to final breakup, increasing magmatic activity occurred along the outermost margin and formed the so-called *outer highs* (Péron-Pinvidic and Osmundsen, 2018, and references therein).

The rift domains of the Mid-Norwegian margin were mapped by Péron-Pinvidic *et al.* (2013), who placed the termination of the proximal domain at the outer edge of the Trøndelag Platform (Figure 10a). In their view, the necking domain corresponds largely to the Halten Terrace and continues further south as a narrower domain. The Møre and Vøring basins (Figure 10a) belong to the

hyperextended (and possibly exhumed mantle) domain of the mid-Norwegian margin because they display a crustal thickness of less than 10 km (Funk *et al.* 2017). The nature of the seismic basement beneath these basins is the matter of much debate, especially about the proportion of pre-rift continental crust with respect to magmatic underplate, inherited Caledonian basement, altered continental crust and serpentinized mantle (e.g., Osmundsen *et al.*, 2016; Péron-Pinvidic and Osmundsen, 2018; Zastrozhnov *et al.*, 2020). The resolution is especially low in the outer part of the Møre and Vøring basins due to significant breakup-related magmatic additions.

The Norwegian margin benefited recently from a careful three-dimensional mapping of major tectonic structures by Osmundsen and Péron-Pinvidic (2018). These authors suggested that each rift domain is framed by laterally persistent tectonic structures that allow for significant changes in the margin architecture, which they termed *breakaway fault complexes*.

5.2.2. The calibrated proximal and necking domains

The tectono-stratigraphy of the Trøndelag Platform was recently reviewed by Péron-Pinvidic *et al.* (2020). These authors highlighted a complex extensional history following the post-orogenic collapse of the Caledonian belt. Extension was accommodated via both normal faulting and extensional reactivation of core complex structures inherited from the post-orogenic collapse. The Trøndelag Platform displays post-tectonic sedimentation from Late Triassic onward.

The necking domain width ranges between 20 and 80 km (Figure 10a). It is framed by two crustal-scale, *breakaway fault complexes*, namely the *inner*- and *outer necking breakaway complex* at its inner and outer edge, respectively (Figure 10b; Osmundsen and Péron-Pinvidic, 2018). Both necking breakaway

complexes are often composite structures in that they comprise both high-β (large fault heave) detachment faults and low-β (minor fault heave) normal faults.

The main fault of the inner necking breakaway complex roots within the ductile middle or lower crust and is related to an abrupt but moderate increase in accommodation (> 20 km of basement exhumation along dip overlain with ca. 2.5 km of Jurassic and Lower Cretaceous sediments in Figure 10b). From south to north along the Norwegian margin, the inner necking breakaway complex is represented by the Møre–Trøndelag, Vingleia, Bremstein, and Revfallet Fault Complexes (Figure 10a). The main fault of the outer necking breakaway complex cuts through the entire crust, down to the upper lithospheric mantle. It is usually associated with significant accommodation creation (> 20 km of basement exhumation along dip overlain with > 4 km of Lower Cretaceous sediments, in addition to the unknown thickness of Jurassic sediments in Figure 10b). From south to north along the Norwegian margin, it is represented by the Main Møre Boundary Fault and the Ytreholmen Fault Complex (Figure 10a). However, the three-dimensional architecture of the inner- and outer necking breakaway complexes is complicated since the two merge in places, so that the necking domain locally coincides with a unique breakaway fault complex. This is the case south of the Halten Terrace (i.e., the Klakk Fault Complex; Figure 10a).

The stratigraphy of the Norwegian necking domain often displays erosional truncations. For instance, at the outer edge of southern Halten Terrace, the Jurassic sequence on the inner side of both the Klakk (outer) and Vingleia (inner) Fault Complexes are deeply eroded before the deposition of deep-marine Lower Cretaceous sediments (e.g., Bell *et al.*, 2014, and references therein; Figure 10c). At the northern Halten Terrace, Breivik *et al.* (2010) and Osmundsen and Péron-Pinvidic (2018) interpreted erosion both at the

Ytreholmen (outer) and Revfallet (inner) Fault Complex. In the inner part of the Halten Terrace, Elliott *et al.* (2012) highlighted erosion at the Bremstein (inner) Fault Complex. South of the Halten Terrace, Osmundsen and Ebbing (2008) reported erosion along the Main Møre Fault (inner breakaway fault complex). In all cases, erosion is reckoned to be of latest Jurassic–earliest Cretaceous age, which corresponds to the end of the necking phase. The resulting unconformity is sealed by a regionally correlatable shale event of early Barremian age (Ian Sharp personal communication). The latest Jurassic–earliest Cretaceous unconformity can be linked to the so-called *Base Cretaceous Unconformity* or *BCU* that is widely recognized across the Norwegian margin (e.g., Brekke, 2000).

Early Jurassic deposits in the necking domain are syn-tectonic sediments dominated by shallow-marine sandstones (Faleide *et al.*, 2010). Late Jurassic sedimentary facies indicate rapid deepening, as shown by prevailing first shallow- and then deep-marine shales. The deepening sequence is interrupted by an episode of major uplift and erosion that affected the necking domain but not the inner part of the shallow-water proximal domain, dismissing the hypothesis of a thermally driven dynamic topography. Indeed, as the latter process involves uplift over several hundreds of kilometers (Campbell, 2005), dynamic topography in the necking domain would have necessarily generated erosion in the adjacent thick-crusted proximal domain, and thus shallow-water proximal domain.

5.2.3. The poorly calibrated hyperextended domain

In the hyperextended domain offshore the mid-Norwegian margin, the thickness of sedimentary deposits may be over 7 sTWT in the axial part of the Møre and

Vøring basins. Drill holes penetrate only as deep as the Late Cretaceous (e.g., Zastrozhnov *et al.*, 2020, and references therein). The base of the Cretaceous sequence is interpreted to be marked by a strong reflection, supposed to correspond to both an erosional hiatus and to the base of passive onlap in the proximal and necking domains (i.e., the *BCU* mentioned above). Underlying deposits are usually interpreted as undifferentiated pre-Cretaceous sediments. Basement is consensually interpreted as affected by a series of oceanward-dipping, in-sequence detachment faults (e.g., Abdelmalak *et al.*, 2017; Osmundsen *et al.*, 2002; Zastrozhnov *et al.*, 2020), which suggests that the mid-Norwegian margin is a lower-plate margin (e.g., Mosar *et al.*, 2002). This is further supported by the shorter along-dip width of the eastern-Greenland conjugate margin (e.g., Péron-Pinvidic *et al.*, 2013).

5.2.4. Summary and predictions

The evolution of the Norwegian margin is consistent with that of our idealized model in that: (1) it displays a sequential localization of deformation, starting with discontinuous Permo–Triassic extension distributed over at least the future proximal and necking domains, and probably also over the future hyperextended domain. Distributed deformation stopped in the Late Triassic and focused in the future necking domain during the Late Jurassic (i.e., necking phase); (2) The main structures allowing for crustal thinning (the *inner-* and *outer necking breakaway complexes* of Osmundsen and Péron-Pinvidic, 2018) are crustal-scale detachment faults, possibly associated with minor normal faults; (3) The necking phase was often associated with erosion at both the inner-and outer necking breakaway complexes; (4) the late stage of the necking phase was associated with an erosional unconformity (the *BCU*) that affected both the future necking domain, and at least the inner part of the hyperextended domain.

Based on our model, we interpret the BCU either as an unconformity that marks the erosion of the keystone block during the necking phase, comparable with the unconformity interpreted at the top of the necking TS in the South China Sea; or as a onlap surface marking the onset of rapid deepening of the hyperextended domain following extreme crustal thinning and/or the onset of thermal relaxation. In both cases, we expect that the overlying Early Cretaceous sediments display sedimentary facies testifying to a rapid deepening associated with the dismembering of the keystone block during hyperextension. This interpretation is supported by the massive thickness of Cretaceous deposits (locally > 7 km) in both the Møre and Vøring basins (Brekke, 2000; Faleide *et al.*, 2010). Besides, the pattern of subsidence–uplift/erosion–subsidence observed on the Halten Terrace (necking domain) can be compared to that of the Briançonnais domain and explained by a flexural rebound following early necking of the upper mantle with respect to the crust (Chenin *et al.*, 2019).

5.3. The southeastern margin of the Gulf of Aden: the Socotra region

5.3.1. Geological setting

Socotra Island is located at the eastern edge of the Gulf of Aden southern margin. The western part of the island was interpreted to expose part of a former necking domain, while its eastern part would correspond to the outer part of a proximal domain (Ahmed *et al.*, 2014; Nonn *et al.*, 2017). In between, Socotra Island is crossed by an ENE–WSW transfer zone (Hadibo Transfer Zone; HTZ on the map of Figure 11). Socotra is one of the rare places in the world where a necking domain and the outer part of a proximal domain crop out. Emergence of these regions, which usually lie in relatively deep-marine environments, is

related to a late-rift regional uplift (the *syn-OCT uplift* of Leroy *et al.*, 2012, and references therein, where *OCT* stands for *Ocean–Continent Transition*).

The oldest sediments recovered in Socotra are Early Triassic and Jurassic in the eastern part of the island, and Cretaceous in the west (Samuel *et al.*, 1997). These were deposited during a phase of discontinuous, broadly distributed extension (stretching phase) that lasted from the Permo-Triassic to the Eocene in the future Gulf of Aden region. Localized extension (necking) initiated during the Priabonian (ca. 34 Ma; Leroy *et al.*, 2012, and references therein). The timing of hyperextension is not constrained. The onset of seafloor spreading occurred during the Burdigalian (ca. 20 Ma in eastern Socotra; Fournier *et al.*, 2007) and was accompanied by regional uplift and significant erosion of both conjugate proximal margins (the *syn-OCT uplift* mentioned above).

5.3.2. The calibrated (onshore) proximal and inner necking domains

At Socotra, necking was associated with significant tectonic exhumation and denudation that removed the entire pre-rift sedimentary cover and part of the exposed basement both in the east and in the west of the island (Pik *et al.*, 2013) We note that this geometry is compatible with basement exhumation related to the activity of crustal-scale detachment faults (dotted blue lines on transects A–A' and C–C' of Figure 11). This episode of tectonic exhumation occurred earlier in the east (ca. 38 Ma) compared to the west (ca. 32 Ma; Pik *et al.*, 2013).

From late Priabonian to Rupelian time, sediments were deposited in graben-type depocenters displaying subsidence and progressive deepening adjacent to the detachment faults (Nonn *et al.*, 2017, and references therein). Subsidence climax was reached during Rupelian–Chattian time (deep-marine deposits).

1283 Then, a *syn-OCT uplift* brought Socotra Island to emergence (Leroy *et al.*, 2012,
1284 and references therein).

1285

1286 5.3.3. The uncalibrated (offshore) outer necking and hyperextended domains

1287 Offshore Socotra, Nonn *et al.* (2017) recognized usually two crustal-scale
1288 extensional faults that exhumed basement to the seafloor over several
1289 kilometers along dip (up to 10 km in transect B–B' in Figure 11). However, in
1290 easternmost Socotra, they recognized only one major detachment fault that
1291 exhumed basement over 13 km along dip.

1292 Further outboard, top basement deepens abruptly from ca. 2 km to 4 km below
1293 sea level over ca. 10 km. This morphostructural step is interpreted to mark the
1294 transition between the necking and hyperextended domain and can be regarded
1295 as a mega fault scarp (Nonn *et al.*, 2017; Ribes *et al.*, 2019a). The
1296 hyperextended domain is structured by a series of oceanward dipping
1297 detachment faults (transect B–B' and D–D' in Figure 11), which prompted Nonn
1298 *et al.* (2017) to interpret the Socotra margin as a lower plate. This hypothesis is
1299 consistent with their interpretation of a residual keystone and of continent-ward-
1300 dipping faults in the hyperextended domain of the conjugate (Oman) margin.

1301

1302 5.3.4. Summary and predictions

1303 The Socotra necking domain provides thermochronological data testifying to a
1304 phase of necking starting at ca. 34 Ma (Leroy *et al.*, 2012), which was
1305 accompanied with basement exhumation and emergence (Pik *et al.*, 2013) that
1306 presumably occurred along detachment faults. Stratigraphy indicates a rapid
1307 deepening of sedimentary deposits in adjacent depocenters. The climax of

subsidence rate was reached during the Rupelian–Chattian (ca. 28 Ma). Yet, according to our model, the highest subsidence rates in the necking domain occur during the hyperextension phase. In the case of Socotra, this would imply that the necking phase was relatively short (< 34 – 28, namely < 6 My).

The occurrence of a mega-fault scarp at the transition between the necking and hyperextended domain of a lower-plate margin is not expected in our idealized model. However, whether this mega-fault scarp formed during necking/hyperextension or corresponds to a late rift feature associated with the syn-OCT uplift of the proximal margin described by Leroy *et al.* (2012, and references therein) remains to be determined. That the Socotra margin is not an upper plate remains also to be confirmed.

Relying on our model, we expect that the presence of Priabonian (syn-necking) and older sediments in the hyperextended domain is limited to the top of the tilted blocks, and that they display shallow-water facies and possibly erosional unconformities. We expect the hyperextension phase to start during the Rupelian–Chattian and to be associated with a rapid increase in water depth, which would be recorded by sedimentary facies both on top and between the tilted blocks in the hyperextended domain.

6. Discussion

6.1. Tectono-stratigraphic model vs. reality: first-order trends and simplifications

As a generic template, our tectono-stratigraphic model is necessarily simplified with respect to the evolution of rift systems worldwide. Below, we discuss the relevance of our simplifications and the reliability of the first-order features we identified as characteristic of rift phases or domains.

6.1.1. The stretching phase

In our model, we consider that the stretching phase is achieved via broadly distributed, synchronous extension over the entire rift domains. Yet it has been proven that, for many rift systems and rifted margins, the stretching phase included several extension pulses that were offset in time and/or space (e.g., Alves *et al.*, 2002; Bosworth *et al.*, 2005; Péron-Pinvidic and Osmundsen, 2018; Sinclair, 1993). Due to the absence of localized deformation during the stretching phase, it is very difficult to distinguish stretching-related structures from those generated by orogenic collapse or far-field effects of other tectonic events. Conversely, the onset of the subsequent phase of localized deformation (i.e., necking) is relatively easy to identify.

Besides, the distribution of deformation during the stretching phase is largely controlled by inheritance (Manatschal *et al.*, 2015), and thus specific to each tectonic system. As our model aims to provide a template as general as possible to interpret the tectono-stratigraphic record of distal margins, it is sensible to limit our description of the stretching phase to a very first-order, considering that the detailed stretching evolution can only be unraveled on the basis of regional data.

6.1.2. The necking phase

6.1.2.1. Formation of a keystone

The formation of a keystone as part of the necking phase is predicted by both analogue and numerical models. It has also been suggested in the balanced kinematic restorations from Sutra *et al.* (2013) and Chao *et al.* (2021). Several field and seismic studies also provide good evidence for it (e.g., Haupert *et al.*, 2016, and references therein). It is, however, extremely difficult to prove the systematic formation of a keystone during

rifting since this phase is transient and the keystone is thought to be subsequently dismembered during hyperextension. One exception may be the Briançonnais domain which, because of its particular position between two overstepping en-échelon rift segments, may have "fossilized" the necking stage just prior to the reorganization of the segmented Alpine rift system into a unique rift basin, and preserved it during later Alpine convergence (Lescoutre and Manatschal, 2020; Manatschal *et al.*, 2021).

6.1.2.2. Formation of tens of kilometer-scale detachment faults

Although only rarely described until the last decade, a growing body of evidence suggests the existence of major detachment faults that would exhume basement over up to several tens of kilometers along dip (Chao *et al.*, 2021; Osmundsen and Péron-Pinvidic, 2018; Ribes *et al.*, 2020; Sutra and Manatschal, 2012). Reasons why such structures have been seldom identified so far may be: (1) the poor calibration of the necking domain because it lies in relatively deep-water settings in thermally equilibrated rifted margins; (2) our preconceived idea on rifted margins being formed of tilted blocks (Figure 12a); and (3) the difficulty to distinguish between the top of pre-rift basement and top of new real estate basement (i.e., basement exhumed to the seafloor via an extensional detachment fault). Further studies are needed to determine whether such structure represent the rule or the exception at rift systems/rifted margins.

6.1.3. The hyperextension phase: formation of upper- vs. lower plate margins

The formation of upper- vs. lower-plate margins at magma-poor rift systems is predicted by numerical modelling (Lavier and Manatschal, 2006; Peron-Pinvidic

and Naliboff, 2020) and supported by morphological observations (Haupert *et al.*, 2016; Nirrengarten *et al.*, 2016; Péron-Pinvidic *et al.*, 2015; Ranero and Pérez-Gussinyé, 2010; Sutra *et al.*, 2013). Note that flip in the polarity of upper- vs lower plate margins may occur across transform faults along strike of rift systems (Decarlis *et al.*, 2017).

Significant thermal weakening prior to/during the hyperextension phase may instead generate a symmetrical evolution (Buck, 1991). However, magma-rich/volcanic rift systems are not necessarily symmetrical and may go through a comparable early rift evolution as magma-poor ones (e.g., Eldholm *et al.*, 1995; Péron-Pinvidic *et al.*, 2013). Thus, whether magma-rich rift systems develop an upper- vs. lower-plate architecture remains to be determined.

6.1.4. The mantle exhumation phase: “symmetrical” pattern of detachment faulting

It is generally accepted that mantle exhumation is achieved via extensional detachment faulting, however the details of this process are difficult to unravel based on field observations and direct seismic imaging only. Several pieces of evidence suggest that mantle exhumation is achieved via flip-flop detachment faulting, rather than via a unique detachment fault, namely: (1) the fact that seafloor spreading initiates usually in the center of an exhumed mantle or proto-oceanic domain; (2) the relatively symmetrical pattern of magnetic anomalies over exhumed mantle with respect to the final seafloor spreading axis (Gillard *et al.*, 2016b, and references therein); (3) the symmetrical pattern of over-tilted sedimentary sequences in the exhumed mantle domain (Gillard *et al.*, 2016a, 2015).

6.2. Characteristics of rift systems

6.2.1. Spatial and temporal scaling of margin domains and rifting events

In Table 1, we summarize the duration of the rift phases, as well as the width of the rift domains for the examples presented above. We did not attempt to provide duration ranges for the stretching phase because it is a phase of diffuse deformation, and thus hard to distinguish from the "noise" generated by potential preceding orogenic collapse or far-field effects of adjacent tectonic events. In most examples, necking appears to have been achieved rapidly (< 10 My). One exception is the Norwegian rift system, for which a late Mid-Jurassic to latest Jurassic necking phase (ca. 25 My?; Table 1) is usually considered (Peron-Pinvidic and Osmundsen, 2018, and references therein). Yet the Norwegian rifting is often described as a succession of extension phases separated by tectonic pauses, rather than one continuous polyphase extensional event (see Fig. 20 in Zastrozhnov *et al.*, 2020). Short necking phase durations are consistent with numerical models by Chenin *et al.* (2020), which explore a wide range of crust and mantle rheologies and predict the duration of the necking phase to range between 3.3 for strong lithospheres and 8 My for weak lithospheres submitted to a bulk extension rate of 10^{-15} s^{-1}. The necking domain width of all examples above ranges from 20 to 100 km, consistent with the range observed by Chenin *et al.* (2017).

Hyperextension also appears to have been achieved rapidly in most examples (< 10 My). It may have taken longer at the Norwegian margin, however the transition between the phase of hyperextension and a potential phase of mantle exhumation is not constrained, which makes it a poorly calibrated example. The hyperextended domain widths of all examples above (from 25 to 60 km; Table 1) fall within the range observed by Chenin *et al.* (2017). Considering that the hyperextended domain is the domain that displays the smaller variability in width (Chenin *et al.*, 2017) and is characterized by relatively consistent angles of

aperture between top basement and Moho amongst rifted margins (Nirrengarten *et al.*, 2016), we can also expect the hyperextension phase to be relatively consistent among rifting events. This hypothesis needs however to be confirmed.

The duration of the mantle exhumation phase is poorly constrained from the examples presented above; however, we expect it to be highly variable given the variability of exhumed mantle domain widths reported by Chenin *et al.* (2017). At Socotra, the small width (ca. 10 km) of the exhumation domain reported by Nonn *et al.* (2017) falls below the range observed by Chenin *et al.* (2017). We can either conclude that the latter range is underestimated because mantle exhumation can occur over a very short period/distance; or that mantle may not have been exhumed at the Socotra margin, and thus that the domain between the hyperextended crust and first mature oceanic crust may rather be interpreted as a proto-oceanic domain like in the South China Sea. The latter interpretation may be supported by the presence of outer highs, which are regarded as magmatic extrusions by Nonn *et al.* (2017). The duration of mantle exhumation may be largely controlled by the capacity of underlying asthenosphere to produce magma (temperature, fertility, upwelling rate conditions), and thus the rapidity of steady-state seafloor spreading to take over, however these hypotheses need to be tested.

6.2.2. Spatio-temporal evolution of accommodation and related sedimentary facies

There are two ways to create accommodation, namely vertical deepening and horizontal widening. Accommodation space is more or less efficiently and rapidly filled with sediments depending on the ratio between sedimentation- vs. accommodation creation rate (Tugend *et al.*, 2014). In the following, we describe

the relative contribution of vertical vs horizontal accommodation creation in the different rift domains and provide insight into the likely evolution of depositional environment. For the sake of simplicity, we consider a sediment-rich, siliciclastic-dominated setting like in the NW-South China Sea, for which the tectonic history is efficiently captured by the sedimentary record and its relationship to tectonic structures (e.g., faults; Figure 12). Sediment-starved rift systems will be discussed in section 6.4.1.

6.2.2.1. The proximal domain

The proximal domain is well-calibrated by drilling, seismic imaging, and field data. The low heave and throw of normal faults and associated limited crustal thinning (continental crust remains usually > 25 km thick; Figure 3a) results in limited tectonic accommodation creation (grey curves in Figure 13a). Besides, minor lithospheric thinning beneath the proximal domain accounts for the lack of significant thermal subsidence.

The proximal domain is usually characterized by accommodation-limited settings during the entire rifting period, which means an excess of sediments with respect to the overall available accommodation space (Prosser, 1993). As a result, facies usually range between subaerial and shallow-marine *sensu lato*, while a significant part of sediments bypass the domain and feed more distal basinal areas. Most common sediments within proximal half-graben depocenters include siliciclastic, salt and/or carbonate platform deposits. Massive salt deposition may also characterize proximal domain depocenters, in particular in arid rift settings (Prosser, 1993).

6.2.2.2. The necking domain

The necking domain is characterized by both moderate horizontal widening (up to a few tens kilometers; e.g., Figure 8b2) due to the creation of new real estate via extensional detachment faults, and moderate- to high crustal (30–10 km) and lithospheric thinning (blue curves in Figure 13a). The necking stage is thought to display a largely undeformed keystone block between two crustal-scale necking faults (Figure 5c).

The tectono-stratigraphic evolution during the necking phase is complex and may vary among rift systems depending on the inherited rheological architecture of the involved lithosphere. In the early stages of necking, the necking domain remains in shallow water (e.g., Iberia margin; Mohn *et al.*, 2015, and references therein, mid-Norwegian margin; Faleide *et al.*, 2010, and references therein, northern North Sea; McLeod et al., 2002) or may even be locally and temporarily uplifted above sea level (e.g., Socotra margin; Pik *et al.*, 2013, Campos Basin; Lewis *et al.*, 2014, East-India margin; Haupert *et al.*, 2016, Mont Blanc; Ribes *et al.*, 2020, Porcupine Basin; Whiting *et al.*, 2020, NW-South China Sea; Chao *et al.* 2021). At this stage, the necking domain is confined and may still be accommodation-limited. Sediment deposits may include shallow-marine carbonates and/or shallow-marine- or terrestrial sandstones (e.g., Newfoundland margin; Wielens *et al.*, 2006, Norwegian margin; Faleide *et al.*, 2010, Porcupine Basin; Whiting *et al.*, 2020). Syn-necking sandstones are possibly derived from immediately adjacent exhumed basement domes/core complexes (e.g., the G*rès Singuliers* close to Mont Blanc; Ribes *et al.*, 2020). They may contrast with those deposited during the stretching TS, which are usually sourced from more regional sources.

Subsequently, when significant new real estate has been created and/or significant thermal subsidence has occurred and/or the flexural rebound of

the underlying lithospheric mantle has stopped, the necking domain may rapidly evolve into open-marine and sediment-limited settings (Figure 6c). Depositional environments evolve from continental and/or shallow-marine during the stretching and early necking TS, to deep marine/continental slope environments during the late necking/hyperextension and subsequent TS (e.g., shale deposition over the syn-necking shallow-water *Grès Singulier* in the Alpine necking domain, Ribes *et al.*, 2020; turbidites deposition over syn-necking (Tithonian) shallow-water deposits in the distal Iberian margin, Mohn *et al.*, 2015; Upper Jurassic deep-marine shales deposited over shallow marine sand-dominated Bathonian deposits and Callovian shallow-marine shales in the necking zone of the Norwegian margin, Faleide *et al.*, 2010 and Bell *et al.*, 2014, early Cretaceous shales in the Newfoundland necking domain, Wielens *et al.*, 2006; sediment starvation contemporaneous with strain localization at the Horda Platform in the North Sea; Tillmans *et al.*, 2021).

Note that the deposits of the stretching TS are partially dismembered an potentially tilted by syn-necking detachment and normal faults, whereas deposits of the late necking TS are continuous.

6.2.2.3. The hyperextended domain

The hyperextended domain is characterized by substantial horizontal widening, especially on the lower plate, due to the creation of new real estate via successive, in-sequence detachment faults (red curves in Figure 13a; see also Fig. 7 in Manatschal *et al.*, 2001, and Figs. 10c and 10d in Epin and Manatschal, 2018). It also displays extreme crustal thinning from ca. 10 to > 0 km (Figure 3a), which is accompanied by immediate tectonic

subsidence, and followed by significant thermal subsidence owing to major lithosphere thinning.

The hyperextended domains of conjugate margins correspond to the former keystone blocks that used to be framed by the two major necking faults during the necking phase (Lavier and Manatschal, 2006; Chao *et al.* 2021). At that time (necking TS), the keystone was at shallow water depths or even emerged (cf. previous section; Figure 6c). During the subsequent hyperextension phase, it was intensively delaminated via extensional detachment faults. As a result, both the stretching and necking TS are largely dismembered in the hyperextended domain (Figure 6b). From the late necking or early hyperextension TS onward, sediment deposits testify to a switch from an accommodation-limited to a sediment-limited environment, which is expressed by a rapid deepening of sedimentary facies up to deep-marine or abyssal conditions (Figure 6c; e.g., Masini *et al.*, 2011; Mohn *et al.*, 2015). The available accommodation during subsequent rift stages is thus essentially inherited from the unfilled accommodation created during hyperextension, and to a lesser extent due to lithosphere thermal relaxation.

The sediments of the late hyperextension TS are the first to be continuous along dip of the hyperextended domain.

6.2.2.4. The exhumed mantle domain

The exhumed mantle domain is characterized by extreme horizontal widening since this domain is entirely made of new real estate. When the distal rift basin is not isolated, mantle is exhumed in deep-marine or abyssal settings (e.g., Epin *et al.*, 2021; Steinmann, 1905) and is

subjected to significant thermal subsidence once it has moved away from the spreading center.

The first sediments deposited onto the exhumed mantle belong to the mantle exhumation TS (Figure 6a). Siliciclastic sedimentary sources may be lacking since the exhumed mantle domain is usually more than 100 km away from the emerged continent (Chenin *et al.*, 2017). Instead, deposition may be dominated by axial sedimentation (i.e., perpendicular to the margin dip-direction). Deposits may either arise from local gravitational reworking, turbidity or contour currents, pelagic sedimentation, or chemical precipitation (e.g., oversaturated SiO_2 rich fluids precipitating cherts), all of which usually characterize abyssal depositional environments (below the Carbonate Compensation Depth or *CCD*). Exceptions may occur at transform margins, where the exhumed mantle domain may be directly fed by the adjacent continent.

6.3. Projections and correlations from proximal to distal domains

6.3.1. New aspects of the interpretation of distal domains

Due to the significantly greater depth of the distal margin with respect to the proximal domain, the necking zone has for a long time represented an "interpretation frontier" between a well-calibrated domain continent-ward, and a much more enigmatic and largely inaccessible domain oceanward (Doran and Manatschal, 2017). The first attempts of distal margin interpretation naturally considered that observations made at the proximal domain can be transposed to the distal one (Figure 12a). Therefore, rift-related deformation was regarded as synchronous along the entire margin and achieved via planar high angle normal faulting between rigid tilted blocks (Waltham *et al.*, 1993). The understanding of

where, when and how deformation and sediments are distributed during rifting underwent a significant paradigm shift since the 1990's (Figure 12b). It is now generally acknowledged that rifting is a localizing process that focuses toward the locus of future lithospheric breakup (Pérez-Gussinyé *et al.*, 2020; Ribes *et al.*, 2019b; Whiting *et al.*, 2020; Luo *et al.*, 2021; Chao *et al.* 2021), and thus the base of post-tectonic deposits should be regarded as younging oceanward. Practically, (1) syn-tectonic sediments of the distal domain are likely to correspond (timewise) to post-tectonic deposits in the proximal domain; and (2) sediment deposits of early rift phases are going to be increasingly fragmented oceanward (Figure 12b).

6.3.2. Correlating timelines across rifted margins

In our tectono-stratigraphic model, we associated each of the successive deformation phases at play during rifting to one Tectonic Sequence (TS). A Tectonic Sequence encompasses all stratigraphic packages synchronous to the corresponding deformation phase, therefore the base and the top of each TS are by definition timelines along-dip of a given transect. Due to the polyphase and localizing nature of rifting, their correlation across the margin is difficult. Below we provide a set of characteristic timelines that may be generally recognized at rifted margins and discuss what the formerly defined *Rift Onset Unconformity* and *Breakup Unconformity* (Falvey, 1974) and *Necking Unconformity* (Chenin *et al.*, 2015) become in our new model.

6.3.2.1. The Base of the Syn-Rift megasequence vs. the Rift Onset Unconformity

In the mid-1970's, the onset of rifting was thought to be immediately preceded by a phase of large-scale (several hundreds of km)

doming/arching of the continental crust that produces widespread erosion in the future region of rifting and breakup (Falvey, 1974). By the late 1970's, such a phase of thermal doming/dynamic topography was thought to be characteristic of the onset of *active/volcanic rifting* only, while *passive/magma-poor rifting* was supposed to start with subsidence (Sengör and Burke, 1978), as predicted by the Pure-Shear Model of McKenzie (1978). More recently, Menzies *et al.* (2002) concluded that pre-rift dynamic topography was not systematic enough to be diagnostic of volcanic rifting. Dynamic topography produces a major unconformity over a wide domain (> 600 km; Campbell, 2005; Figure 13b). This unconformity can be used as a proxy for the Base Syn-Rift timeline (BSR in Figures 6, 12a and 12b) when the related doming precedes the stretching phase.

Whether or not initial doming takes place, the stretching phase is characterized by widely distributed normal faulting that forms numerous half-graben depocenters. In sediment-rich rift systems, the BSR corresponds within the basins to a shift from pre-tectonic to half-graben wedge-shaped deposits. Such a shift may be identifiable on both seismic sections and at the outcrop scale.

The formation of high-angle normal faults is often associated with the uplift of the corresponding footwall and local erosion of its crest (Yielding, 1990) over a width usually less than 5 km (Figure 13b). This erosional unconformity and its correlative conformities can be used as a proxy for the age of the BSR.

6.3.2.2. The Base of the Necking Tectonic Sequence vs. the Necking Unconformity

Chenin *et al.* (2015) defined the necking unconformity as the transition from syn- to post-tectonic deposits in the proximal domain (for sufficiently sediment-rich rift systems). In our model this “unconformity” corresponds to the timeline at the base of the necking TS (BNk in Figures 6 and 12a and 12b).

The “necking unconformity” is difficult to correlate across more distal domains. In the future necking and hyperextended domains, we notice that the necking phase is often associated with the formation of erosional unconformities. In the necking domain, erosion occurs at the breakaway of the necking fault (e.g., Norwegian margin; Bell *et al.*, 2014) and/or along upper- to mid-crustal basement exhumed by this fault (e.g., Mont Blanc; Ribes *et al.*, 2020). The new real estate created by activity on detachment faults corresponds also to a discordance since sedimentary deposits cannot be older than local basement exhumation age. Distinguishing between exhumed basement and eroded top basement may be difficult, especially because one does not exclude the other.

In-between the main necking fault systems, the keystone block (future hyperextended domains) seems to remain at shallow water depths during (part of) the necking phase, or to be even temporarily emergent. Illustrative examples include the early Jurassic karst of the Briançonnais (section 4.2.2; Claudel and Dumont, 1999), Tithonian offshore shelf deposits at the Iberian hyperextended domain (section 4.3.3; Mohn *et al.*, 2015, and references therein), lack of deposition in the central part of the northwestern South China sea (section 5.1.4 and Figure 9e; Chao *et al.* subm), shallow water deposits on the Halten Terrace at the mid-Norwegian margin (section 5.2.2; Bell *et al.*, 2014), and basement subaerial exhumation at the Socotra margin (section 5.3.2; Pik *et al.*, 2013). The

width of such necking-related uplift is of the order of a few tens of kilometers (Figure 13b; Chenin *et al.*, 2019, and references therein).

Thus, the necking phase may be associated with several unconformities and/or discordances in both the necking and hyperextended domains. Although these may not be synchronous, they are largely limited to the necking TS, which seems to usually encompass only a short period of time (section 6.2.1), and thus can be reasonably correlated with the “necking unconformity” of the proximal domain.

6.3.2.3. The Base of the Post-Rift megasequence vs. the Breakup Unconformity

Falvey (1974) suggested that continental breakup results in a rapid increase in the subsidence rate at the two conjugate margins. The resulting rapid marine transgression produces either a backstep of the onlapping sediments towards the continent when accommodation creation rate dominates over sedimentation rate at the coast, or a progressive onlap otherwise. In both cases it would produce an unconformity, often named the *Breakup Unconformity*. This hypothesis was supported by dynamic thermo-mechanical modelling (Braun and Beaumont, 1989). Although the existence of such discordance has been highlighted in several margins (e.g., Iberia–Newfoundland; Tucholke *et al.*, 2007, Santos Basin, Grand Banks and Beaufort Sea; Hubbard, 1988, Amerasian Basin; Embry and Dixon, 1990), its cause and synchronicity became debated from the 2000’s (e.g., Masini *et al.*, 2013; Wilson *et al.*, 2001). Gillard *et al.* (2015) highlighted that, in the exhumed mantle domain, each detachment fault was associated with a specific discordance, ruling out the existence of a unique *breakup unconformity* at the scale of an entire margin. More

recently, Pérez-Gussinyé *et al.* (2020) advocated, based on dynamical thermo-mechanical numerical modeling, that the “breakup unconformity” was restricted to the most distal part of the margin because lithospheric breakup is not associated with a sudden stress drop.

The Base of the Post-rift timeline (BPR in Figures 6, 12a and 12b) and onset of seafloor spreading are often difficult to define, either because of scattered and sporadic incipient magmatic activity in magma-poor rift systems (Bronner *et al.*, 2011; Epin *et al.*, 2019; Epin *et al.*, 2021; Jagoutz *et al.*, 2007), or because of excess magma prior to onset of steady-state seafloor spreading in magma-rich rift systems (Tugend et al., 2020). When the first-formed oceanic crust can be identified, the age of breakup corresponds to the age of the first overlying sediments in most sediment-rich rift systems (in sediment-starved systems the first overlying sediments provide only a minimum age). On seismic sections, the corresponding seismic reflection could theoretically be correlated across the entire margin. It may correspond to a discordance in the most distal part of the margin since it expresses the transition from syn- to post tectonic settings, however it is likely a conformable reflection in the proximal domain since deformation therein ceased earlier than the time of breakup. In the field, the BPR is practically impossible to identify based on geometrical criteria. In the past, it was considered to be marked by the biostratigraphic hiatus related to the backstep/progressive onlap mentioned above. However, given that breakup is not associated with a sudden stress drop in the proximal domain (Pérez-Gussinyé *et al.*, 2020), the contemporality between this paraconformity recorded in the proximal domain and the BPR is unlikely.

It is important not to automatically interpret unconformities at proximal margins as marking the BPR because numerous unconformities in the proximal domain may relate either to local tectonic events, or to large-scale, unrelated processes (e.g., climate, or far-field influence of a large-scale tectonic event). Indeed, as the top of the proximal domain remains at shallow depths due to its thick crust (30 ± 5 km) and the absence of significant lithospheric thinning, it may be very sensitive to eustatic changes (Prosser, 1993). Therefore, the timing of breakup cannot be accurately determined from seismic reflector relationship the proximal and necking domains.

6.4. Model limitations

The tectono-stratigraphic evolution presented in this contribution provides a powerful template to guide the seismic interpretation of distal margins and to unravel the complexity of rift systems exposed in orogens, where they are usually dismembered by thrust tectonics. However, as a model it remains a simplification, and thus it should not be used without taking the regional specificities of individual rift systems. Below we briefly review the main potential pitfalls to keep in mind when using this template:

6.4.1. Completeness and quality of the tectono-stratigraphic record

The efficient record of the tectono-stratigraphic evolution depends primarily on the ratio between sedimentation- and accommodation creation rate (e.g., Ravnås and Steel, 1998 and references therein; Martins-Neto and Catuneanu, 2010). A sediment-starved system will incompletely or even not record syn-tectonic deformation (Figure 14a; e.g., Barr, 1991). Note that the sedimentary budget available during rifting depends largely on the climate, in that humid

conditions favor increased erosion, and hence prolific sediment sources, conversely to arid climates that favor sediment starvation (Prosser, 1993).

The presence of pre- or syn-rift low frictional materials like salt and/or clay may also be a problem since they can induce deformation and accommodation creation not necessarily related to the rifting event itself (e.g., Rowan and Ratliff, 2012).

6.4.2. Presence of magmatic systems

The presence of magmatic systems may represent a difficulty because (1) magmatic crust may be hard to distinguish from pre-rift continental crust (Osmundsen et al., 2016; Tugend et al., 2020); (2) magmatic intrusions may perturb or overprint the tectono-sedimentary record, rendering its unravelling difficult (Zhang et al., 2021); and (3) magma-related heat may modify the rheology of the lithosphere involved, and thus lead to different deformation modes compared to magma-poor rifting; in particular, significant magmatic activity and related diking may trigger both crustal and lithospheric breakup before the continental crust was thinned to 0 km (Bialas et al., 2010; Ebinger and Casey, 2001; Sun et al., 2019). Otherwise, magmatic lava flows may behave comparably to sediments, and can thus be interpreted in a similar way (e.g., Chao et al., 2021)

6.4.3. The three-dimensional aspect of rift systems

Rift systems are often segmented by transform faults (Figure 14b1), especially during crustal thinning (necking and hyperextension; Nirrengarten *et al.*, 2018). Transform systems can separate segments with distinct margin architectures, as

exemplified by the differing domains width between the northern and central segment of the Iberia margin (Sutra and Manatschal, 2012) and between the southern (Møre), central (Vøring) and northern (Lofoten) segment of the mid-Norwegian margin (Péron-Pinvidic and Osmundsen, 2018). Transfer faults can also delimit segments with different timings of extension (e.g., the sequential northward propagation of crustal extension along the Iberian margin; Alves *et al.*, 2009, the sequential evolution along the Norwegian–Greenland conjugate margins; Gernigon *et al.*, 2020, or the westward younging of extension across the transform fault of the Socotra margin; Pik *et al.*, 2013). Therefore, the timing of necking, hyperextension and mantle exhumation, as well as the age of the various unconformities mentioned above, vary presumably from one segment to another (Nirrengarten *et al.*, 2018; Péron-Pinvidic *et al.*, 2013).

Individual faults have a limited extent along strike (Lescoutre and Manatschal, 2020; Lymer *et al.*, 2019; Nonn *et al.*, 2017; Péron-Pinvidic *et al.*, 2007) and major structures may change their tectonic role along the margin (e.g., local merging of breakaway complexes in Osmundsen and Péron-Pinvidic, 2018; Figure 10a).

The correlation of timelines is particularly tricky in propagating rift systems (e.g., the V-shaped South China Sea, Gulf of Aden, Bay of Biscay, Porcupine Basin, early stages of the southern North-Atlantic rifting, etc.; Nirrengarten *et al.*, 2018, and references therein; Luo *et al.*, 2021). Indeed, the migration of deformation toward both the rift center and the tip of the propagator renders timelines oblique to the conjugate margins (Figure 14b2).

6.4.4. Multistage rifting (out-of-sequence deformation)

Rifting may not always initiate on a thermally and gravitationally equilibrated lithosphere (Manatschal *et al.*, 2021; Zhang *et al.*, 2020) and/or the pre-rift sediments may display variable thicknesses inherited from previous tectonic events. In Western Europe, for instance, the Alpine Tethys rifting overprinted an area that was formerly affected by the Meliata-Vardar rifting, which is expressed by a thickening of the pre-Alpine Tethys rifting sedimentary sequence to the east (Manatschal *et al.*, this vol. and references therein). In Grand Banks, the Jeanne d'Arc stretching basin underwent post-Iberia–Newfoundland rifting extension related to the opening of the Orphan Basin (e.g., Skogseid, 2010). We refer to these spatially overprinting but temporally distinct extension phases as *multistage rifting* (Cadenas *et al.*, 2020). The consequence of multistage rifting may be the local incorporation and/or reactivation of older tectono-stratigraphic features into the ongoing rift system (Figure 14c). Examples include the Permian and Triassic basins incorporated in the Jurassic hyperextended domain of the Alpine rift system (Epin and Manatschal, 2018); and Jurassic salt-bearing basins in the Cretaceous hyperextended domain of the Basque-Cantabrian basin (Manatschal *et al.*, 2021; Miró *et al.*, 2021).

7. Conclusion

In this contribution, we propose a tectono-stratigraphic model describing the primary spatio-temporal evolution of active deformation during rifting. We show that the different rift domains of rifted margins are associated with specific (1) periods of tectonic activity; (2) styles of deformation and related tectono-stratigraphic architecture; (3) amounts of horizontal and vertical accommodation creation; and (4) depositional environments. We demonstrate that the sequential localization of extension during rifting results in both a younging of the base of passive infill and an increasing fragmentation of early rift-related

deposits oceanward. We propose a panel of Tectonic Sequences that may be correlated more or less easily and continuously across rifted margins. This model provides a new template to help correlate observations made at the well-calibrated and understood proximal domain with the more inaccessible and enigmatic distal domain. It highlights the necessity of jettisoning outdated dogma on rifted margins and changing our routines when interpreting seismic sections and correlating remnants of dismembered rifted margins exposed in orogens.

Acknowledgments: The authors are grateful to C.A.L. Jackson, I. Sharp, L. Whitting, and an anonymous reviewer for thorough, constructive and stimulating reviews that helped improving the manuscript. We also thank Editor K. Gallagher for handling both the present manuscript and its companion. The concepts presented in this work benefited from fruitful discussions with Garry Karner. M. Nirrengarten is acknowledged for providing the NW-SCS domain map shown in Figure 9a.

Author contributions:
Pauline Chenin: Writing – original draft, Conceptualization, Investigation
Gianreto Manatschal: Writing – review & editing, Conceptualization, Investigation, Funding acquisition
Jean-François Ghienne: Writing – review & editing, Conceptualization, Investigation
Peng Chao: Writing – review & editing, Conceptualization, Investigation

Data Availability Statement:
Data sharing is not applicable to this article as no new data were created or analyzed in this study.

REFERENCES

Abdelmalak, M.M., Faleide, J.I., Planke, S., Gernigon, L., Zastrozhnov, D., Shephard, G.E., Myklebust, R., 2017. The T-Reflection and the Deep Crustal Structure of the Vøring Margin, Offshore mid-Norway. Tectonics 36, 2497–2523. https://doi.org/10.1002/2017TC004617

Ahmed, A., Leroy, S., Keir, D., Korostelev, F., Khanbari, K., Rolandone, F., Stuart, G., Obrebski, M., 2014. Crustal structure of the Gulf of Aden southern margin: Evidence from receiver functions on Socotra Island (Yemen). Tectonophysics 637, 251–267. https://doi.org/10.1016/j.tecto.2014.10.014

Alves, T., Moita, C., Cunha, T., Ullnaess, M., Myklebust, R., Monteiro, J.H., Manuppella, G., 2009. Diachronous evolution of Late Jurassic–Cretaceous continental rifting in the northeast Atlantic (west Iberian margin). Tectonics 28, n/a-n/a. https://doi.org/10.1029/2008TC002337

Alves, T.M., Gawthorpe, R.L., Hunt, D.W., Monteiro, J.H., 2003. Post-Jurassic tectono-sedimentary evolution of the Northern Lusitanian Basin (western Iberian margin). Basin Res. 15, 227–249. https://doi.org/10.1046/j.1365-2117.2003.00202.x

Alves, T.M., Gawthorpe, R.L., Hunt, D.W., Monteiro, J.H., 2002. Jurassic tectono-sedimentary evolution of the Northern Lusitanian Basin (offshore Portugal). Mar. Pet. Geol. 19, 727–754. https://doi.org/10.1016/S0264-8172(02)00036-3

Alves, T.M., Moita, C., Sandnes, F., Cunha, T., Monteiro, J.H., Pinheiro, L.M., 2006. Mesozoic-Cenozoic evolution of North Atlantic continental-slope basins: The Peniche basin, western Iberian margin. Am. Assoc. Pet. Geol. Bull. 90, 31–60. https://doi.org/10.1306/08110504138

Andersen, T.B., Corfu, F., Labrousse, L., Osmundsen, P.-T., 2012. Evidence for hyperextension along the pre-Caledonian margin of Baltica. J. Geol. Soc. London. 169, 601–612. https://doi.org/10.1144/0016-76492012-011

Angrand, P., Mouthereau, F., Masini, E., Asti, R., 2020. A reconstruction of Iberia accounting for Western Tethys-North Atlantic kinematics since the late-Permian-Triassic. Solid Earth 11, 1313–1332. https://doi.org/10.5194/se-11-1313-2020

Argand, E., 1916. Sur l'arc des Alpes occidentales. Bridel, G.

Aubouin, J., 1965. Geosynclines. Elsevier Publishing Company, Amsterdam - London - New York.

Barr, D., 1991. Subsidence and sedimentation in semi-starved half-graben: A model based on North Sea data. Geol. Soc. Spec. Publ. 56, 17–28. https://doi.org/10.1144/GSL.SP.1991.056.01.02

Barr, D., 1987. Structural/stratigraphic models for extensional basins of half-graben type. J. Struct. Geol. 9, 491–500. https://doi.org/10.1016/0191-8141(87)90124-6

Bell, R.E., Jackson, C.A.L., Elliott, G.M., Gawthorpe, R.L., Sharp, I.R., Michelsen, L., 2014. Insights into the development of major rift-related unconformities from geologically constrained subsidence modelling: Halten Terrace, offshore mid Norway. Basin Res. 26, 203–224. https://doi.org/10.1111/bre.12049

Beltrando, M., Stockli, D.F., Decarlis, A., Manatschal, G., 2015. A crustal-scale view at rift localization along the fossil Adriatic margin of the Alpine Tethys preserved in NW Italy. Tectonics 34, 1927–1951. https://doi.org/10.1002/2015TC003973

Bernoulli, D., 1964. Zur Geologie des Monte Generoso (Lombardische Alpen): ein Beitrag zur Kenntnis der südalpinen Sedimente.

Bertotti, G., Picotti, V., Bernoulli, D., Castellarin, A., 1993. From rifting to drifting: tectonic evolution of the South-Alpine upper crust from the Triassic to the Early Cretaceous. Sediment. Geol. 86, 53–76. https://doi.org/10.1016/0037-0738(93)90133-P

Bialas, R.W., Buck, W.R., Qin, R., 2010. How much magma is required to rift a continent? Earth Planet. Sci. Lett. 292, 68–78. https://doi.org/10.1016/J.EPSL.2010.01.021

Boillot, G., Winterer, E.L., 1988. Drilling on the Galicia margin: retrospect and prospect 1, Scientific

Results.

Bond, G.C., Kominz, M.A., 1988. Evolution of thought on passive continental margins from the origin of geosynclinal theory (~1860) to the present. Bull. Geol. Soc. Am. 100, 1909–1933. https://doi.org/10.1130/0016-7606(1988)100<1909:EOTOPC>2.3.CO;2

Bosworth, W., Huchon, P., McClay, K., 2005. The Red Sea and Gulf of Aden Basins. J. African Earth Sci. 43, 334–378. https://doi.org/10.1016/j.jafrearsci.2005.07.020

Braun, J., Beaumont, C., 1989. A physical explanation of the relation between flank uplifts and the breakup unconformity at rifted continental margins. Geology 17, 760–764. https://doi.org/10.1130/0091-7613(1989)017<0760:APEOTR>2.3.CO

Breivik, A., Mjelde, R., Raum, T., 2010. Crustal structure beneath the Trøndelag Platform and adjacent areas of the Mid-Norwegian margin, as derived from wide-angle seismic and potential field data. Nor. J. Gology 90, 141–161.

Brekke, H., 2000. The tectonic evolution of the Norwegian Sea continental margin, with emphasis on the Voring and More basins. Spec. Publ. Soc. London 167, 327–378.

Bronner, A., Sauter, D., Manatschal, G., Péron-Pinvidic, G., Munschy, M., 2011. Magmatic breakup as an explanation for magnetic anomalies at magma-poor rifted margins. Nat. Geosci. 4, 549–553.

Brune, S., Heine, C., Pérez-Gussinyé, M., Sobolev, S. V, 2014. Rift migration explains continental margin asymmetry and crustal hyper-extension. Nat. Commun. 5, 4014. https://doi.org/10.1038/ncomms5014

Buchanan, P.G., McClay, K.R., 1991. Sandbox experiments of inverted listric and planar fault systems. Tectonophysics 188, 97–115. https://doi.org/10.1016/0040-1951(91)90317-L

Buck, W.R., 1991. Modes of continental lithospheric extension. J. Geophys. Res. 96, 20,161-20,178.

Cadenas, P., Manatschal, G., Fernández-Viejo, G., 2020. Unravelling the architecture and evolution of the inverted multi-stage North Iberian-Bay of Biscay rift. Gondwana Res. 88, 67–87. https://doi.org/10.1016/j.gr.2020.06.026

Cameselle, A.L., Ranero, C.R., Franke, D., Barckhausen, U., 2017. The continent-ocean transition on the northwestern South China Sea. Basin Res. 29, 73–95. https://doi.org/10.1111/bre.12137

Campbell, I.H., 2005. Large Igneous Provinces and the Mantle Plume Hypothesis. Elements 1, 265–269. https://doi.org/10.2113/gselements.1.5.265

Causer, A., Pérez-Díaz, L., Adam, J., Eagles, G., 2020. Uncertainties in break-up markers along the Iberia-Newfoundland margins illustrated by new seismic data. Solid Earth 11, 397–417. https://doi.org/10.5194/se-11-397-2020

Chao, P., Manatschal, G., Chenin, P., Ren, J., Zhang, C., Pang, X., Zheng, J., Yang, L., Kusznir, N.J., 2021. The tectono-stratigraphic and magmatic evolution of conjugate rifted margins: insights from the NW South China Sea. J. Geodyn.

Chenin, P., Manatschal, G., Decarlis, A., Schmalholz, S.M., Duretz, T., Beltrando, M., 2019. Emersion of distal domains in advanced stages of continental rifting explained by asynchronous crust and mantle necking. Geochemistry, Geophys. Geosystems 20, 2019GC008357. https://doi.org/10.1029/2019GC008357

Chenin, P., Manatschal, G., Lavier, L.L., Erratt, D., 2015. Assessing the impact of orogenic inheritance on the architecture, timing and magmatic budget of the North Atlantic rift system: a mapping approach. J. Geol. Soc. London. 172, 711–720. https://doi.org/10.1144/jgs2014-139

Chenin, P., Manatschal, G., Picazo, S., Müntener, O., Karner, G.D., Johnson, C., Ulrich, M., 2017. Influence of the architecture of magma-poor hyperextended rifted margins on orogens produced by the closure of narrow versus wide oceans. Geosphere 13, 1–18. https://doi.org/10.1130/GES01363.1

Chenin, P., Schmalholz, S.M., Manatschal, G., Duretz, T., 2020. Impact of crust–mantle mechanical coupling on the topographic and thermal evolutions during the necking phase of ‘magma-poor’

and ‘sediment-starved’ rift systems: A numerical modeling study. Tectonophysics 228472. https://doi.org/10.1016/j.tecto.2020.228472

Chenin, P., Schmalholz, S.M., Manatschal, G., Karner, G.D., 2018. Necking of the lithosphere: A reappraisal of basic concepts with thermo-mechanical numerical modeling. J. Geophys. Res. Solid Earth 123, 5279–5299. https://doi.org/10.1029/2017JB014155

Chester, F.M., Logan, J.M., 1986. Implications for mechanical properties of brittle faults from observations of the Punchbowl fault zone, California. Pure Appl. Geophys. PAGEOPH 124, 79–106. https://doi.org/10.1007/BF00875720

Chevalier, F., 2002. Vitesse et cyclicité de fonctionnement des failles normales de rift: implication sur le remplissage stratigraphique des bassins et sur les modalités d’extension d’une marge passive fossile: aplication au demi-graben liasique de Bourg d’Oisans (Alpes occid. Université de Bourgogne.

Claudel, M.E., Dumont, T., 1999. A record of multistage continental break-up on the Briançonnais marginal plateau (Western Alps): Early and Middle-Late Jurassic rifting. Eclogae Geol. Helv. 92, 45–61.

Clerc, C., Ringenbach, J.C., Jolivet, L., Ballard, J.F., 2018. Rifted margins: Ductile deformation, boudinage, continentward-dipping normal faults and the role of the weak lower crust. Gondwana Res. 53, 20–40. https://doi.org/10.1016/j.gr.2017.04.030

CNLOPB, C.-N.-L.O.P.B., 2010. Jeanne d’Arc Basin lithostratigraphy [WWW Document]. URL https://www.cnlopb.ca/wp-content/uploads/maps/xdb_lith.pdf%0A

Collettini, C., 2011. The mechanical paradox of low-angle normal faults: Current understanding and open questions. Tectonophysics. https://doi.org/10.1016/j.tecto.2011.07.015

Coltat, R., Boulvais, P., Branquet, Y., Collot, J., Epin, M.E., Manatschal, G., 2019. Syntectonic carbonation during synmagmatic mantle exhumation at an ocean-continent transition. Geology 47, 183–186. https://doi.org/10.1130/G45530.1

Conti, P., Manatschal, G., Pfister, M., 1994. Synrift sedimentation, Jurassic and Alpine tectonics in the central Ortler nappe (Eastern Alps, Italy). Eclogae Geol. Helv. 87, 63–90.

Dana, J.D., 1873. On some results of the Earth’s contraction from cooling including a discussion of the origin of mountains and the nature of the Earth’s interior. Am. J. Sci. 3, 423–443.

De Graciansky, P.C., Roberts, D.G., Tricart, P., 2011. The Western Alps, from rift to passive margin to orogenic belt: an integrated geoscience overview, Developments in Earth Surface Processes 14. Elsevier.

Decandia, F.A., Elter, P., 1972. La “zona” ofiolitifera del Bracco nel settore compreso fra Levento e la Val Graveglia (Appenino ligure). Mem. Soc. Geol. Ital. 11, 503–530.

Decandia, F.A., Elter, P., 1969. Riflessioni sul problema delle ofioliti nell’Appennino settentrionale (nota preliminare). Atti della Soc. Toscana di Sci. Nat.

Decarlis, A., Beltrando, M., Manatschal, G., Ferrando, S., Carosi, R., 2017. Architecture of the Distal Piedmont-Ligurian Rifted Margin in NW Italy: Hints for a Flip of the Rift System Polarity. Tectonics 36, 2388–2406. https://doi.org/10.1002/2017TC004561

Deemer, S., Hall, J., Solvason, K., Lau, K.W.H., Louden, K., Srivastava, S., Sibuet, J.C., 2009. Structure and development of the southeast Newfoundland continental passive margin: Derived from SCREECH Transect 3. Geophys. J. Int. 178, 1004–1020. https://doi.org/10.1111/j.1365-246X.2009.04162.x

Desmurs, L., Müntener, O., Manatschal, G., 2002. Onset of magmatic accretion within a magma-poor rifted margin: a case study from the Platta ocean-continent transition, eastern Switzerland. Contrib. to Mineral. Petrol. 144, 365–382. https://doi.org/10.1007/s00410-002-0403-4

Doran, H., Manatschal, G., 2017. Breaking up is never easy: The complexities that create opportunities in the distal domain. GeoExPro 58–61.

Doré, A.G., Lundin, E.R., Jensen, L.N., Birkelan, Ø., Eliassen, P.E., Fichler, C., 1999. Principal tectonic events in the evolution of the northwest European Atlantic margin, in: Fleet, A.J., Boldy, S.A.R. (Eds.), Petroleum Geology of Northwest Europe: Proceedings of the 5th Conference. The Geological Society, London, pp. 41–61.

Dumont, T., Champagnac, J.D., Crouzet, C., Rochat, P., 2008. Multistage shortening in the Dauphiné zone (French Alps): The record of Alpine collision and implications for pre-Alpine restoration, in: Swiss Journal of Geosciences. SpringerOpen, pp. 89–110. https://doi.org/10.1007/s00015-008-1280-2

Duretz, T., Asti, R., Lagabrielle, Y., Brun, J.P., Jourdon, A., Clerc, C., Corre, B., 2019. Numerical modelling of Cretaceous Pyrenean Rifting: The interaction between mantle exhumation and syn-rift salt tectonics. Basin Res. 32, 0–1. https://doi.org/10.1111/bre.12389

Eberli, G.P., 1988. The evolution of the southern continental margin of the Jurassic Tethys Ocen as recorded in the Allgäu Formation of the Austroalpine Nappes of Graubünden (Switzerland). Eclogae Geol. Helv. 81, 175--214.

Ebinger, C.J., Casey, M., 2001. Continental breakup in magmatic provinces: An Ethiopian example. Geology 29, 530.

Eldholm, O., Skogseid, J., Planke, S., Gladczenko, T.P., 1995. Volcanic margin concepts, in: Banda, E., Torné, M., Talwani, M. (Eds.), Rifted Ocean-Continent Boundaries. Springer, Dordrecht, pp. 1–16. https://doi.org/10.1007/978-94-011-0043-4_1

Elliott, G.M., Wilson, P., Jackson, C.A. -L., Gawthorpe, R.L., Michelsen, L., Sharp, I.R., 2012. The linkage between fault throw and footwall scarp erosion patterns: an example from the Bremstein Fault Complex, offshore Mid-Norway. Basin Res. 24, 180–197. https://doi.org/10.1111/J.1365-2117.2011.00524.X

Embry, A.F., Dixon, J., 1990. The breakup unconformity of the Amerasia Basin, Arctic Ocean: evidence from Arctic Canada. Geol. Soc. Am. Bull. 102, 1526–1534. https://doi.org/10.1130/0016-7606(1990)102<1526:TBUOTA>2.3.CO;2

Enachescu, M.E., 1987. Tectonic and Structural Framework of the Northeast Newfoundland Continental Margin, in: Sedimentary Basins and Basin-Forming Mechanisms — Memoir 12. CSPG Special Publications, pp. 117–146.

Epin, M.-E., Manatschal, G., Amann, M., Ribes, C., Clausse, A., Guffon, T., Lescanne, M., 2019. Polyphase tectono-magmatic evolution during mantle exhumation in an ultra-distal, magma-poor rift domain: example of the fossil Platta ophiolite, SE Switzerland. Int. J. Earth Sci. https://doi.org/10.1007/s00531-019-01772-0

Epin, M.-E., Manatschal, G., Sapin, F., Rowan, M.G., 2021. The tectono-magmatic and subsidence evolution during lithospheric breakup in a salt-rich rifted margin: Insights from a 3D seismic survey from southern Gabon. Mar. Pet. Geol. 128, 105005. https://doi.org/10.1016/j.marpetgeo.2021.105005

Epin, M.E., Manatschal, G., 2018. Three-dimensional architecture, structural evolution, and role of inheritance controlling detachment faulting at a hyperextended distal margin: the example of the Err detachment system (SE Switzerland). Tectonics 37, 4494–4514. https://doi.org/10.1029/2018TC005125

Epin, M.E., Manatschal, G., Amann, M., 2017. Defining diagnostic criteria to describe the role of rift inheritance in collisional orogens: the case of the Err-Platta nappes (Switzerland). Swiss J. Geosci. 110, 419–438. https://doi.org/10.1007/s00015-017-0271-6

Faleide, J.I., Bjorlykke, K., Gabrielsen, R.H., 2010. Geology of the norwegian continental shelf, in: Petroleum Geoscience: From Sedimentary Environments to Rock Physics. Springer Berlin Heidelberg, pp. 467–499. https://doi.org/10.1007/978-3-642-02332-3_22

Falvey, D.A., 1974. The development of continental margins in Plate Tectonics theory. APPEA J. 14, 95. https://doi.org/10.1071/aj73012

Fletcher, R.C., Hallet, B., 1983. Unstable extension of the lithosphere: A mechanical model for Basin-

and-Range structure. J. Geophys. Res. 88, 7457. https://doi.org/10.1029/JB088iB09p07457

Fournier, M., Huchon, P., Khanbari, K., Leroy, S., 2007. Segmentation and along-strike asymmetry of the passive margin in Socotra, eastern Gulf of Aden: Are they controlled by detachment faults? Geochemistry, Geophys. Geosystems 8, n/a-n/a. https://doi.org/10.1029/2006GC001526

Froitzheim, N., Eberli, G.P., 1990. Extensional detachment faulting in the evolution of a Tethys passive continental margin, Eastern Alps, Switzerland. Geol. Soc. Am. Bull. 102, 1297–1308. https://doi.org/10.1130/0016-7606(1990)102

Gao, J., Wu, S., McIntosh, K., Mi, L., Liu, Z., Spence, G., 2016. Crustal structure and extension mode in the northwestern margin of the South China Sea. Geochemistry, Geophys. Geosystems 17, 2143–2167. https://doi.org/10.1002/2016GC006247

Gawthorpe, R.L., Fraser, A.J., Collier, R.E.L., 1994. Sequence stratigraphy in active extensional basins: implications for the interpretation of ancient basin-fills. Mar. Pet. Geol. 11, 642–658. https://doi.org/10.1016/0264-8172(94)90021-3

Gawthorpe, R.L., Leeder, M.R., 2000. Tectono-sedimentary evolution of active extensional basins. Basin Res. 12, 195–218. https://doi.org/10.1111/j.1365-2117.2000.00121.x

Gawthorpe, R.L., Leeder, M.R., Kranis, H., Skourtsos, E., Andrews, J.E., Henstra, G.A., Mack, G.H., Muravchik, M., Turner, J.A., Stamatakis, M., 2018. Tectono-sedimentary evolution of the Plio-Pleistocene Corinth rift, Greece. Basin Res. 30, 448–479. https://doi.org/10.1111/bre.12260

Gee, J.S., Kent, D. V., 2007. Source of oceanic magnetic anomalies and the geomagnetic polarity time scale. https://doi.org/10.7916/D8DV1V8P

Gernigon, L., Franke, D., Geoffroy, L., Schiffer, C., Foulger, G.R., Stoker, M., 2020. Crustal fragmentation, magmatism, and the diachronous opening of the Norwegian-Greenland Sea. Earth-Science Rev. https://doi.org/10.1016/j.earscirev.2019.04.011

Gillard, M., Autin, J., Manatschal, G., 2016a. Fault systems at hyper-extended rifted margins and embryonic oceanic crust: Structural style, evolution and relation to magma. Mar. Pet. Geol. 76, 51–67. https://doi.org/10.1016/j.marpetgeo.2016.05.013

Gillard, M., Autin, J., Manatschal, G., Sauter, D., Munschy, M., Schaming, M., 2015. Tectonomagmatic evolution of the final stages of rifting along the deep conjugate Australian-Antarctic magma-poor rifted margins: Constraints from seismic observations. Tectonics 34, 753–783. https://doi.org/10.1002/2015TC003850.Received

Gillard, M., Manatschal, G., Autin, J., 2016b. How can asymmetric detachment faults generate symmetric Ocean Continent Transitions? Terra Nov. 28, 27–34. https://doi.org/10.1111/ter.12183

Hall, J., 1859. Description and Figures of the Organic Remains of the Lower Helderberg Group and Orinskany Sandstone. Natural History of New-York, Paleontology. Geol. Surv. N.Y., Albany.

Hardy, S., 1993. Numerical modelling of the response to variable stretching rate of a domino fault block system. Mar. Pet. Geol. 10, 145–152. https://doi.org/10.1016/0264-8172(93)90019-O

Haug, E., 1900. Les géosynclinaux et les aires continentales: contribution à l'étude des transgressions et des regressions marines. Au siège de la Société géologique de France.

Haupert, I., Manatschal, G., Decarlis, A., Unternehr, P., 2016. Upper-plate magma-poor rifted margins: stratigraphic architecture and structural evolution. Mar. Pet. Geol. 69, 241–261. https://doi.org/10.1016/j.marpetgeo.2015.10.020

Hopper, J.R., Funck, T., Tucholke, B.E., Louden, K.E., Holbrook, W.S., Larsen, H.C., 2006. A deep seismic investigation of the Flemish Cap margin: Implications for the origin of deep reflectivity and evidence for asymmetric break-up between Newfoundland and Iberia. Geophys. J. Int. 164, 501–515. https://doi.org/10.1111/j.1365-246X.2006.02800.x

Hubbard, R.J., 1988. Age and significance of sequence boundaries on Jurassic and Early Cretaceous rifted continental margins. Am. Assoc. Pet. Geol. Bull. 72, 49–72. https://doi.org/10.1306/703c81c8-1707-11d7-8645000102c1865d

2096 Huismans, R., Beaumont, C., 2011. Depth-dependent extension, two-stage breakup and cratonic
2097 underplating at rifted margins. Nature 473, 74–78. https://doi.org/10.1038/nature09988

2098 Jagoutz, O., Müntener, O., Manatschal, G., Rubatto, D., Péron-Pinvidic, G., Turrin, B.D., Villa, I.M.,
2099 2007. The rift-to-drift transition in the North Atlantic: A stuttering start of the MORB machine?
2100 Geology 35, 1087–1090. https://doi.org/10.1130/G23613A.1

2101 Jarvis, G.T., McKenzie, D.P., 1980. Sedimentary basin formation with finite extension rates. Earth
2102 Planet. Sci. Lett. 48, 42–52. https://doi.org/10.1016/0012-821X(80)90168-5

2103 Jourdon, A., Le Pourhiet, L., Mouthereau, F., May, D., 2020. Modes of Propagation of Continental
2104 Breakup and Associated Oblique Rift Structures. J. Geophys. Res. Solid Earth 125,
2105 e2020JB019906. https://doi.org/10.1029/2020JB019906

2106 Karner, G.D., Shillington, D.J., 2005. Basalt sills of the U reflector, Newfoundland basin: A
2107 serendipitous dating technique. Geology 33, 985–988. https://doi.org/10.1130/G21971.1

2108 Kay, M., 1951. North American geosynclines. Geological Society of America.

2109 Kober, L., 1923. Bau und Entstehung der Alpen. Berlin.

2110 Krawczyk, C.M., Reston, T.J., Boillot, G., Beslier, M.-O., 1996. Evidence for detachment tectonics on
2111 the Iberia Abyssal Plain rifted margin, Proceedings of the Ocean Drilling Program: Scientific
2112 Results.

2113 Kusznir, N.J., Ziegler, P.A., 1992. The mechanics of continental extension and sedimentary basin
2114 formation: A simple-shear/pure-shear flexural cantilever model. Tectonophysics 215, 117–131.
2115 https://doi.org/10.1016/0040-1951(92)90077-J

2116 Larsen, H.C., Mohn, G., Nirrengarten, M., Sun, Z., Stock, J., Jian, Z., Klaus, A., Alvarez-Zarikian, C.A.,
2117 Boaga, J., Bowden, S.A., Briais, A., Chen, Y., Cukur, D., Dadd, K., Ding, W., Dorais, M., Ferré,
2118 E.C., Ferreira, F., Furusawa, A., Gewecke, A., Hinojosa, J., Höfig, T.W., Hsiung, K.H., Huang, B.,
2119 Huang, E., Huang, X.L., Jiang, S., Jin, H., Johnson, B.G., Kurzawski, R.M., Lei, C., Li, B., Li, L.,
2120 Li, Y., Lin, J., Liu, C., Liu, C., Liu, Z., Luna, A.J., Lupi, C., McCarthy, A., Ningthoujam, L., Osono,
2121 N., Peate, D.W., Persaud, P., Qiu, N., Robinson, C., Satolli, S., Sauermilch, I., Schindlbeck, J.C.,
2122 Skinner, S., Straub, S., Su, X., Su, C., Tian, L., van der Zwan, F.M., Wan, S., Wu, H., Xiang, R.,
2123 Yadav, R., Yi, L., Yu, P.S., Zhang, C., Zhang, J., Zhang, Y., Zhao, N., Zhong, G., Zhong, L.,
2124 2018. Rapid transition from continental breakup to igneous oceanic crust in the South China Sea.
2125 Nat. Geosci. 11, 782–789. https://doi.org/10.1038/s41561-018-0198-1

2126 Lavier, L.L., Manatschal, G., 2006. A mechanism to thin the continental lithosphere at magma-poor
2127 margins. Nature 440, 324–328. https://doi.org/10.1038/nature04608

2128 Le Breton, E., Brune, S., Ustaszewski, K., Zahirovic, S., Seton, M., Müller, R.D., 2020. Kinematics and
2129 extent of the Piemont-Liguria Basin – implications for subduction processes in the Alps. Solid
2130 Earth Discuss. 1–42. https://doi.org/10.5194/se-2020-161

2131 Leeder, M.R., Gawthorpe, R.L., 1987. Sedimentary models for extensional tilt-block/half-graben
2132 basins, in: Coward, M.P., Dewey, J.F., Hancock, P.L. (Eds.), Continental Extensional Tectonics.
2133 Geological Society of London, Special publications No. 28, pp. 139–152.
2134 https://doi.org/10.1144/gsl.sp.1987.028.01.11

2135 Leleu, S., Hartley, A.J., van Oosterhout, C., Kennan, L., Ruckwied, K., Gerdes, K., 2016. Structural,
2136 stratigraphic and sedimentological characterisation of a wide rift system: The Triassic rift system
2137 of the Central Atlantic Domain. Earth-Science Rev.
2138 https://doi.org/10.1016/j.earscirev.2016.03.008

2139 Lemoine, M., 1985. Structuration jurassique des Alpes occidentales et palinspastique de la Tethys
2140 ligure. Bull. la Soc. Geol. Fr. 8, 126--137.

2141 Lemoine, M., Bas, T., Arnaud-Vanneau, A., Arnaud, H., Dumont, T., Gidon, M., Bourbon, M., de
2142 Graciansky, P.C., Rudkiewicz, J.L., Megard-Galli, J., Tricart, P., 1986. The continental margin of
2143 the Mesozoic Tethys in the Western Alps. Mar. Pet. Geol. 3, 179–199.
2144 https://doi.org/10.1016/0264-8172(86)90044-9

Lemoine, M., Tricart, P., Boillot, G., 1987. Ultramafic and gabbroic ocean floor of the Ligurian Tethys (Alps, Corsica, Apennines): In search of a genetic imodel. Geology 15, 622–625. https://doi.org/10.1130/0091-7613(1987)15

Leroy, S., Razin, P., Autin, J., Bache, F., d'Acremont, E., Watremez, L., Robinet, J., Baurion, C., Denèle, Y., Bellahsen, N., Lucazeau, F., Rolandone, F., Rouzo, S., Kiel, J.S., Robin, C., Guillocheau, F., Tiberi, C., Basuyau, C., Beslier, M.O., Ebinger, C., Stuart, G., Ahmed, A., Khanbari, K., Al Ganad, I., de Clarens, P., Unternehr, P., Al Toubi, K., Al Lazki, A., 2012. From rifting to oceanic spreading in the Gulf of Aden: A synthesis. Arab. J. Geosci. 5, 859–901. https://doi.org/10.23919/RADIO.2017.8242234

Lescoutre, R., Manatschal, G., 2020. Role of rift-inheritance and segmentation for orogenic evolution: example from the Pyrenean-Cantabrian system. Bull. la Soc. Geol. Fr. 191.

Lewis, D.S., Ross, E., Leander, M., 2014. New insights into late synrift subsidence from detailed well ties and seismic mapping, Campos Basin, Brazil, in: Pindell, J., Horn, B., Rosen, N., Weimer, P., Dinkleman, M., Lowrie, A., Fillon, R., Granath, J., Kennan, L. (Eds.), Sedimentary Basins: Origin, Depositional Histories and Petroleum Systems. SEPM Society for Sedimentary Geology, Houston, pp. 98–115.

Li, F., Sun, Z., Yang, H., 2018. Possible Spatial Distribution of the Mesozoic Volcanic Arc in the Present-Day South China Sea Continental Margin and Its Tectonic Implications. J. Geophys. Res. Solid Earth 123, 6215–6235. https://doi.org/10.1029/2017JB014861

Luo, P., Manatschal, G., Ren, J., Zhao, Z., Wang, H., Tong, D., 2021. Tectono-magmatic and stratigraphic evolution of final rifting and breakup: evidence from the tip of the southwestern propagator in the South China Sea. Mar. Pet. Geol. 105079. https://doi.org/10.1016/J.MARPETGEO.2021.105079

Lymer, G., Cresswell, D.J.F., Reston, T.J., Bull, J.M., Sawyer, D.S., Morgan, J.K., Stevenson, C., Causer, A., Minshull, T.A., Shillington, D.J., 2019. 3D development of detachment faulting during continental breakup. Earth Planet. Sci. Lett. 515, 90–99. https://doi.org/10.1016/j.epsl.2019.03.018

Manatschal, G., 2004. New models for evolution of magma-poor rifted margins based on a review of data and concepts from West Iberia and the Alps. Int. J. Earth Sci. 93, 432–466. https://doi.org/10.1007/s00531-004-0394-7

Manatschal, G., 1999. Fluid- and reaction-assisted low-angle normal faulting: evidence from rift-related brittle fault rocks in the Alps (Err Nappe, eastern Switzerland). J. Struct. Geol. 21, 777–793. https://doi.org/10.1016/S0191-8141(99)00069-3

Manatschal, G., Bernoulli, D., 1999. Architecture and tectonic evolution of nonvolcanic margins: Present-day Galicia and ancient Adria. Tectonics 18, 1099–1119. https://doi.org/10.1029/1999TC900041

Manatschal, G., Chenin, P., Ghienne, J.-F., Ribes, C., Masini, E., n.d. A tectono-stratigraphic model for the syn-rift sequence of a magma-poor rifted margin (Part 1): insights from the Alpine Tethys. Basin Res.

Manatschal, G., Chenin, P., Lescoutre, R., Miró, J., Cadenas, P., Saspiturry, N., Masini, E., Chevrot, S., Ford, M., Jolivet, L., Mouthereau, F., Thinon, I., Issautier, B., Calassou, S., 2021. The role of inheritance in forming rifts and rifted margins and building collisional orogens: a Biscay-Pyrenean perspective. Bull. la Société Géologique Fr.

Manatschal, G., Engström, A., Desmurs, L., Schaltegger, U., Cosca, M., Müntener, O., Bernoulli, D., 2006. What is the tectono-metamorphic evolution of continental break-up: The example of the Tasna Ocean-Continent Transition. J. Struct. Geol. 28, 1849–1869. https://doi.org/10.1016/j.jsg.2006.07.014

Manatschal, G., Froitzheim, N., Rubenach, M., Turrin, B.D., 2001. The role of detachment faulting in the formation of an ocean-continent transition: Insights from the Iberia Abyssal Plain. Geol. Soc. Spec. Publ. 187, 405–428. https://doi.org/10.1144/GSL.SP.2001.187.01.20

Manatschal, G., Lavier, L.L., Chenin, P., 2015. The role of inheritance in structuring hyperextended rift

systems: Some considerations based on observations and numerical modeling. Gondwana Res. 27, 140–164. https://doi.org/10.1016/j.gr.2014.08.006

Manatschal, G., Marquer, D., Früh-Green, G.L., 2000. Channelized fluid flow and mass transfer along a rift-related detachment fault (Eastern Alps, Southeast Switzerland). Bull. Geol. Soc. Am. 112, 21–33. https://doi.org/10.1130/0016-7606(2000)112<21:CFFAMT>2.0.CO;2

Manatschal, G., Müntener, O., 2009. A type sequence across an ancient magma-poor ocean--continent transition: the example of the western Alpine Tethys ophiolites. Tectonophysics 473, 4–19. https://doi.org/10.1016/j.tecto.2008.07.021

Manatschal, G., Nievergelt, P., 1997. A continent-ocean transition recorded in the Err and Platta nappes (Eastern Switzerland). Eclogae Geol. Helv. 90, 3–27.

Manatschal, G., Sauter, D., Karpoff, A.M., Masini, E., Mohn, G., Lagabrielle, Y., 2011. The Chenaillet Ophiolite in the French/Italian Alps: An ancient analogue for an Oceanic Core Complex? Lithos 124, 169–184. https://doi.org/10.1016/j.lithos.2010.10.017

Martins-Neto, M.A., Catuneanu, O., 2010. Rift sequence stratigraphy. Mar. Pet. Geol. 27, 247–253. https://doi.org/10.1016/J.MARPETGEO.2009.08.001

Masini, E., Manatschal, G., Mohn, G., 2013. The Alpine Tethys rifted margins: Reconciling old and new ideas to understand the stratigraphic architecture of magma-poor rifted margins. Sedimentology 60, 174–196. https://doi.org/10.1111/sed.12017

Masini, E., Manatschal, G., Mohn, G., Ghienne, J.F., Lafont, F., 2011. The tectono-sedimentary evolution of a supra-detachment rift basin at a deep-water magma-poor rifted margin: The example of the Samedan Basin preserved in the Err nappe in SE Switzerland. Basin Res. 23, 652–677. https://doi.org/10.1111/j.1365-2117.2011.00509.x

Masini, E., Manatschal, G., Mohn, G., Unternehr, P., 2012. Anatomy and tectono-sedimentary evolution of a rift-related detachment system: The example of the Err detachment (central Alps, SE Switzerland). Bull. Geol. Soc. Am. 124, 1535–1551. https://doi.org/10.1130/B30557.1

McAlpine, K.D., 1990. Mesozoic stratigraphy, sedimentary evolution, and petroleum potential of the Jeanne d'Arc Basin, Grands Banks of Newfoundland.

McKenzie, D., 1978. Some remarks on the development of sedimentary basins. Earth Planet. Sci. Lett. 40, 25–32. https://doi.org/10.1016/0012-821X(78)90071-7

McLeod, A.E., Underhill, J.R., Davies, S.J., Dawers, N.H., 2002. The Influence of Fault Array Evolution on Synrift Sedimentation Patterns: Controls on Deposition in the Strathspey-Brent-Statfjord Half Graben, Northern North Sea. Am. Assoc. Pet. Geol. Bull. 86, 1061–1093. https://doi.org/10.1306/61EEDC24-173E-11D7-8645000102C1865D

Menzies, Martin A, Klemperer, Simon L, Ebinger, Cynthia J, Baker, Joel, 2002. Characteristics of volcanic rifted margins, in: Menzies, M. A., Klemperer, S. L., Ebinger, C .J., Baker, J. (Eds.), Volcanic Rifted Margins. Geological Society of America Special Paper 362, Boulder, Colorado, pp. 1–14.

Merino-Perez, I., 2016. Stratigraphic evolution of a segmented hyper-extended rifted margin: The example of the Western Iberia Margin (Master Thesis). Université de Strasbourg.

Miró, J., Cadenas, P., Manatschal, G., Munoz, J.A., 2021. Reactivation of a hyperextended rift system: the Basque-Cantabrian Pyrenees case. Basin Res. 00, 1–25. https://doi.org/10.1111/bre.12595

Miró, J., Cadenas, P., Manatschal, G., Muñoz, J.A., n.d. Reactivation of a hyperextended rift system: the Basque-Cantabrian Pyrenees case.

Mohn, G., Karner, G.D., Manatschal, G., Johnson, C.A., 2015. Structural and stratigraphic evolution of the Iberia–Newfoundland hyper-extended rifted margin: a quantitative modelling approach. Geol. Soc. London, Spec. Publ. 413, 53–89. https://doi.org/10.1144/SP413.9

Mohn, G., Manatschal, G., Beltrando, M., Masini, E., Kusznir, N., 2012. Necking of continental crust in magma-poor rifted margins: Evidence from the fossil Alpine Tethys margins. Tectonics 31, TC1012. https://doi.org/10.1029/2011TC002961

Mohn, G., Manatschal, G., Müntener, O., Beltrando, M., Masini, E., 2010. Unravelling the interaction between tectonic and sedimentary processes during lithospheric thinning in the Alpine Tethys margins. Int. J. Earth Sci. 99, 75–101. https://doi.org/10.1007/s00531-010-0566-6

Montadert, L., de Charpal, O., Roberts, D., Guennoc, P., Sibuet, J.-C., 1979. Northeast Atlantic passive continental margins: Rifting and subsidence processes, in: Talwani, M., Hay, W., Ryan, W.B.F. (Eds.), Deep Drilling Results in the Atlantic Ocean: Continental Margins and Paleoenvironment, Volume 3. American Geophysical Union (AGU), pp. 154–186. https://doi.org/10.1029/me003p0154

Mosar, J., Eide, E. a., Osmundsen, P.T., Sommaruga, A., Torsvik, T.H., 2002. Greenland - Norway separation: A geodynamic model for the North Atlantic. Nor. Geol. Tidsskr. 82, 281–298.

Murillas, J., Mougenot, D., Boulot, G., Comas, M.C., Banda, E., Mauffret, A., 1990. Structure and evolution of the Galicia Interior Basin (Atlantic western Iberian continental margin). Tectonophysics 184, 297–319. https://doi.org/10.1016/0040-1951(90)90445-E

Naliboff, J.B., Buiter, S.J.H., Péron-Pinvidic, G., Osmundsen, P.T., Tetreault, J., 2017. Complex fault interaction controls continental rifting. Nat. Commun. 8. https://doi.org/10.1038/s41467-017-00904-x

Nirrengarten, M., Manatschal, G., Tugend, J., Kusznir, N., Sauter, D., 2018. Kinematic Evolution of the Southern North Atlantic: Implications for the Formation of Hyperextended Rift Systems. Tectonics 37, 89–118. https://doi.org/10.1002/2017TC004495

Nirrengarten, M., Manatschal, G., Yan, X., Kusznir, N., Millot, B., 2016. Application of the critical Coulomb wedge theory to hyper-extended, magma-poor rifted margins. Earth Planet. Sci. Lett. 442, 121–132.

Nirrengarten, M., Mohn, G., Kusznir, N.J., Sapin, F., Despinois, F., Pubellier, M., Chang, S.P., Larsen, H.C., Ringenbach, J.C., 2020. Extension modes and breakup processes of the southeast China-Northwest Palawan conjugate rifted margins. Mar. Pet. Geol. 113, 104123. https://doi.org/10.1016/j.marpetgeo.2019.104123

Nonn, C., Leroy, S., Khanbari, K., Ahmed, A., 2017. Tectono-sedimentary evolution of the eastern Gulf of Aden conjugate passive margins: Narrowness and asymmetry in oblique rifting context. Tectonophysics 721, 322–348. https://doi.org/10.1016/j.tecto.2017.09.024

Olsen, K.H., Morgan, P., 2006. Introduction: Progress in understanding continental rifts. Dev. Geotecton. https://doi.org/10.1016/S0419-0254(06)80005-4

Osmundsen, P.T., Ebbing, J., 2008. Styles of extension offshore mid-Norway and implications for mechanisms of crustal thinning at passive margins. Tectonics 27. https://doi.org/10.1029/2007TC002242

Osmundsen, P.T., Péron-Pinvidic, G., 2018. Crustal-scale fault interaction at rifted margins and the formation of domain-bounding breakaway complexes: Insights from offshore Norway. Tectonics 37, 935–964.

Osmundsen, P.T., Péron-Pinvidic, G., Ebbing, J., Erratt, D., Fjellanger, E., Bergslien, D., Syvertsen, S.E., 2016. Extension, hyperextension and mantle exhumation offshore Norway: a discussion based on 6 crustal transects. Nor. J. Gology 96, 343–372. https://doi.org/10.17850/njg96-4-05

Osmundsen, P.T., Sommaruga, A., Skilbrei, J.R., Olesen, O., 2002. Deep structure of the Mid Norway rifted margin. Nor. J. Geol. 82, 205–224.

Pérez-Gussinyé, M., Andrés-Martínez, M., Araújo, M., Xin, Y., Armitage, J., Morgan, J.P., 2020. Lithospheric Strength and Rift Migration Controls on Synrift Stratigraphy and Breakup Unconformities at Rifted Margins: Examples From Numerical Models, the Atlantic and South China Sea Margins. Tectonics 39, e2020TC006255. https://doi.org/10.1029/2020TC006255

Pérez-Gussinyé, M., Ranero, C.R., Reston, T.J., 2003. Mechanisms of extension at nonvolcanic margins: Evidence from the Galicia interior basin, west of Iberia. J. Geophys. Res. 108. https://doi.org/10.1029/2001JB000901

Péron-Pinvidic, G., Manatschal, G., 2009. The final rifting evolution at deep magma-poor passive margins from Iberia-Newfoundland: A new point of view. Int. J. Earth Sci. 98, 1581–1597. https://doi.org/10.1007/s00531-008-0337-9

Péron-Pinvidic, G., Manatschal, G., Masini, E., Sutra, E., Flament, J.M., Haupert, I., Unternehr, P., 2015. Unravelling the along-strike variability of the Angola – Gabon rifted margin: a mapping approach. Geol. Soc. London, Spec. Publ. 438. https://doi.org/10.1144/SP438.1 #

Péron-Pinvidic, G., Manatschal, G., Minshull, T. a., Sawyer, D.S., 2007. Tectonosedimentary evolution of the deep Iberia-Newfoundland margins: Evidence for a complex breakup history. Tectonics 26, n/a-n/a. https://doi.org/10.1029/2006TC001970

Péron-Pinvidic, G., Manatschal, G., Osmundsen, P.T., 2013. Structural comparison of archetypal Atlantic rifted margins: A review of observations and concepts. Mar. Pet. Geol. 43, 21–47. https://doi.org/10.1016/j.marpetgeo.2013.02.002

Peron-Pinvidic, G., Naliboff, J., 2020. The exhumation detachment factory. Geology 48, 635–639. https://doi.org/10.1130/G47174.1

Péron-Pinvidic, G., Osmundsen, P.T., 2018. The Mid Norwegian - NE Greenland conjugate margins: Rifting evolution, margin segmentation, and breakup. Mar. Pet. Geol. https://doi.org/10.1016/j.marpetgeo.2018.08.011

Péron-Pinvidic, G., Osmundsen, P.T., Bunkholt, H., 2020. The proximal domain of the Mid-Norwegian rifted margin: The Trøndelag Platform revisited. Tectonophysics 790, 228551. https://doi.org/10.1016/j.tecto.2020.228551

Petri, B., Duretz, T., Mohn, G., Schmalholz, S.M., Karner, G.D., Müntener, O., 2019. Thinning mechanisms of heterogeneous continental lithosphere. Earth Planet. Sci. Lett. 512, 147–162. https://doi.org/10.1016/J.EPSL.2019.02.007

Picazo, S., Müntener, O., Manatschal, G., Bauville, A., Karner, G.D., Johnson, C., 2016. Mapping the nature of mantle domains in Western and Central Europe based on clinopyroxene and spinel chemistry: evidence for mantle modification during an extensional cycle. Lithos. https://doi.org/10.1016/j.lithos.2016.08.02

Pik, R., Bellahsen, N., Leroy, S., Denèle, Y., Razin, P., Ahmed, A., Khanbari, K., 2013. Structural control of basement denudation during rifting revealed by low-temperature (U-Th-Sm)/He thermochronology of the Socotra Island basement-Southern Gulf of Aden margin. Tectonophysics 607, 17–31. https://doi.org/10.1016/j.tecto.2013.07.038

Planke, S., Symonds, P.A., Alvestad, E., Skogseid, J., 2000. Seismic volcanosratigraphy of large-volume basaltic extrusive complexes on rifted margins. J. Geophys. Res. 105, 19,335-19,351.

Posamentier, H.W., Vail, P.R., 1988. Eustatic controls on clastic deposition II—sequence and systems tract models. Spec. Publ. SEPM 42.

Prosser, S., 1993. Rift-related linked depositional systems and their seismic expression, in: Williams, G.D., Dobb, A. (Eds.), Tectonics and Seismic Sequence Stratigraphy. Geological Society Special Publication. pp. 35–66.

Ranero, C.R., Pérez-Gussinyé, M., 2010. Sequential faulting explains the asymmetry and extension discrepancy of conjugate margins. Nature 468, 294–299. https://doi.org/10.1038/nature09520

Ravnås, R., Steel, R.J., 1998. Architecture of marine rift-basin successions. Am. Assoc. Pet. Geol. Bull. 82, 110–146. https://doi.org/10.1306/1D9BC3A9-172D-11D7-8645000102C1865D

Ravnås, R., Windelstad, J., Mellere, D., Nøttvedt, A., Sjøblom, T.S., Steel, R.J., Wilson, R.C.L., 1997. A marine Late Jurassic syn-rift succession in the Lusitanian Basin, western Portugal — tectonic significance of stratigraphic signature. Sediment. Geol. 114, 237–266. https://doi.org/10.1016/S0037-0738(97)00068-7

Ren, J., Pang, X., Lei, C., Yu, P., Luo, P., 2018. Characteristics and formation mechanism of deepwater and ultra-deepwater basins in the northern continental margin of the South China Sea. Chinese J. Geophys. 61, 4901–4920. https://doi.org/１０．６０３８／

2344 Reston, T.J., McDermott, K.G., 2011. Successive detachment faults and mantle unroofing at magma-
2345 poor rifted margins. Geology 39, 1071–1074. https://doi.org/10.1130/G32428.1

2346 Ribes, C., Ghienne, J.-F., Manatschal, G., Decarlis, A., Karner, G.D., Figueredo, P.H., Johnson, C.A.,
2347 2019a. Long-lived mega fault-scarps and related breccias at distal rifted margins: insights from
2348 present-day and fossil analogues. J. Geol. Soc. London. 176, 801–816.
2349 https://doi.org/10.1144/jgs2018-181

2350 Ribes, C., Ghienne, J.F., Manatschal, G., Dall'Asta, N., Stockli, D.F., Galster, F., Gillard, M., Karner,
2351 G.D., 2020. The Grès Singuliers of the Mont Blanc region (France and Switzerland): stratigraphic
2352 response to rifting and crustal necking in the Alpine Tethys. Int. J. Earth Sci. 109, 2325–2352.
2353 https://doi.org/10.1007/s00531-020-01902-z

2354 Ribes, C., Manatschal, G., Ghienne, J.-F., Karner, G.D., Johnson, C.A., Figueredo, P.H., Incerpi, N.N.,
2355 Epin, M., 2019b. The syn-rift stratigraphic record across a fossil hyper-extended rifted margin:
2356 the example of the northwestern Adriatic margin exposed in the Central Alps. Int. J. Earth Sci.
2357 108, 2071–2095. https://doi.org/DOI: 10.1007/s00531-019-01750-6

2358 Ribes, C., Petri, B., Ghienne, J., Manatschal, G., Galster, F., Karner, G.D., Figueredo, P.H., Johnson,
2359 C.A., Karpoff, A., 2019c. Tectono-sedimentary evolution of a fossil ocean-continent transition:
2360 Tasna nappe, central Alps (SE Switzerland). Geol. Soc. Am. Bull. 1–20.
2361 https://doi.org/10.1130/B35310.1/4863878/b35310.pdf

2362 Ros, E., Pérez-Gussinyé, M., Araújo, M., Thoaldo Romeiro, M., Andrés-Martínez, M., Morgan, J.P.,
2363 2017. Lower crustal strength controls on melting and serpentinization at magma-poor margins:
2364 Potential implications for the South Atlantic. Geochemistry, Geophys. Geosystems 18, 4538–
2365 4557. https://doi.org/10.1002/2017GC007212

2366 Rowan, M.G., Ratliff, R.A., 2012. Cross-section restoration of salt-related deformation: Best practices
2367 and potential pitfalls. J. Struct. Geol. https://doi.org/10.1016/j.jsg.2011.12.012

2368 Samuel, M.A., Harbury, N., Bott, R., Thabet, A.M., 1997. Field observations from the Socotran
2369 platform: Their interpretation and correlation to Southern Oman. Mar. Pet. Geol. 14, 661–673.
2370 https://doi.org/10.1016/s0264-8172(96)00033-5

2371 Schlische, R.W., 1995. Geometry and Origin of Fault-Related Folds in Extensional Settings. Am.
2372 Assoc. Pet. Geol. Bull. 79, 1661–1678. https://doi.org/10.1306/7834DE4A-1721-11D7-
2373 8645000102C1865D

2374 Sengör, A.M.C., Burke, K., 1978. Relative timing of rifting and volcanism on Earth and its tectonic
2375 implications. Geophys. Res. Lett. 5, 419–421. https://doi.org/10.1029/GL005i006p00419

2376 Serck, C.S., Braathen, A., Olaussen, S., Osmundsen, P.T., Midtkandal, I., van Yperen, A.E., Indrevær,
2377 K., 2021. Supradetachment to rift basin transition recorded in continental to marine deposition;
2378 Paleogene Bandar Jissah Basin, NE Oman. Basin Res. 33, 544–569.
2379 https://doi.org/10.1111/bre.12484

2380 Sharp, I., Higgins, S., Scott, M., Freitag, U., Allsop, C., Kane, K., Sultan, A., Doubleday, P., Leppard,
2381 C., Bloomfield, J., Cody, J., Rait, G., Haynes, S., 2017. Rift to drift evolution and hyperextension
2382 in the North Atlantic – Insights from a super-regional approach, in: Davies, M., Carlisle, C. (Eds.),
2383 Atlantic Ireland 2017. Dublin, pp. 22–23.

2384 Sinclair, I.K., 1994. ectonism and sedimentation in the Jeanne d'Arc Basin, Grand Banks of
2385 Newfoundland. University of Aberdeen.

2386 Sinclair, I.K., 1993. Tectonism: the dominant factor in mid-Cretaceous deposition in the Jeanne d'Arc
2387 Basin, Grand Banks. Mar. Pet. Geol. 10, 530–549. https://doi.org/10.1016/0264-8172(93)90058-
2388 Z

2389 Sinclair, I.K., 1988. Evolution of Mesozoic-Cenozoic sedimentary basins in the Grand Banks area of
2390 Newfoundland and comparison with Falvey's (1974) rift model, Bulletin of Canadian Petroleum
2391 Geology. GeoScienceWorld.

Skogseid, J., 2010. The Orphan Basin - a key to understanding the kinematic linkage between North and NE Atlantic Mesozoic rifting. II Cent. North Atl. Conjug. Margins Conf. II, 13–23.

Spencer, J.E., 1984. Role of tectonic denudation in warping and uplift of low-angle normal faults. Geology 12, 95–98.

Steinmann, G., 1905. Geologische Beobachtungen in den Alpen. Wagners Universitäts-Buchdruckerei.

Stille, H., 1936. The Present Tectonic State of the Earth. Am. Assoc. Pet. Geol. Bull. 20, 849–880. https://doi.org/10.1306/3d932dfa-16b1-11d7-8645000102c1865d

Stille, H., 1924. Grundfragen der vergleichenden Tektonik. Berlin.

Stille, H., 1913. Evolution und Revolutionen in der Erdgeschichte. Berlin.

Stockli, D.F., Bosworth, W.B., 2018. Timing of extensional faulting along the magma-poor central and northern red sea rift margin-transition from regional extension to necking along a hyperextended rifted margin, in: Geological Setting, Palaeoenvironment and Archaeology of the Red Sea. Springer International Publishing, pp. 81–111. https://doi.org/10.1007/978-3-319-99408-6_5

Sun, Z., Lin, J., Qiu, N., Jian, Z., Wang, P., Pang, X., Zheng, J., Zhu, B., 2019. The role of magmatism in the thinning and breakup of the South China Sea continental marginSpecial Topic: The South China Sea Ocean Drilling. Natl. Sci. Rev. 6, 871–876. https://doi.org/10.1093/NSR/NWZ116

Sutra, E., Manatschal, G., 2012. How does the continental crust thin in a hyperextended rifted margin? Insights from the Iberia margin. Geology 40, 139–142. https://doi.org/10.1130/G32786.1

Sutra, E., Manatschal, G., Mohn, G., Unternehr, P., 2013. Quantification and restoration of extensional deformation along the Western Iberia and Newfoundland rifted margins. Geochemistry, Geophys. Geosystems 14, 2575–2597. https://doi.org/10.1002/ggge.20135

Tillmans, F., Gawthorpe, R.L., Jackson, C.A.L., Rotevatn, A., 2021. Syn-rift sediment gravity flow deposition on a Late Jurassic fault-terraced slope, northern North Sea. Basin Res. 33, 1844–1879. https://doi.org/10.1111/bre.12538

Tucholke, B.E., Sawyer, D.S., Sibuet, J., Brest, I.C. De, 2007. Breakup of the Newfoundland--Iberia rift, in: Karner, G.D., Manatschal, G., Pinheiro, L.M. (Eds.), Imaging, Mapping and Modelling Continental Lithosphere Extension and Breakup; Geological Society, London, Special Publications, 282. The Geological Society of London, pp. 9–46. https://doi.org/10.1144/SP282.2

Tugend, J., Gillard, M., Manatschal, G., Nirrengarten, M., Harkin, C., Epin, M.-E., Sauter, D., Autin, J., Kusznir, N., McDermott, K., 2020. Reappraisal of the magma-rich versus magma-poor rifted margin archetypes. Geol. Soc. London, Spec. Publ. 476, 23–47. https://doi.org/10.1144/SP476.9

Tugend, J., Manatschal, G., Kusznir, N.J., Masini, E., Mohn, G., Thinon, I., 2014. Formation and deformation of hyperextended rift systems: Insights from rift domain mapping in the Bay of Biscay-Pyrenees. Tectonics 33, 1239–1276. https://doi.org/10.1002/2014TC003529

Urquhart, E., 2001. Depositional environment of synrift sediments on the Iberia margin, in: AGU Fall Meeting Abstracts. pp. PP42B-0505.

Waltham, D., Hardy, S., Abousetta, A., 1993. Sediment geometries and domino faulting. Geol. Soc. Spec. Publ. 71, 67–85. https://doi.org/10.1144/GSL.SP.1993.071.01.04

Welford, J.K., Smith, J.A., Hall, J., Deemer, S., Srivastava, S.P., Sibuet, J.-C., 2010. Structure and rifting evolution of the northern Newfoundland Basin from Erable multichannel seismic reflection profiles across the southeastern margin of Flemish Cap. Geophys. J. Int. 180, 976–998. https://doi.org/10.1111/j.1365-246X.2009.04477.x

Wernicke, B., 1985. Uniform-sense normal simple shear of the continental lithosphere. Can. J. Earth Sci. 22, 108–125. https://doi.org/10.1139/e85-009

Whiting, L., Haughton, P.D.W., Shannon, P.M., 2020. From rifting to hyperextension: Upper Jurassic–Lower Cretaceous tectono-stratigraphy of the Porcupine Basin, Irish Atlantic Margin. Basin Res. 33, 1662–1696. https://doi.org/10.1111/bre.12530

Wielens, J.B.W., Jauer, C.D., Williams, G.L., 2006. Is there a viable petroleum system in the Carson and Salar Basins, offshore Newfoundland? J. Pet. Geol. 29, 303–326. https://doi.org/10.1111/j.1747-5457.2006.00303.x

Wilson, R.C.L., Manatschal, G., Wise, S., 2001. Rifting along non-volcanic passive margins: Stratigraphic and seismic evidence from the Mesozoic successions of the Alps and Western Iberia. Geol. Soc. London, Spec. Publ. 187, 429–452. https://doi.org/10.1144/gsl.sp.2001.187.01.21

Withjack, M.O., Schlische, R.W., Olsen, P.E., 2002. Rift-Basin Structure and Its Influence on Sedimentary Systems. Spec. Publ. SEPM 57–81.

Xie, X., Ren, J., Pang, X., Lei, C., Chen, H., 2019. Stratigraphic architectures and associated unconformities of Pearl River Mouth basin during rifting and lithospheric breakup of the South China Sea. Mar. Geophys. Res. 40, 129–144. https://doi.org/10.1007/s11001-019-09378-6

Yang, P., Welford, J.K., 2021. Investigating the Porcupine Atlantic margin, offshore Ireland, through integration of new seismic reflection and gravity data. Tectonophysics 807, 228809. https://doi.org/10.1016/j.tecto.2021.228809

Yielding, G., 1990. Footwall uplift associated with Late Jurassic normal faulting in the northern North Sea. J. - Geol. Soc. 147, 219–222. https://doi.org/10.1144/gsjgs.147.2.0219

Zastrozhnov, D., Gernigon, L., Gogin, I., Planke, S., Abdelmalak, M.M., Polteau, S., Faleide, J.I., Manton, B., Myklebust, R., 2020. Regional structure and polyphased Cretaceous-Paleocene rift and basin development of the mid-Norwegian volcanic passive margin. https://doi.org/10.1016/j.marpetgeo.2020.104269

Zhang, C., Manatschal, G., Pang, X., Sun, Z., Zheng, J., Li, H., Sun, L., Zhang, J., Zhao, Y., 2020. Discovery of Mega-Sheath Folds Flooring the Liwan Subbasin (South China Sea): Implications for the Rheology of Hyperextended Crust. Geochemistry, Geophys. Geosystems 21, e2020GC009023. https://doi.org/10.1029/2020GC009023

Zhang, C., Su, M., Pang, X., Zheng, J., Liu, B., Sun, Z., Manatschal, G., 2019. Tectono-Sedimentary Analysis of the Hyperextended Liwan Sag Basin (Midnorthern Margin of the South China Sea). Tectonics 38, 470–491. https://doi.org/10.1029/2018TC005063

Zhang, C., Sun, Z., Manatschal, G., Pang, X., Qiu, N., Su, M., Zheng, J., Li, H., Gu, Y., Zhang, J., Zhao, Y., 2021. Syn-rift magmatic characteristics and evolution at a sediment-rich margin: Insights from high-resolution seismic data from the South China Sea. Gondwana Res. 91, 81–96. https://doi.org/10.1016/j.gr.2020.11.012

TABLE CAPTION

	Necking			Hyperextension			Mantle exhumation			Proto-oceanic	
	phase duration		domain width	phase duration		domain width	phase duration		domain width	Phase duration	domain width
Alps	6 My (Ribes et al. 2019)	ca. 10 My (Manatschal et al. this vol.)	unknown	5 My (Ribes et al. 2019)	ca. 10 My (Manatschal et al. this vol.)	unknown	18 My (Ribes et al. 2019)	ca. 10 My (Manatschal et al. this vol.)	unknown	X	unknown
Iberia–Newfnd.	ca. 10 My (Mohn et al. 2015, with ref.)		ca. 100 (E) & 45 (W) km (Sutra et al. 2013)	ca. 5 My (Mohn et al. 2015, with ref.)		ca. 60 & 45 km (Sutra et al. 2013)	ca. 25 My (Mohn et al. 2015, with ref.)		ca. 80 (E) & 90(W) km (Sutra et al. 2013)	X	X
NW SCS	7 My (Chao et al. subm.)		N margin: ca. 60 km (Chao et al. Subm.)	4 My (Chao et al. Subm.)		ca. 25 (N) & 30 (S) km (Chao et al. Subm.)	X		X	2 My (Chao et al. subm)	X
Norway	Late Mid-Jurassic–base Cretaceous (ca. 25 My? Péron-Pinvidic et al. 2018, with ref.)		20–80 km (Osmundsen & Péron-Pinvidic 2018)	Base Cretaceous–Late Cretaceous (ca. 60 My? Péron- Pinvidic et al. 2018, with ref.)		unknown	unknown		unknown	Late Cretaceous–Paleocene (ca. 30 My? Péron-Pinvidic et al. 2018, with ref.)	unknown
Socotra	< 6 My? (This study)		unknown	ca. 10 My? (This study)		20–30 km (Nonn et al. 2017)	unknown		ca. 10 km (Nonn et al. 2017)	X	X

Table 1: Summary of the duration of the different rift phases and width of the different rift domains at the rift systems presented in this study.

FIGURE CAPTIONS

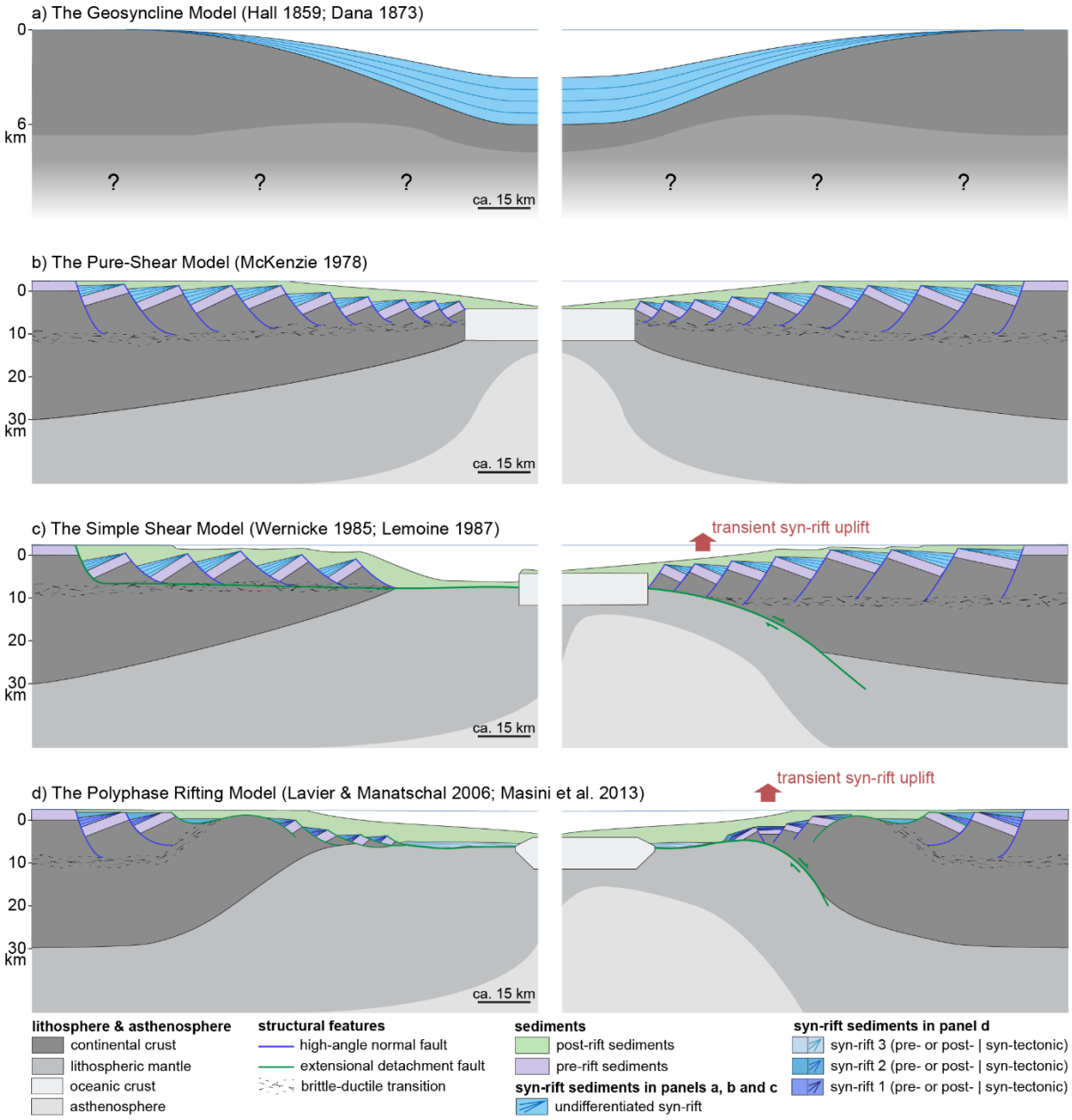


Figure 1: Schematic illustration of the evolution of stratigraphic models for rifted margins: a) the Geosyncline Model (Dana, 1873; Hall, 1859); b) the Pure-Shear or Depth-Uniform Thinning Model by McKenzie (1978); c) the Simple-Shear Model by Wernicke (1985); and d) the Polyphase Stretching–Thinning–Exhumation Model by Lavier and Manatschal (2006). Note that the scale for sedimentary deposits is vertically exaggerated compared to that of the crust.

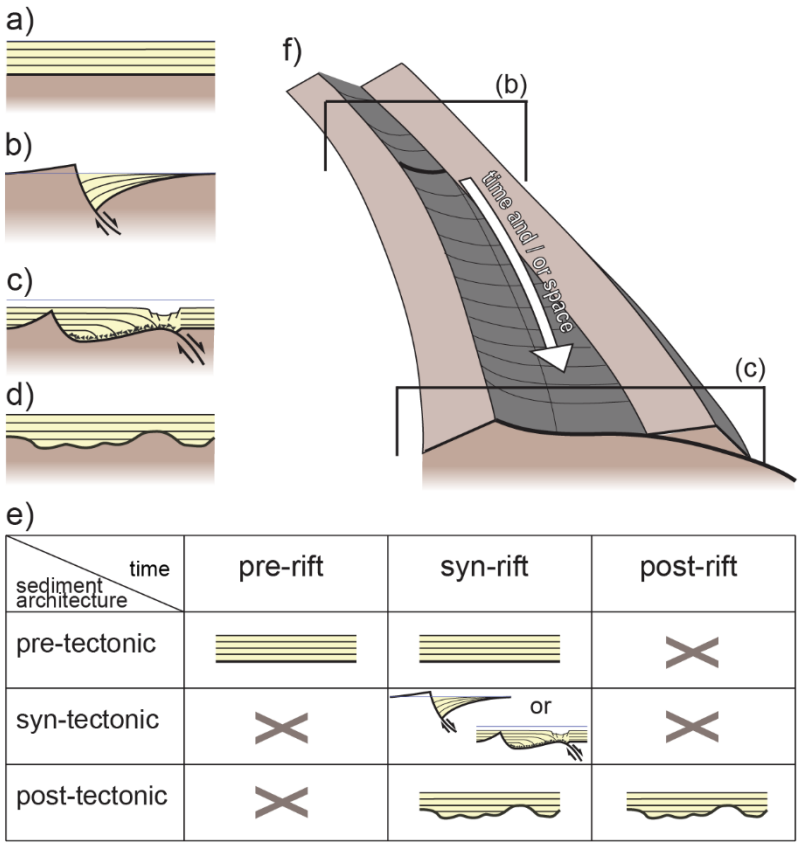


Figure 2: Schematic stratigraphic architectures depending on the tectonic context during sediment deposition: a) pre-tectonic; b) syn-tectonic half-graben wedge-shaped; c) syn-tectonic supra-detachment wedge-shaped; d) post-tectonic. e) relationships between the pre-, syn-, post-rift time intervals and the pre-, syn-, post-tectonic sedimentary architectures; f) schematic illustration of the evolution of a high-angle normal fault into a low-angle extensional detachment fault as extension progresses (modified from Péron-Pinvidic et al., 2007). Note that all schematics represent idealized architectures deposited in sediment-rich systems.

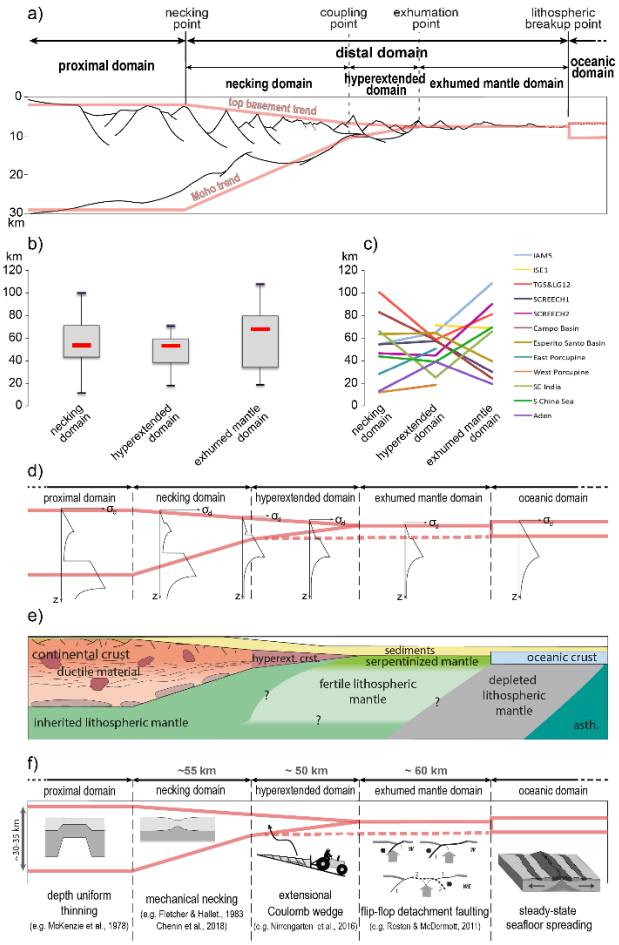


Figure 3: a) Schematic cross section highlighting the primary morphology of magma-poor rifted margins (from Chenin *et al.*, 2017); b) Width of the different distal domains in magma-poor rifted margins (from Chenin *et al.*, 2017); c) Width relationships among the different distal domains in magma-poor rifted margins (from Chenin *et al.*, 2017); d) First-order rheological evolution across a typical magma-poor rifted margin represented by schematic depth-dependent stress profiles; σ_d: deviatoric stress; z: depth; e) Schematic cross section displaying the first-order lithology across a typical magma-poor rifted margin (modified from Chenin *et al.*, 2017). f) Schematic cross section displaying the dominant deformation mechanism associate with the different rift domains of magma-poor rifted margins.

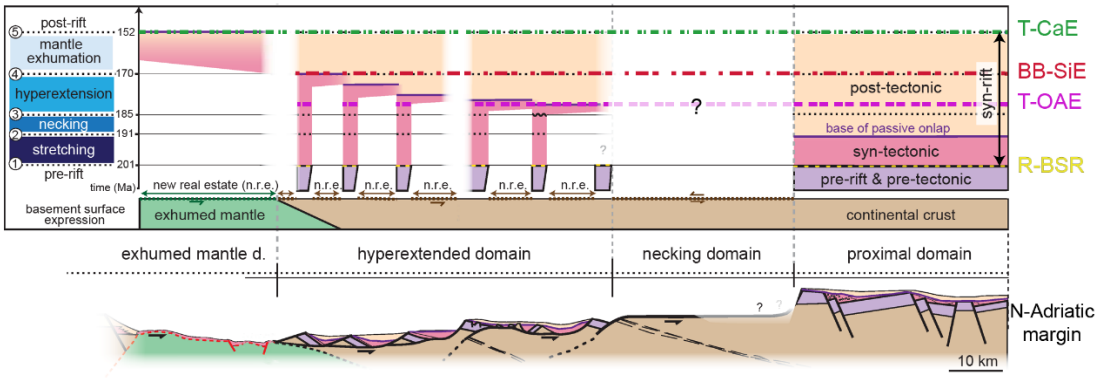


Figure 4: Wheeler diagram representing the spatio-temporal distribution of pre-, syn- and post-tectonic sedimentary sequences across the Adriatic margin of the Alpine Tethys (modified from Ribes *et al.*, 2019b). The dotted lines in the Wheeler diagram represent timelines that correspond to dated global or local events, namely: BB-SiE: Bajocian-Bathonian bio-Siliceous Event; R-BSR: Rhaetian Base of the Syn-rift sequence; T-CaE Tithonian Carbonate Event; T-OAE: Toarcian Oceanic Anoxic Event. Abbreviation n.r.e. stands for *new real estate*.

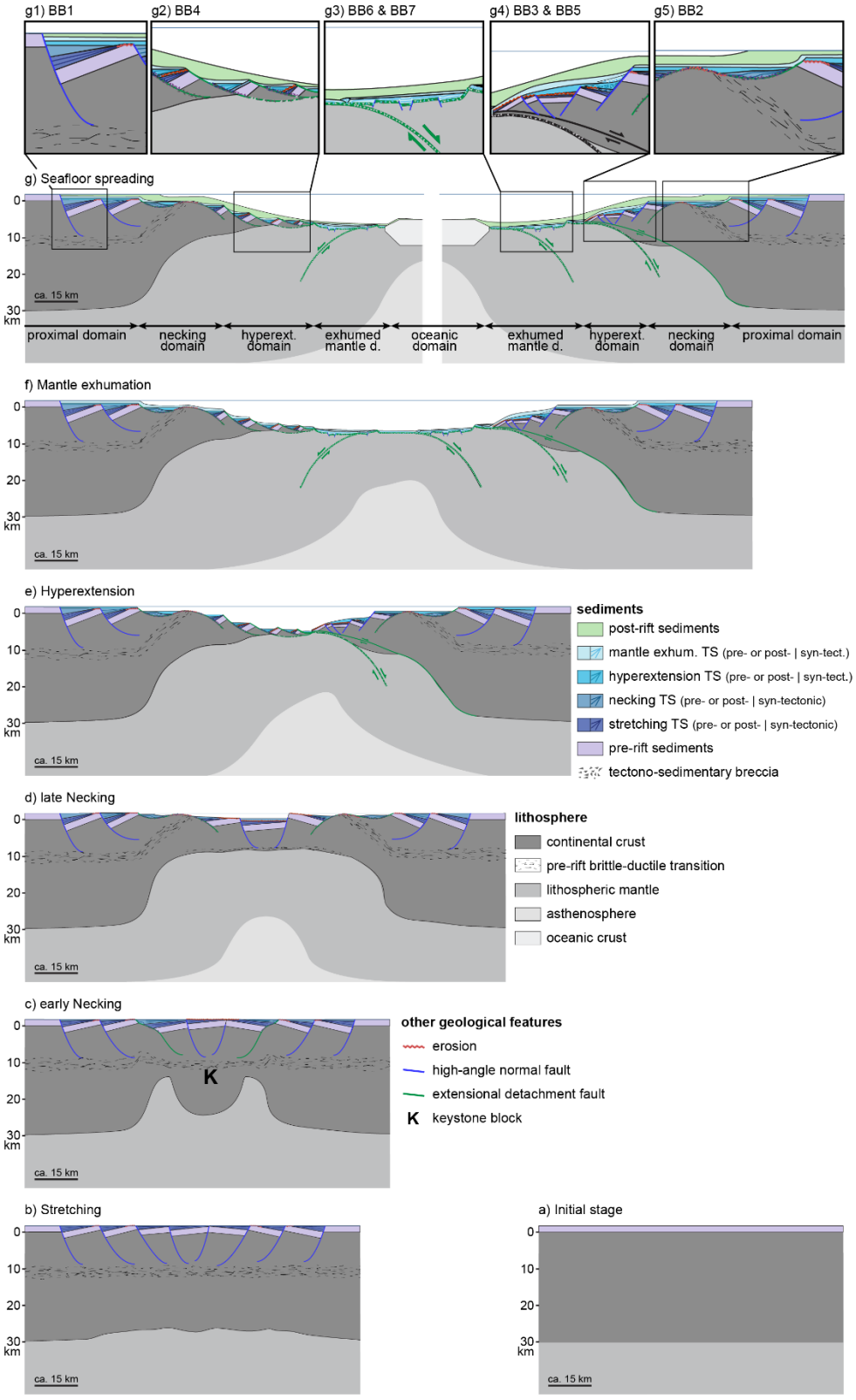


Figure 5: Schematic evolution of an idealized magma-poor rifting (crustal surface and pre-rift sediment length are conserved among the different stages): a) pre-rift setting; b) stretching phase; c) early necking phase; d) late necking phase; e) hyperextension phase; f) mantle exhumation phase g) seafloor spreading phase. Insets g1-g5 zoom on characteristic “Building Blocks” (BB1-BB7) of rifted margins (see Manatschal *et al.*, this volume, for a description of the different Building Blocks).

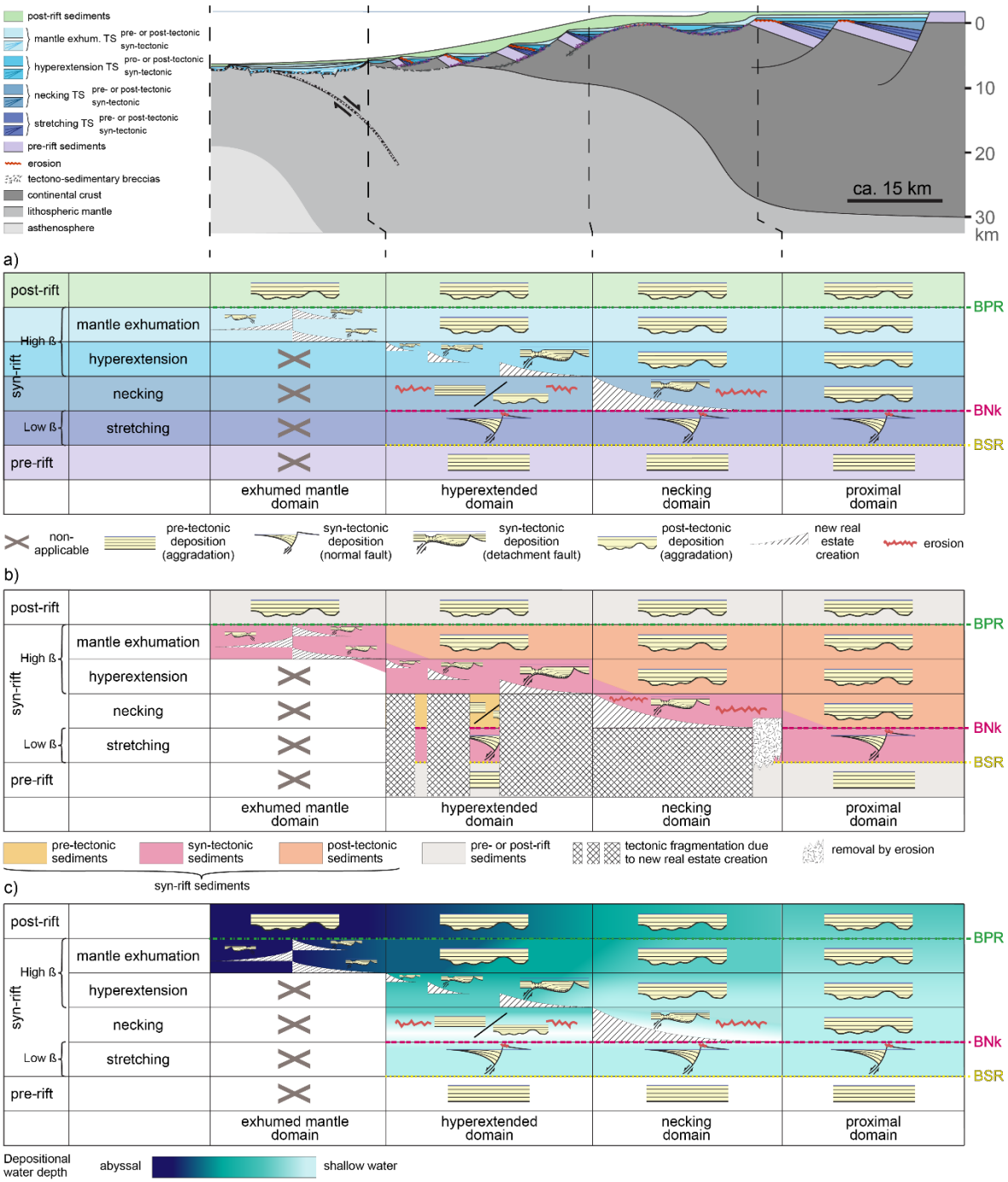


Figure 6: Tables summarizing the main characteristics of each system tract in the different rift domains of our idealized model: a) main structures and related stratigraphic architecture; b) distribution of pre-, syn- and post-tectonic sedimentation and tectonic fragmentation; c) evolution of the depositional water depth.

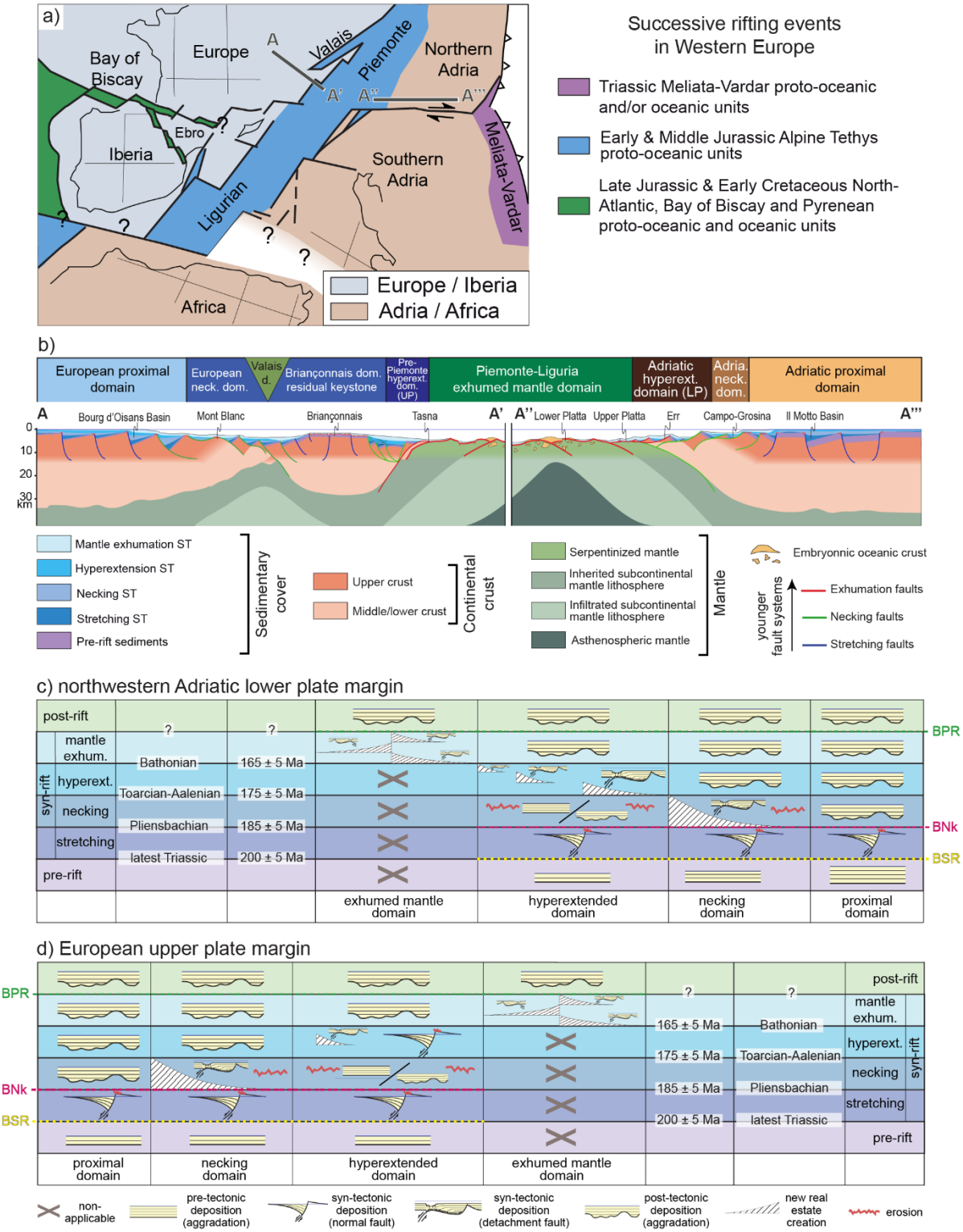


Figure 7: a) Schematic map showing the succession of rifting events in Western Europe (modified from Manatschal and Müntener, 2009).; b) Reconstruction of a synthetic section across the former Alpine Tethys rift system during the Late Jurassic margins. See panel (a) for location and note that section A—A' across the European margin is offset from section A''—A''' across the Adriatic margin. Abbreviations: hyperext.: hyperextended; d.: domain; Low. Aust. N.: Lower Austroalpine nappes; OCT: Ocean–Continent Transition; c) and d) Tables synthetizing the sedimentary architectures in each system tract in the different rift domains of the northwestern Adriatic and European margin, respectively.

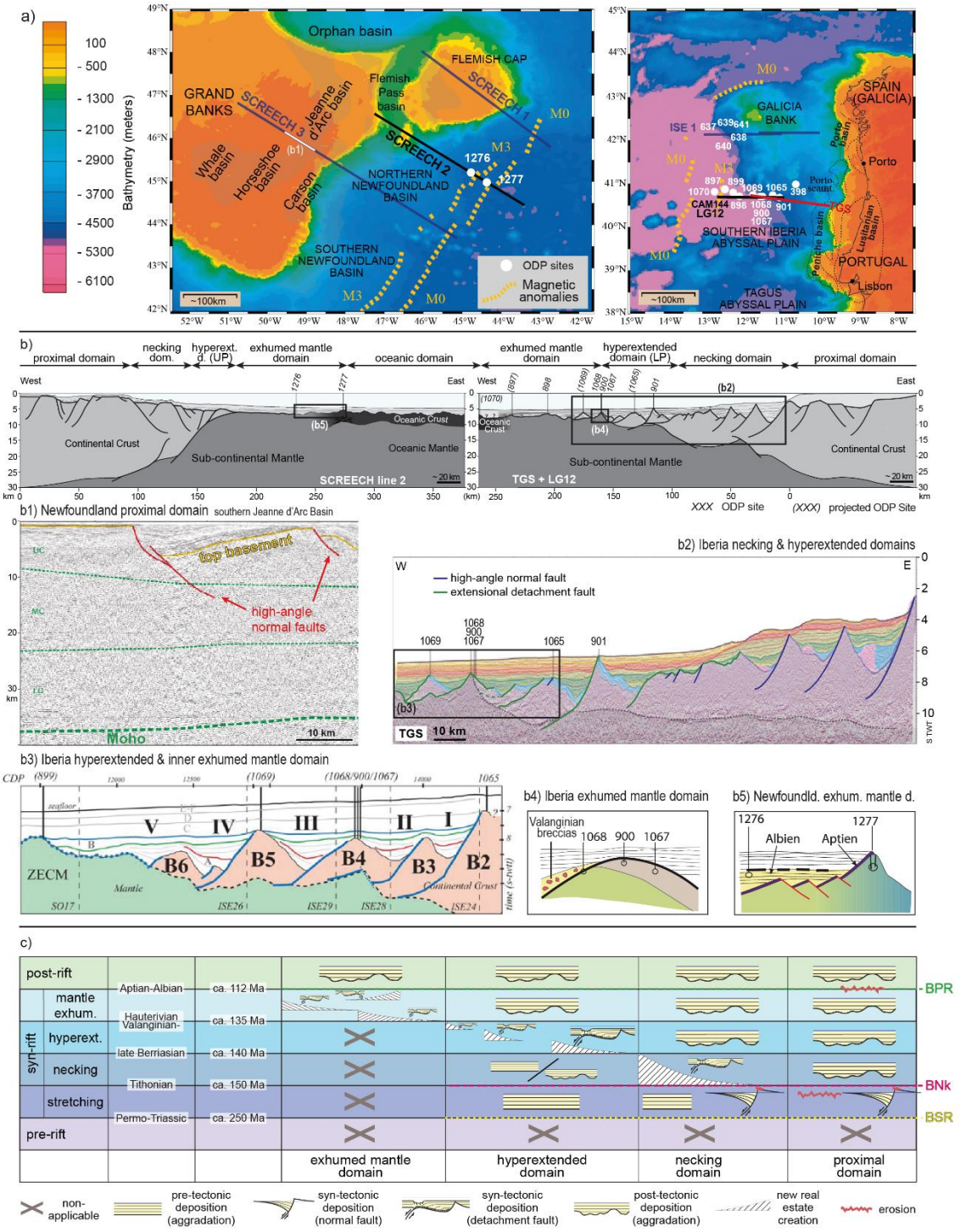


Figure 8: a) map of the Iberia–Newfoundland margins and location of the public seismic profiles and drill holes (modified from Sutra *et al.*, 2013); b) interpreted SCREECH 2, TGS and LG 12 seismic sections across the conjugate Iberia–Newfoundland rifted margins (modified from Sutra *et al.*, 2013); b1) close up on the southern Jeanne d'Arc Basin on the SCREECH 3 seismic transect (modified from Deemer *et al.*, 2009); b2) stratigraphic overview of the Iberian necking and hyperextended domains (from Merino-Perez, 2016, and references therein); b3) stratigraphic interpretation of the CAM 144 seismic line imaging the Iberian hyperextended domain (from Péron-Pinvidic *et al.*, 2007); b4) and b5) stratigraphic overview from the exhumed mantle domain of Iberia and Newfoundland, respectively (modified from Sutra *et al.*, 2013); c) Table synthetizing the sedimentary architectures in each system tract in the different rift domains of the Iberian margin.

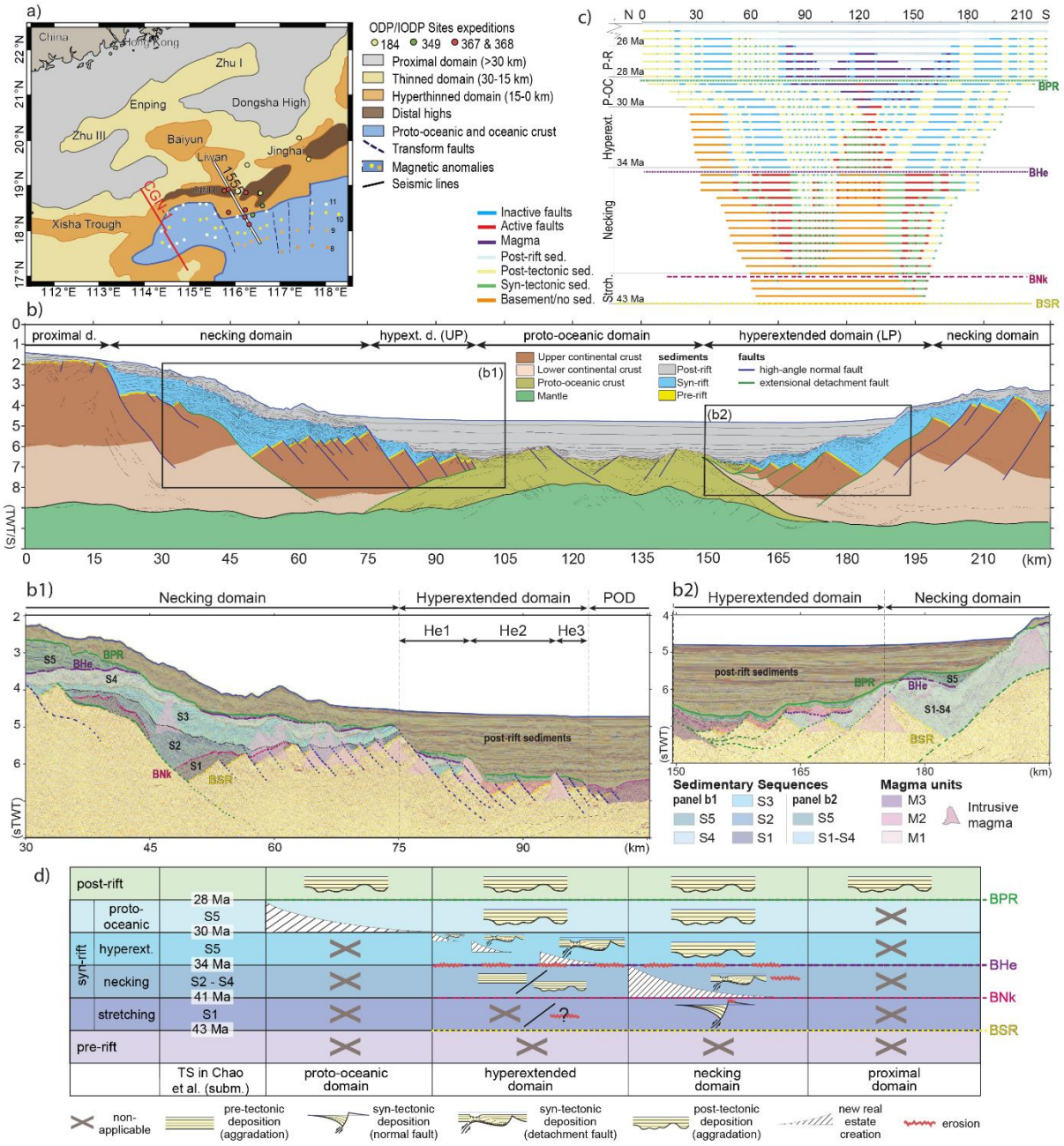


Figure 9: a) Rift domain map showing the location of the CGN-1 transect and IODP Sites (modified from Nirrengarten *et al.* 2020); b) linedrawing of the CGN-1 line by Chao *et al.* (2021); b1) and b2) close-up of the outer necking - inner hyperextended domains of the northern and southern margin, respectively; c) spatio-temporal evolution of active vs inactive faulting and sedimentation along the studied transect (from Chao *et al.* 2021); f) Table synthetizing the sedimentary architectures of each system tract in the different rift domains of the northern margin of the NW-SCS. Abbreviation POD stands for Proto-Oceanic Domain.

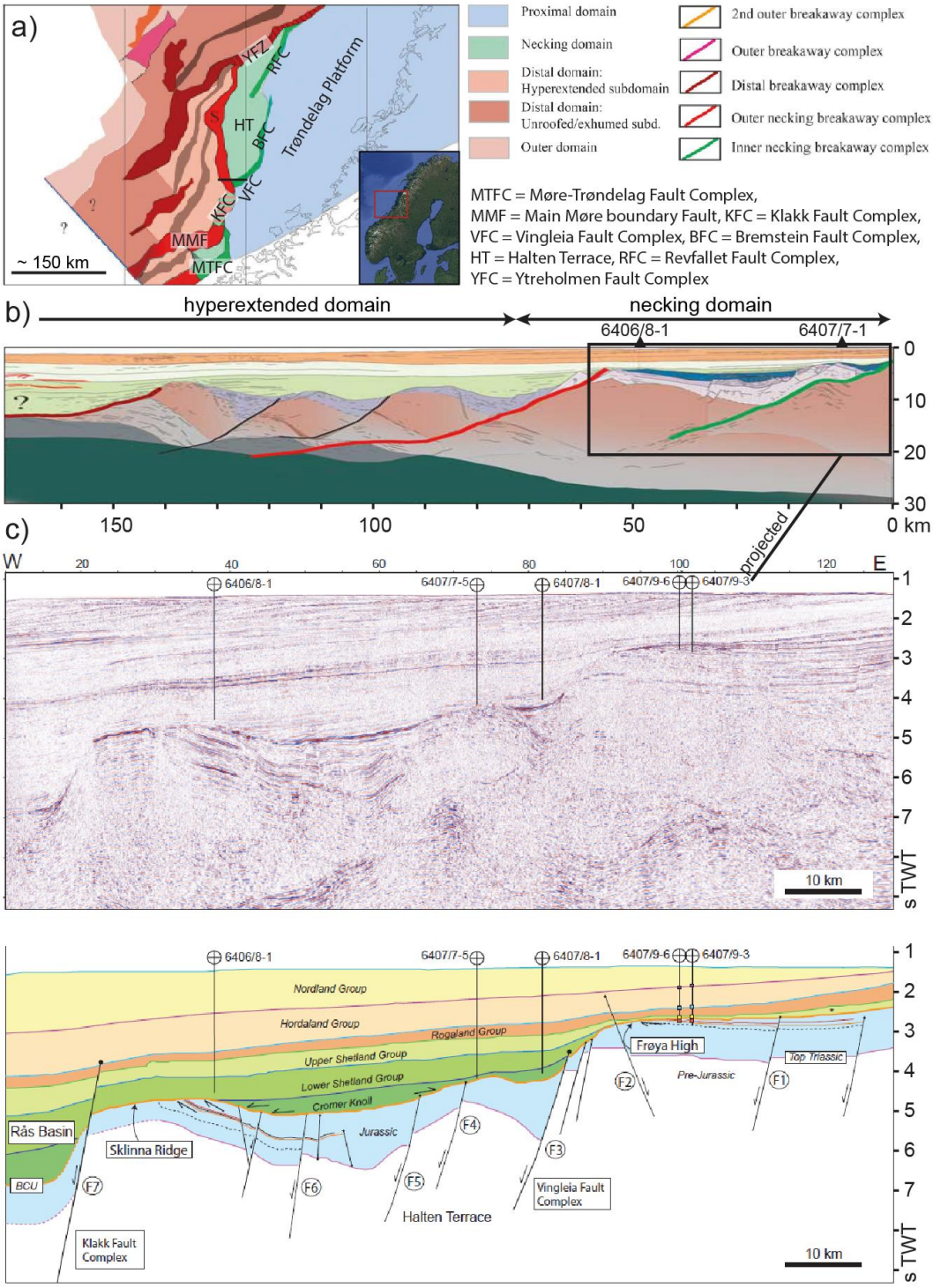


Figure 10: a) Map of the rift domains and intervening breakaway fault complexes at the mid-Norwegian margin (modified from Osmundsen and Péron-Pinvidic, 2018). Inset map from Google Earth; b) Interpreted seismic transect across the necking and hyperextended domains south of the Halten Terrace (no vertical exaggeration; modified from Osmundsen and Péron-Pinvidic, 2018; see panel a for location); c) uninterpreted and interpreted seismic section highlighting pervasive erosion of the Jurassic sequence at the breakaway of both the Vingleia and Klakk fault complexes (from Bell *et al.*, 2014).

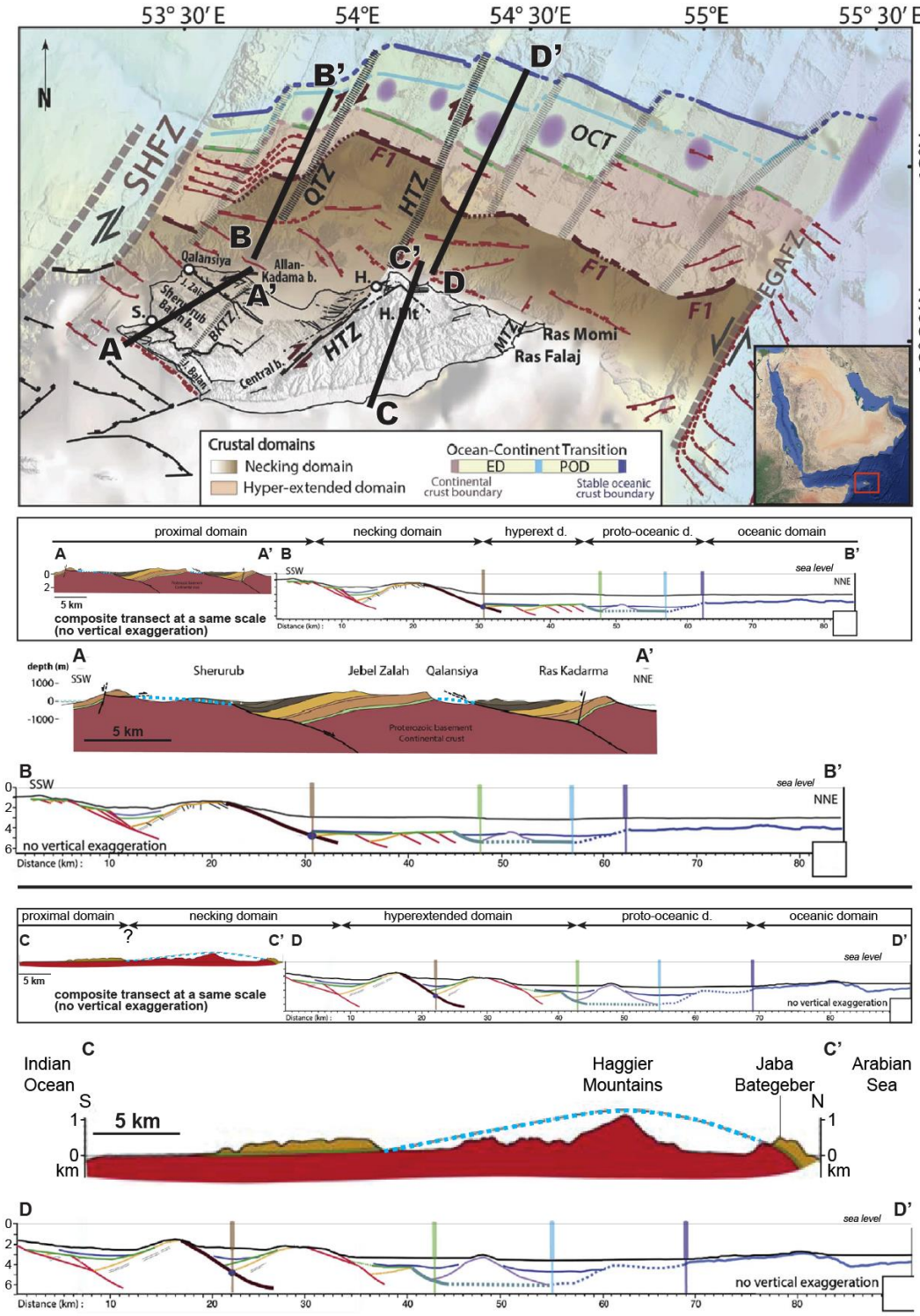


Figure 11: Map of the rift domains in the region of Socotra and interpreted transects onshore (A-A' from Nonn *et al.*, 2017; C-C' from (Fournier *et al.*, 2007) and offshore (B-B' and D-D' from Nonn *et al.*, 2017). Transects are first shown at the same scale and without vertical exaggeration for reference. Inset map from Google Earth.

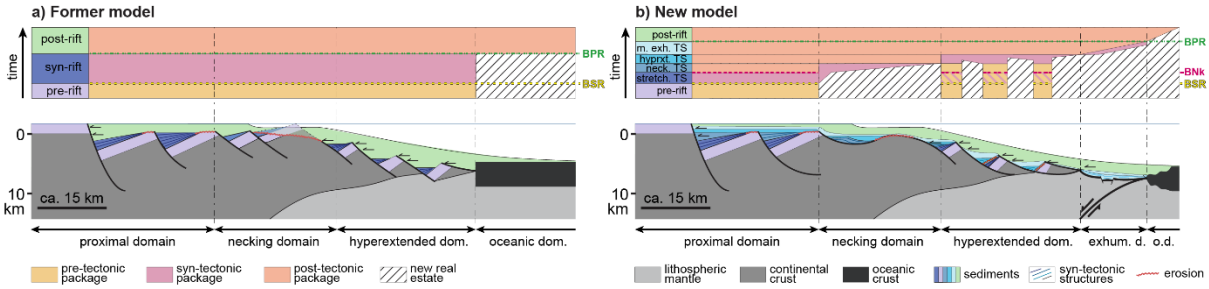


Figure 12: Schematic view of a rifted margin interpretation and corresponding Wheeler diagram according to a) former tectono-stratigraphic models; b) the tectono-stratigraphic presented in this study.

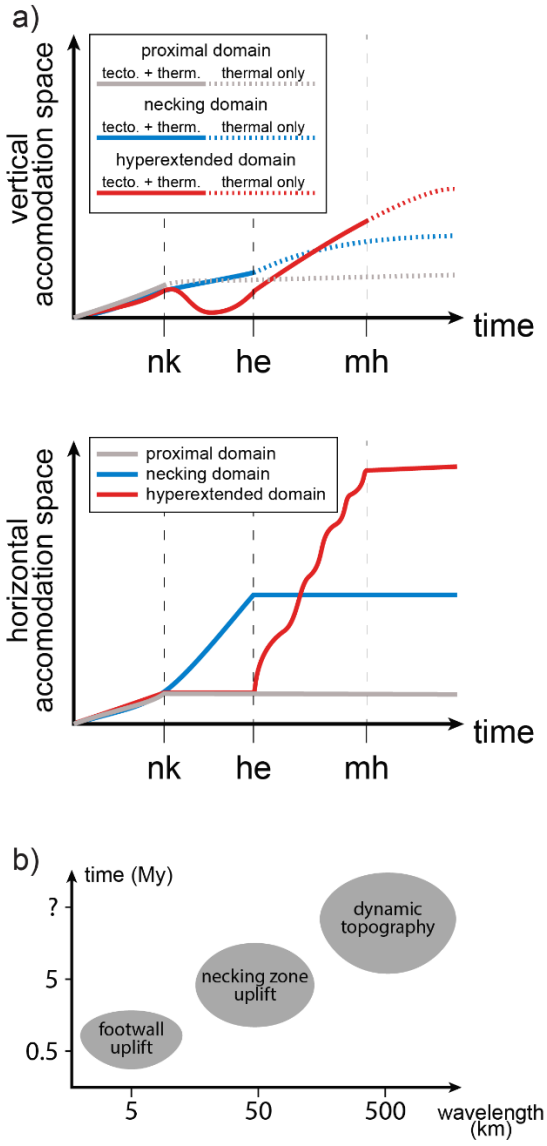


Figure 13: a) Graphs displaying the evolution of vertical and horizontal accommodation creation with time for the different rift domains. Note that vertical accommodation creation may result either from tectonics with a minor thermal component, or from thermal relaxation only. b) Characteristic wavelengths and time of uplift for different tectonic or geodynamic processes.

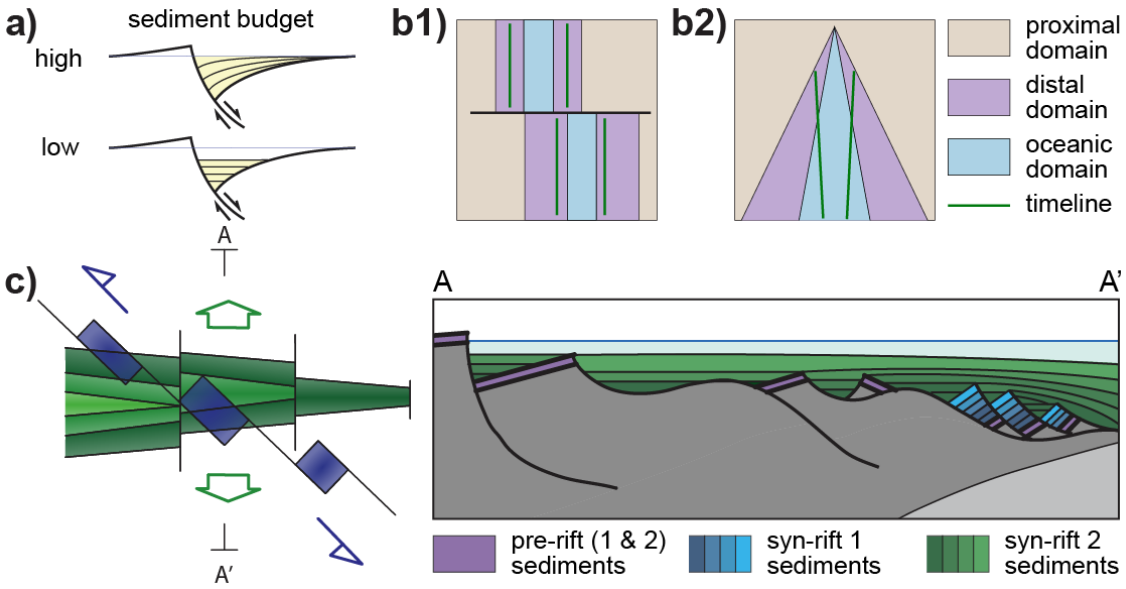


Figure 14: Main pitfalls to be kept in mind when applying a tectono-stratigraphic model to the interpretation of rift systems: a) impact of the ratio between sedimentation- and subsidence rate: sediment-starved systems will incompletely or even not record tectonic activity. b1) impact of segmentation and b2) propagating extension on the correlation of timelines across rift systems. c) impact of spatially overprinting extensional events (i.e., “multi-stage rifting”), which may incorporate sedimentary sequences unrelated to the rifting event considered (modified from Miró *et al.* 2021).